Slip Clutch Design for Position Sensitive Systems in Marine Environments

by

Thomas Patrick Finley

B.S., Naval Architecture, United States Naval Academy (2001)

Submitted to the Department of Mechanical Engineering
in partial fulfillment of the requirements for the degrees of

Naval Engineer

and

Master of Science in Mechanical Engineering

at the

MASSACHUSETTS INSTITUTE OF TECHNOLOGY

June 2017

Signature redacted

Author .....
Department of Mechanical Engineering
May 15, 2017

Signature redacted

Certified by .....
Alexander H. Slocum
Pappalardo Professor of Mechanical Engineering
Thesis Supervisor

Signature redacted

Accepted by .....
Rohan Abeyaratne
Chairman, Department Committee on Graduate Students

Slip Clutch Design for Position Sensitive Systems in Marine Environments

by

Thomas Patrick Finley

Submitted to the Department of Mechanical Engineering
on May 15, 2017, in partial fulfillment of the
requirements for the degrees of
Naval Engineer
and
Master of Science in Mechanical Engineering

Abstract

The Naval Research Laboratory (NRL) requested a two-axis pan tilt mechanism be designed, built, and tested for shipboard deployment of a sensor payload. Of paramount consideration to this design was the robustness of the system in the face of wave impact loading from "green water" taken over the superstructure of naval vessels. Central to providing such a system is the prevention of drive train failures given wave or other forms of impact loading. Through the course of work completed for his Master's thesis, Nathan M. Mills brought the design effort through initial bench testing. Several failures were experienced due to minor design flaws and mechanical component selection. One component selection that required improvement was the torque limiting slip clutch used in both the pan and tilt drive sections. The unit selected induced positioning errors resulting from backlash inherent to its design. The backlash encountered is unavoidable when using the type of slip clutch selected, as it is with many of the slip clutches available to the machine designer. Slip clutches are available that have limited backlash, but the majority of these are friction based and have setpoints that either do not have tight tolerances or change as the component is cycled. The goal of the present work was to design a slip clutch that maintains its setpoint and minimizes backlash to allow for its shipboard use in the NRL sponsored pan tilt system. The design was completed in a manner that supports the use of the slip clutch in other systems that require accurate positioning and torque overload protection in both marine and non-marine environments.

Thesis Supervisor: Alexander H. Slocum
Title: Pappalardo Professor of Mechanical Engineering

Acknowledgments

Throughout the course of the work presented, my wife, Elizabeth, and children, Katherine and Reagan, have been my greatest supporters. I thank them for being understanding when I am not at home and for brightening my life when I am. Thank you to my parents for always believing in me and for celebrating my accomplishments and showing me how to make meaning from my defeats. Thank you to my advisor, Dr. Alex Slocum, who has provided me with an invaluable educational opportunity. Thank you to the PERG lab group for their support throughout this project. Specifically, Kevin Simon and David Taylor, have always been willing to take time away from their work to help me work through a problem. Thank you to Herb Connors and Professor Richard Roberts at the Wentworth Institute of Technology. Their support during the testing phase of this project was a significant contributor to the completion of the work as a whole.

THIS PAGE INTENTIONALLY LEFT BLANK

Contents

THIS PAGE INTENTIONALLY LEFT BLANK

List of Figures

THIS PAGE INTENTIONALLY LEFT BLANK

List of Tables

THIS PAGE INTENTIONALLY LEFT BLANK

Introduction

The Naval Research Laboratory (NRL) requested a two-axis pan tilt mechanism be designed, built, and tested for shipboard deployment of a sensor payload. Of paramount consideration to this design was the robustness of the system in the face of wave impact loading from "green water" taken over the superstructure of naval vessels. Central to providing such a system is the prevention of drive train failures given wave or other forms of impact loading. Through the course of work completed for his Master's thesis, Nathan M. Mills brought the design effort through initial bench testing. Several failures were experienced due to minor design flaws and mechanical component selection. One component selection that required improvement was the torque limiting slip clutch used in both the pan and tilt drive sections. A rendering of the pan tilt machine with the torque limiting components shown in red is below.

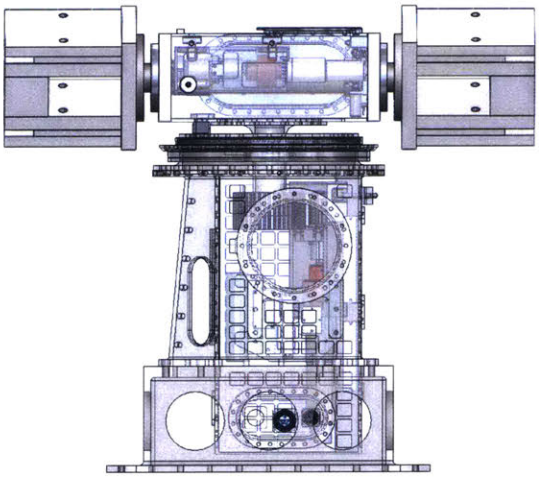

Pan Tilt Machine with Torque Limiting Components Shown in Red [7]

The unit selected induced positioning errors resulting from backlash inherent to its

design. The backlash encountered is unavoidable when using the type of slip clutch selected, as it is with many of the slip clutches available to the machine designer. One of the primary considerations for the torque limiting devices that were used was the constraints with respect to form factor. Since these components typically take a cylindrical shape, these constraints are 64mm diameter by 71mm length for the tilt drive and 73mm diameter by 82mm length for the pan drive. These constraints are imposed by the tilt and pan drive housings are shown below. The existing component is shown in solid red with the space constraints for the design shown in transparent red.

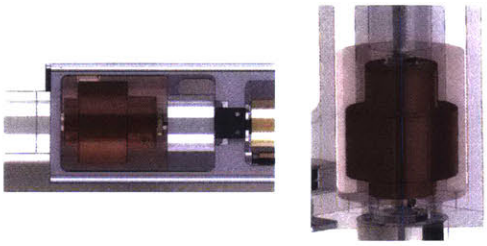

Space Considerations for Pan (right) and Tilt (left) Drives[7]

Slip clutches are available that have limited backlash, but the majority of these are friction based and have setpoints that either do not have tight tolerances or change as the component is cycled. The goal of the present work was to design a slip clutch that maintains its setpoint and minimizes backlash to allow for its shipboard use in the NRL sponsored pan tilt system. The design was completed in a manner that supports the use of the slip clutch in other systems that require accurate positioning and torque overload protection in both marine and non-marine environments.

At the beginning of the design process, a concentrated effort was made to envision the structure that would be followed during process execution. This enabled the balance and preservation of time resources through the elimination of activities that did not contribute to design realization. The design process was structured using four key components that also serve as chapter headings in the documentation of the effort: Literature Review, Strategy and Concept Development, Detailed Engineering and Development, and Manufacturing and Testing. These key components were broken

down into subcomponents until individual actionable items were identified. These items provided the basis for the time line used for scheduling and resource balancing.

The literature review was divided into three key areas. The first of these involved the review of Nate Mills' thesis upon which the present work is based. A general understanding of the work conducted was present, but further development of the specifics was required to establish a knowledge baseline and to properly develop the problem statement. This was done in order to provide context and scope to the remaining portions of the literature review. The second key area was a comprehensive audit of torque limiting devices available to the machine designer in the commercial market. This served the role of providing definition to the existing design space and highlighting the limitations of current designs, specifically with respect to positioning inaccuracies. The market analysis also provided a baseline from which designs developed over the course of this project would be measured. The market research also aided in the overall design process in that the concept development phase benefited from knowledge of the mechanisms in use that serve the intended function of providing torque overload protection. The third key area of the literature review was the research of existing patents. The primary reason for this review was to understand the patented overload devices, so as not to infringe on or recreate work already in existence, but not marketed commercially. The second purpose for this audit of patents was to improve the concept development phase by understanding prior work.

Following the literature review, the execution of the design process started in earnest with the strategy and concept development phase. This phase required the formulation of a detailed problem statement that was framed in a manner that allowed for the definition of functional requirements for the design. This enabled the realization of the feasible conceptual solutions that meet functional requirements. Through an engineering analysis that incorporated parametric and solid modeling, an optimal solution was selected. The output of the strategy and concept development phase was confirmation of optimal solution feasibility through the completion of proof of concept prototype testing.

With the optimal solution for the slip clutch identified, the design entered the de-

tailed engineering and development phase. The first stage in this phase was additional research focused specifically on the optimal solution that had not been previously explored in detail. In conjunction with this research, a significant level of detail was added to the parametric model developed in the strategy and concept development phase to increase model fidelity. This allowed for the identification of any scalability in the design for future development. Using the results of the parametric analysis, the fidelity of the 3D model was also improved and detailed finite element analyses were conducted. Over several iterations, the improvement in the parametric and 3D models enabled the development of a high fidelity prototype.

Following the detailed engineering and development phase the focus was the manufacturing, assembly, and testing of the high fidelity prototype which was used to again demonstrate the viability of the concept. The high fidelity prototype also served to allow for the identification of design changes that could be made to improve the manufacturability of component. Overlap between this and the previous phase occurred through the employment of the design-build-test method. Throughout the previous phase, prototypes were built that informed the design and changes were reflected in the next iteration. Following final assembly of the high fidelity prototype, testing was conducted to validate the parametric model developed over the course of the design effort. These testing results provide information that enable improvements in the performance, manufacturability, and scalability of a production ready unit in a future design iteration.

Chapter 1

Literature Review and Market Gap Analysis

1.1 Literature Review

In order to maximize the aperture of the literature review, with the goal of enabling a robust design process, the review was conducted in three phases. The first of these phases entailed a detailed reading of Nate Mill's thesis[7], proceeded by market research, and concluding with patent research. The sequence was executed in this fashion because it allowed for the later phases to be informed by those conducted earlier. The thesis review ensured that the limitations of components used in the original pan-tilt machine were understood such that a general problem statement could be developed. The previously used components provided two data points and established a baseline for a comparison from which the market research could be expanded. Based on the limited knowledge of torque limiting devices with which the author began this research, it was necessary to gain early exposure to commercially available designs. This exposure provided a foundation from which to build an in-depth understanding of the physical principles and concepts being employed, thus cuing more focused research of patent information. Another very practical reason for undertaking the literature review in this manner was the large quantity of and ease of obtaining information on commercially available torque limiting devices.

1.1.1 Background Thesis Review

The design requirement for a component that provides torque overload protection while minimizing position error arose out of Nathan M. Mill's Master's thesis.[7] This project was sponsored by the Naval Research Lab as detailed in the "Proposal for A Low-Torque Pan Tilt System for Directional Scanning in a Marine Environment".[13] In order to fully understand the system implications of the slip clutch design that was used, it was necessary to perform an in-depth review of both these documents.

While conducting initial testing of the drive train for both the pan and tilt systems, an excessive amount of error was experienced in angular position. This was of concern because the system had strict position accuracy requirements for the attached payload. Although the exact purpose of the payload is unknown, it can be expected that the system would not be able to operate with the position error experienced by the system. There were two design flaws that manifested as angular position inaccuracies. The first, which will not be specifically addressed in the present work, is the means by which the motor drive and the drive pulley shafts were connected. The slip clutch used in the design served as a coupling between these two shafts and the manner in which the shafts were connected resulted in an inability to transmit the required torque. The second factor in the position inaccuracy of the drive train was the backlash associated with the slip clutch. This backlash produced errors in the regulation tuning of the drive systems that manifested as payload position inaccuracy. The specific clutch used for both the pan and tilt drives will be left for discussion in Section 1.1.2.

It was proposed by Mr. Mills that a friction based slip clutch should be used as a temporary means of providing torque overload protection to the pan and the tilt drive systems. The basis for this recommendation was that friction based slip clutches do not experience backlash. It was evaluated that this could not be a permanent solution because the setpoint of these components drift with cycling. Further discussion will be reserved for Section 1.1.2, but the assumption of no backlash with respect to friction based slip clutches is inaccurate. This imposed some immediacy to the development

of a slip clutch that could be used in position sensitive systems, because even the temporary solution proposed to restore pan-tilt system capability was not viable.

1.1.2 Market Research

Based on the very specific application of torque limiting devices, a review of the commercial market was not as daunting as it may have been for another mechanical component that had more variations in form, fit or function. For each clutch that was researched, it was essential to gain an understanding of the fundamental principles that enabled the component to transmit torque and provide for motor and load shaft disengagement upon overload. This understanding allowed the advantages and disadvantages of each clutch to be identified to serve as a means of conducting a market comparison and market gap analysis. It also allowed for the grouping of these components such that an accurate survey of the market, across different manufacturers, could be undertaken. This market survey is presented below according to these groupings or transmission/actuation principles.

Spring Loaded Actuator

As a natural starting point for the market analysis, the slip clutches employed in the existing design of the pan-tilt system were researched. The slip clutches for the pan and tilt drive trains differed only in torque capacity and for the purpose of this analysis are considered in the same functional group, termed the spring loaded actuator group. These units were the Zero-Max® Torque Tender Models TT2-C and TT2X-C, with torque capacities of 85 in-lb (9.6 N-m) and 350 in-lbs (39.5 N-m), respectively.[7] As with all the slip clutches being researched, the orientation of the input and output or load and motor end of the slip clutch is interchangeable. The drive side of the slip clutch is comprised of an actuator that is compressed on both sides by a circumferential spring loaded mechanism. The load side is a receptacle that has a detent into which the actuator seats. If an overload condition is presented, the actuator is rotated against the spring force. Once adequate rotation is experienced,

the actuator clears the detent and the drive side is free to rotate for one revolution, upon which the actuator attempts to reengage the load. Positioning error is induced in this system from the start of torque application until the actuator clears the detent and the drive side is made free to rotate. The stiffness of the circumferential spring affects the accuracy of the overload setpoint and the amount of positioning error experienced by the system. A graphical representation of the arrangement described above is provided in Figure 1-1.

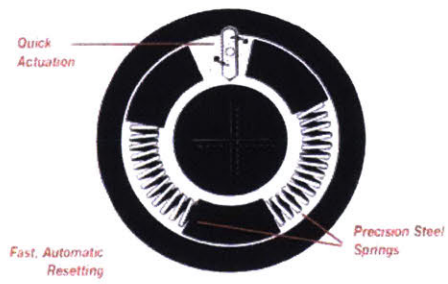

Figure 1-1: Zero-Max® Torque Tender Slip Clutch [15]

Axial Spring Loaded Ball and Detent

As a logical progression, the other type of slip clutch from the same manufacturer, Zero-Max®, was investigated. This research yielded a slip clutch that will be referred to as the axial spring loaded ball and detent. In this configuration, a given number of ball and spring combinations are recessed in one side of the clutch. The springs load the balls into detents in the opposing side of the clutch. The torque for the system is transmitted through these balls until the engagement force contributed by the spring is overcome by the side force resultant from the torque. Once this overload occurs, the clutch releases and ratchets to the next position. A cutaway of this type of clutch is provided.

Figure 1-2: Zero Max® H-TLC Torque Tender Cutaway [15]

Circumferential Ball and Detent

A predominant type of slip clutch available to the machine designer employs several balls that are constrained to an outer radial position by a retainer and loaded by a single spring mechanism on one side. On the opposing side, detents are provided that mate with the balls. This type of slip clutch employs the same actuation as the axial spring loaded ball and detent, just in a different configuration. The system torque is transmitted through the balls until the engagement force is overcome by the side force. At this point the clutch releases and ratchets to the next position. Figure 1-3 provides a cutaway of a representative example of this grouping that is produced by Mayr®. This type of slip clutch is a common design and is produced by several companies.

Figure 1-3: Mayr® EAS®-compact®-R/RA [6]

The manufacturers of several of the slip clutches that employ this method of torque overload protection claim that the devices have zero backlash. Detailed literature is not readily available that supports this catalog information. For this reason, an evaluation of the space available in the pan and tilt drives was conducted to determine

their viability for incorporation. It was found that these space constraints were limiting and therefore this type of slip clutch was not pursued as a solution. If the space constraints had supported, one of these units would have been purchased so that the catalog information regarding backlash could have been verified.

Friction Based

Another predominant grouping of slip clutch designs employ disk pads that are subjected to a loading force. This normal force allows for the transmission of torque though the friction created on the surface of these disk pads. The magnitude of the torque that can be transmitted has a direct correlation to the loading force and the coefficient of static friction of the material used. This phenomena takes advantage of the fact that the coefficient of static friction is always greater that the coefficient of dynamic friction, allowing the clutch to remain disengaged while the overload condition is present. Once the overload condition is removed, the clutch automatically resets as the relative motion of the disk pads approaches zero.

Figure 1-4: Zero Max H-TLC Torque Tender Cutaway [2]

The torque setting for this type of clutch can typically be changed quickly by making an external adjustment that increases the loading force. As mentioned in Section 1.1.1, a friction based slip clutch was proposed as a temporary solution to overcome the limitations of the spring loaded actuator type slip clutch used in the pan and tilt drives. The justification for its use as a temporary solution was that the friction based slip clutch did not have backlash, but that it would have a drifting set point with increased wear on the disk pads induced by component cycling. This justification is correct on the account of the torque tolerance of these slip clutch

designs ranging between 15%-20%. However, it is flawed in that the typical range for backlash is between 2 and 6 degrees.

1.1.3 Patent Research

Following completion of the market research portion of the literature review, an informed understanding had been developed of the types of slip clutches available commercially and where the pan-tilt system requirements stood with respect to those designs. In order to understand designs that may not have been marketed commercially, it was necessary to conduct a review of patent information. In order to ensure that a critical technology was not overlooked, a critical step was the development of an understanding of how to conduct such a review. Through meetings with library staff and other researchers who had an in-depth understanding of the process, a method for conducting this portion of the literature review was developed. The entire patent research process aided in the development of an understanding of the technologies developed for applications requiring torque overload protection. These devices will not be cataloged in the manner done for the market research, as it would be lengthy and not contribute to the reader's understanding of the present work.

1.2 Market Gap Analysis

Through the conduct of the market and patent research presented above, a comprehensive understanding of the types of torque overload devices that have been previously designed was obtained. The development of this understanding was a critical step in the design process because it encouraged thought on how to best capitalize on the advantages of certain designs in order to overcome the disadvantages or limitations of others. Without viewing the broad spectrum provided by this review of prior work as a whole, it would not have been possible to gain this perspective. Throughout the design process, the exposure to concepts that was gained during this period would be referred to frequently. Although several types of slip clutches are available to the machine designer, it is seen that for the majority of these components that the

backlash inherent to their design would not support the strict positioning tolerance of the pan-tilt system. For those devices that have limited or no backlash, their form factor did not allow for their incorporation into the drive trains. The non-union of a design solution that incorporates limited backlash and a compact design is a market gap that the rest of the present work will address.

Chapter 2

Strategy and Concept Development

The Strategy and Concept Development phase of this design effort evaluated numerous solutions using functional requirements and first order mechanics to establish feasibility. The critical first step of this phase was to define the problem in a manner that would allow for the development of this set of functional requirements. Using this approach enabled the brainstorming of conceptual solutions free from a detailed engineering analysis and the generation of potential solutions where first order feasibility of mechanics was satisfied. These conceptual solutions were subjected to further scrutiny leaving a small set of candidate solutions that were carried forward to the detailed engineering effort. The candidate solutions were modeled and moderately detailed calculations were performed. These additional steps allowed for the selection of an optimal solution that was carried forward for prototyping and proof of concept testing.

2.1 Problem Definition

As established in Chapter 1, the pan-tilt machine required a slip clutch that would provide overload protection while limiting the positioning error associated with many commercially available components. The system required a clutch for both the pan and the tilt drive sections that would provide protection at torque loads of 35.0 and 8.5 Newton-meters (N-m), respectively. [7] The system required position accuracy within

0.25 degrees and is expected to operate in a marine environment.[13] The component is not necessarily required to perform while directly exposed to the environment, but should use materials and sub-components that will not corrode if exposed to seawater. In order to provide analytical focus, the slip clutch for the tilt drive will be considered for the remainder of the design effort.

2.2 Deterministic Design

The concept of deterministic design was used throughout the design process. Succinctly put, "Deterministic Design could be described as creativity based on facts." [8] The general progression for deterministic design is to generate ideas based on the list of requirements and to use increasingly detailed engineering analysis as the design progresses to prove that the requirements are satisfied. The use of deterministic design requires early identification of risks associated with a given design and a continuous evaluation of where the design is positioned with respect to those risks. The goal in the early stages of design is to conduct simple experiments and analysis to prove that concept is viable with respect to physical principles.

2.3 Development Candidate Solutions

Considering the time resources available, only a small number of candidate solutions could be brought forward for detailed modeling and analysis. Through careful consideration of the potential for conceptual solutions to satisfy the functional requirements, three candidate solutions were selected and are analyzed in the following sections. Further description is provided in Section 2.4.

2.4 Analysis of Candidate Solutions

As described in Section 2.2, one of the goals of the design effort was to conduct analysis of first order mechanics to prove concept feasibility. This analysis also informed the

design process as to whether or not the concept was viable. One example of where a solution could be feasible yet non-viable would be one that satisfied functional requirements but had a large form factor that would preclude its use. Presented below are analyses for the candidate solutions that informed the selection of the optimal solution that was pursued for detailed engineering analysis and development.

2.4.1 Spiral Magnet

The spiral magnet concept utilizes permanent magnets to transmit torque. The input and output shaft are connected to the left and right end housings which transfer torque to the left and right end pieces via keyed shafts (in the housings) and shaftways (in the end pieces). On each end, between the face of the shaft and shaftway is a spring to maintain preload in the system. Alignment shafts and bearings maintain alignment of the left and right end pieces with their respective center pieces. The coupling spider between the left and right center pieces compensates for misalignment in the input/output shafts. The right and left end pieces could be directly coupled without the use of the center pieces and coupling spider with the sacrifice of misalignment compensation.

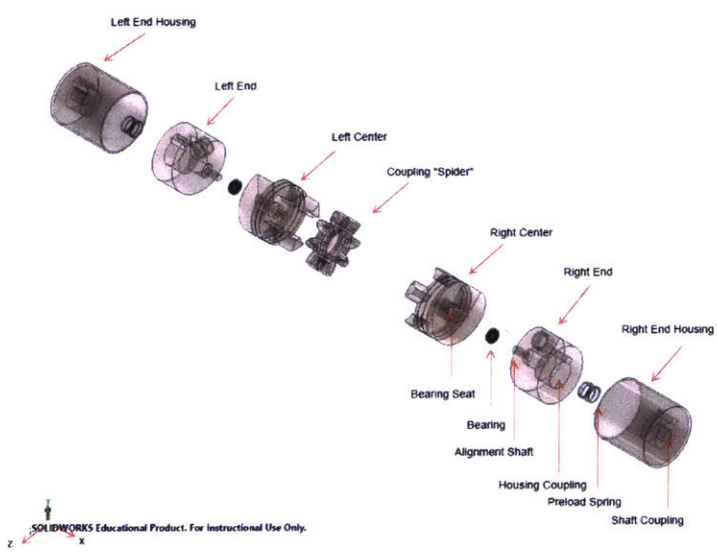

Figure 2-1: Spiral Magnet Conceptual Solution - Isometric View

Upon overload, the magnets in the left end and left center pieces will separate and the left end piece will continue to rotate with the input shaft. This will result in the left end traversing the "ramp" created by the spiral, causing the left end and left center pieces to translate in the -x and +x directions respectively. This movement will be compensated for through preload compression on both sides of the clutch. Overload in the counterclockwise direction is similar but employs the right side of the clutch. In order to develop a first order analysis of the spiral magnet slip clutch the following relationships had to be developed.

- Magnetic force provided by magnets of varying sizes (F_{mag})
- The size of magnet that can be accommodated by the end and center pieces of the clutch (r_{mag},ℓ_{mag})
- The torque required to overcome static friction on the spiral ramp ($T_{friction}$)

The limiting factor for the spiral magnet slip clutch concept is the magnetic force supplied for a given size of commercially available magnet. In order to increase torque capacity, the strength of magnet for a given distance from the clutch centerline must be maximized. The location of the magnet from centerline (r_{eq})is influenced by the outer clutch radius (r_{oc}) that can accommodate the magnet. These relationships are reflected in the following equations:

$$T_{magnet} = F_{mag} * r_{eq} = F_{mag} * \tan\left(\sin^{-1}\left(\frac{\ell_{mag}}{r_{oc}}\right)\right) \tag{2.1}$$

Another contributor to the torque capacity of the spiral magnet concept is the static friction along the ramp section. The derived equation for this torque is given by equation 2.2.

$$T_{friction} = F_s * r_{eq} = \mu_o * F_{preload} * \cos\left(\tan^{-1}\left(\frac{P}{r + \frac{2P}{3}}\right)\right) * r_{eq} \tag{2.2}$$

$$T_{capacity} = T_{magnet} + T_{friction} \tag{2.3}$$

Laboratory notebook exerts establishing these relationships are provided in Appendix A. Given the tilt drive form factor limitation of 64mm outer clutch diameter, the first order estimate of torque capacity of 3.3 N-m falls short of the 8.5 N-m required. Additionally, even at this early stage, the manufacturing complexity of the spiral magnet concept could not be ignored. For these reasons this potential solution was not pursued further.

2.4.2 Socket Ball

The Socket Ball concept utilizes the friction force between a zirconia ball and a stainless steel cup to transmit torque. Referring to Figure 2-2 the concept of operations is described below.

Figure 2-2: Socket Ball Conceptual Solution

The input shaft is connected to the right end piece which is connected to the right cup through a coupling spider which compensates for shaft misalignment. Torque is transmitted through friction created by preload between the right cup, the zirconia ball and the left cup. The torque which can be transmitted is dependent on the preload force ($F_{preload}$), the coefficient of static friction (μ) and the effective radius of the contact area between the cups and the ball (r_{eff}). A first order analysis of this relationship, as presented in Appendix A, yields the following governing equation:

$$T_{capacity} = \mu * F_{preload} * r_{eff} = \mu * F_{preload} * \left(\frac{r_{top} - r_{bottom}}{r_{top} + r_{bottom}}\right) * \left(\frac{2r_{top} + r_{bottom}}{3}\right) \quad (2.4)$$

Given the tilt drive form factor limitation of 64mm outer clutch diameter, the first order estimate, given reasonable assumptions for μ and $F_{preload}$, yielded a torque capacity of 2.5 N-m falling short of the 8.5 N-m required. Varying the magnitude of preload force in equation 2.4 showed that the amount of increase required to achieve the target torque value was excessive and limited the feasibility of the concept. Additionally, while the manner in which the preload would have been incorporated into the system was not identified, it would have required that the overall form factor be increased. This increase, specifically in diameter would have made the concept infeasible for incorporation into the tilt drive system. For these reasons, the Socket Ball concept was not pursued further.

2.4.3 Curved Beam

The Curved Beam concept evolved from the Market Research portion of the Literature Review described in Section 1.1.2. Specifically, the evolution resulted from exposure to a commercially available component known as a spring loaded device (SLD). The most notable example of such a component being incorporated in a slip clutch design is the H-TLC line of torque limiting devices produced by Zeromax, Inc., a cutaway view of which is provided in Figure 1-2.

The generation of ideas around this line of torque limiting devices led to the realization that the rotation of the SLD from an axial to a circumferential orientation would place the reaction point of the ball and detent further from the central axis. This increase in distance would yield a greater torque capacity. Presented below are several drawbacks to both the axial or circumferential arrangement, all of which are inherent to the SLD.

- Corrosive Environment - The inclusion of springs in a component exposed to a marine environment would result in deterioration that affects performance and

service life.

- Spring Housing - The SLD incurs additional friction losses as a result of the vertical displacement of the ball into the housing. This friction again affects torque, is difficult to quantify, and changes as the surfaces wear.

- Ball/Detent Interface - The interface arrangements used in the traditional SLD and the associated slip clutches have sliding friction. This friction affects torque, is difficult to quantify, and changes as the surfaces wear.

Identification of these drawbacks was not seen as limiting to the evolution of conceptual solution, but rather enablers for design improvements. The limitation imposed by the corrosive environment was approached first because of the consequences of engagement spring failure during tilt drive operation. It also served as a logical starting point due to the easy identification of mechanical components that could serve that same purpose as the compression spring. In keeping with the philosophy presented by Occum of maintaining systems as simple as possible, a simple beam was explored as an option of avoiding the use of springs and providing the required engagement force.[12] This solution also avoids the friction that is encountered in the spring housing of the SLD. The first iteration of brainstorming around this concept involved the bending of straight beams that extended radially from the center of the device. A simple sketch of such an arrangement is provided in Figure

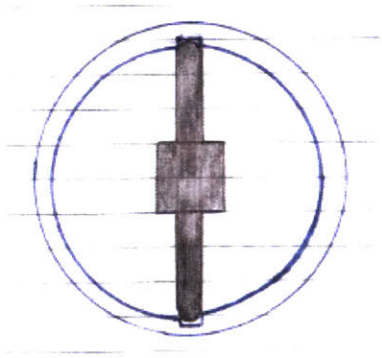

Figure 2-3: Sketch of Straight Beam Configuration

This configuration requires radial displacement of the end of the beam through

bending. This bending results in angular displacement, or rotation, of the beam assembly relative to the detent. This rotation manifests as position error in the system prior to overload protection being provided. The straight beam configuration therefore does not meet the functional requirement of minimizing position error prior to release. The mechanics of the above system can be conceptualized by analyzing a simple cantilever beam. In it's simplest, uniform cross section case, it is readily shown that for an equivalent force, displacement in the direction of loading is larger for a bending force than for an axial force. Invoking reciprocity, the next iteration involved the conceptualization of a method to rotate the beam to take advantage of these mechanics. As such, the beam had to axially support the force enabling torque transmission, while vertical deflection would be resultant from the force applied in bending. Taken in context of the straight beam case presented above, this manner of loading would minimize rotation for a given vertical deflection. Stated in terms of the slip clutch system as a whole, position error would be minimized for a given torque overload set point. Since the rotation of the straight beam to enable loading in this manner is not practical, the curved beam enabled this conceptualization to take form. Thus, the use of a radially curved beam that interfaced with a detent presented itself as a conceptual solution. While not specifically addressed in this formulation of the conceptual solution, the elimination of the spring also mitigated the frictional losses that the SLDs' spring encountered in the housing.

Development of the beam to detent interface allowed the final drawback of the traditional SLD to detent interface to be approached. This development included the use of a ball bearing attached to the end of the curved beam. This resulted in the interface of the curved beam to detent being made through a ball bearing. This formulation of the interface virtually eliminates the sliding friction encountered in the traditional ball and detent configuration. This conceptual solution either eliminated or mitigated all of the drawbacks to the traditional SLD based slip clutch. A simple sketch of this concept is provided in Figure 2-4.

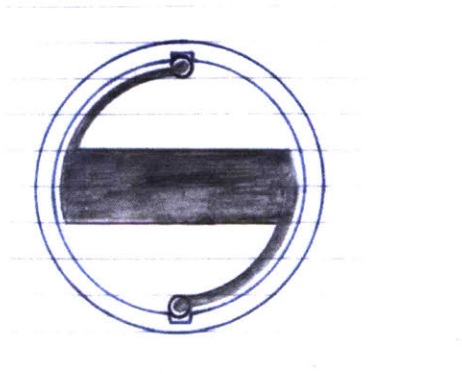

Figure 2-4: Curved Beam Initial Conceptualization

While this configuration presented some attractive properties, analysis was in order to ensure feasibility for the torque range and form factor of the tilt drive, and to better understand the mechanics. This first order analysis is presented in Appendix A and yields a governing equation that is dependent on Engagement Force ($F_{engagement}$), Side Force (F_s), the number of curved beams (N), the radius of the bearing to detent interface (R), and the angle of interface (α).

$$F_{engagement} = \frac{F_s}{tan(\alpha)} \tag{2.5}$$

$$since, F_s = \frac{T_{capacity}}{N * R} \tag{2.6}$$

$$T_{capacity} = F_{engagement} * tan(\alpha) * N * R \tag{2.7}$$

Using reasonable assumptions for the variables, a $T_{capacity}$ of 8.0 N-m can be achieved within the limiting constraints of the tilt drive housing. As can be seen from equation 2.7, torque capacity of this conceptual solution is highly dependent on the interface angle between the ball bearing and the detent. The tangent of interface angle of the ball bearing and detent has such a large effect on the torque capacity because of the behavior of the tangent function between 0 and 90 degrees as shown below.

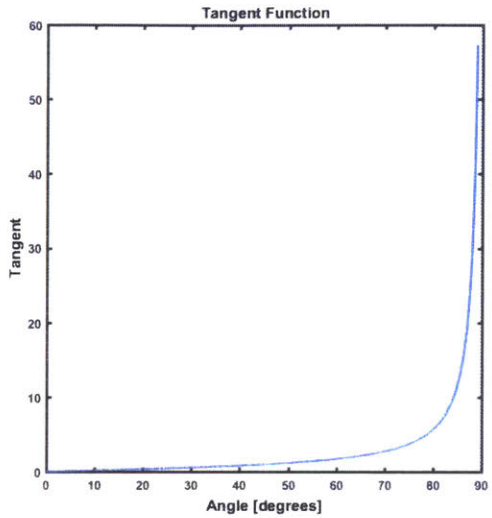

Figure 2-5: Tangent Function from 0° to 90°

The behavior reflected in equation 2.7 is intuitive when taken in the context of the physical relationship between the ball bearing and the detent. The left graphic of Figure 2-6 provides a representation of when the interface angle is 90 degrees. In this condition the Curved Beam can support infinite torque for any engagement force greater than zero, as reflected in equation 2.7.

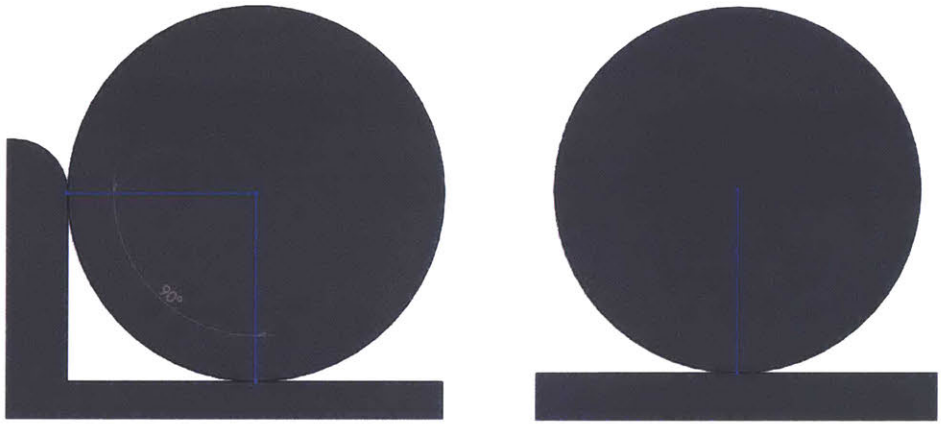

Figure 2-6: Interface Angle Representation for 90° (Left) and 0° (Right)

The right graphic of Figure 2-6 provides the other extreme where the interface angle is 0 degrees. In this condition, the tangent of the interface angle again drives the result, and no torque can be supported, for a finite engagement force, again, as

reflected in equation 2.7.

Another principle addressed during this stage of development was the contribution of the element's stiffness given an applied torque and their corresponding relationship to interface angle. The engagement force contributed by the beam and rolling contact stiffness of the ball bearing result in the element being torsionally stiff until the resultant preload force is overcome. At this point, the displacement of the beam results in an increase in engagement force which effects torque capacity. This displacement also results in the interface angle decreasing with a corresponding effect on torque capacity. The balancing of these effects was viewed as critical further development of this concept.

2.5 Selection of Optimal Solution

Through the analysis presented in Appendix A and amplified in Section 2.4, it was found that the curved beam concept offered the most potential for further development of the slip clutch. This decision was based primarily on a first order analysis that yielded a torque capacity and form factor consistent with the tilt drive requirements. As such, the next step undertaken in the design effort was to develop the concept to the level of fidelity required to perform a functional test. The goal of this test was to ensure that the calculations supporting the first order mechanics could be substantiated through a physical demonstration under the design, build, test paradigm.

2.6 Optimal Solution Validation

Following the selection of the curved beam as the optimal solution, it was necessary to perform a concept validation. This validation was realized through higher fidelity parametric analysis and 3D modeling efforts as well as a test based proof of concept. The tangible result of these validation steps was a prototype which supported initial manufacturing and fit-up evaluations as well as the test based validation.

2.6.1 Parametric Analysis

The parametric analysis completed at this stage of the design was focused on the determination of the required engagement force to support a desired slip clutch torque capacity and the resultant angular displacement. The analysis was structured in this manner to support the concept validation phase of the design. The parametric analysis was completed in MATLAB to allow for easy manipulation and calculations involving matrices. Further development was left to later stages of design and is presented in the detailed engineering and development work contained in Chapter 3. The script used for the concept validation as well as the detailed engineering analysis was founded on the calculations presented in Section 2.4.3 and as amplified in Appendix A. As stated above, analysis was structured such that the engagement force required to support a given torque capacity and detent incident angle was calculated. Curved Beam Analysis was conducted to determine the vertical displacement of the curved beam element as torque is increased. Several items were excluded to simplify the analysis and allow for solution validation and progression of the design. These exclusions were acknowledged explicitly as presented below and are addressed as appropriate in Chapter 3 and are reflected in the script containing the final parametric analysis presented in Appendix C.

- Cross Section - The cross section of the curved beam used at this stage of design was of uniform cross section. The simplification was most significant in that it greatly eased the analysis of the beam bending equations. Despite this approach, it was acknowledged that the stresses encountered in the beam would have to be managed at a later stage through the use of a non-uniform or tapered beam cross section.

- Detent Angle - The detent angle was maintained constant in the analysis which was not reflected in the validation prototype. In the prototype, the transition of the detent to the inner cup radius was rounded to avoid excessive stress concentrations as the ball bearing was displaced.

- Engagement Force - The Engagement Force was kept constant through the range

of the curved beam element's deflection. This is a simplification because the engagement force of the element increases proportionally to its displacement by the stiffness constant.

- Hertzian Contact Stress - The cup detent and ball bearing experience line loading along their interface. At this stage, the hertzian contact stress was not analyzed in relation to yield stress of the components.

- Stiffness Constant - The engagement force is a product of the displacement of the curved beam and the stiffness constant. There are both vertical and horizontal components of displacement, stiffness, and Engagement Force. For simplification, this stage of analysis only incorporated the vertical components.

2.6.2 3D Modeling

As it was during the development of candidate solutions, the three dimensional Computer Aided Design (CAD) tool Solidworks was used to model and analyze the prototype during concept validation. The functionality afforded by this program was critical to the development of the prototype and the associated test rig. The curved beam was modeled and Finite Element Analysis conducted using the Design Study functionality. The FEA allowed for the determination of the displacement of the curved beam that was necessary to impart the appropriate amount of engagement force required for a given torque capacity. In order to achieve this result, the curved beam element was subjected to a loading condition of 1N, 10N and 100N. These conditions were then graphed versus the displacements calculated through the FEA, allowing for a spring constant for the curved beam element to be determined. Using this spring constant and the engagement force required, the displacement of the beam required to achieve adequate preload could be determined. This in turn dictated the location of the interface of the ball bearing and detent, therefore dictating the cup dimensions. Examples of the results of these first analyses is provided in Figures 2-7 and 2-8.

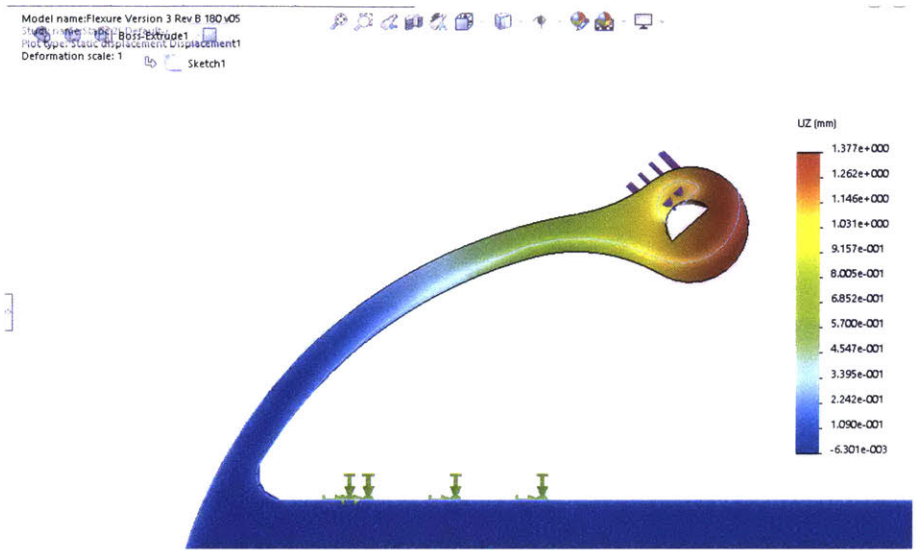

Figure 2-7: Optimal Solution Validation Finite Element Analysis - Displacement

It is seen from the analysis that the use of the uniform cross section results in an area of concern near the base of the beam with respect to stress. As mentioned in Section 2.6.1 this result was acknowledged and was addressed in the next iteration of the design.

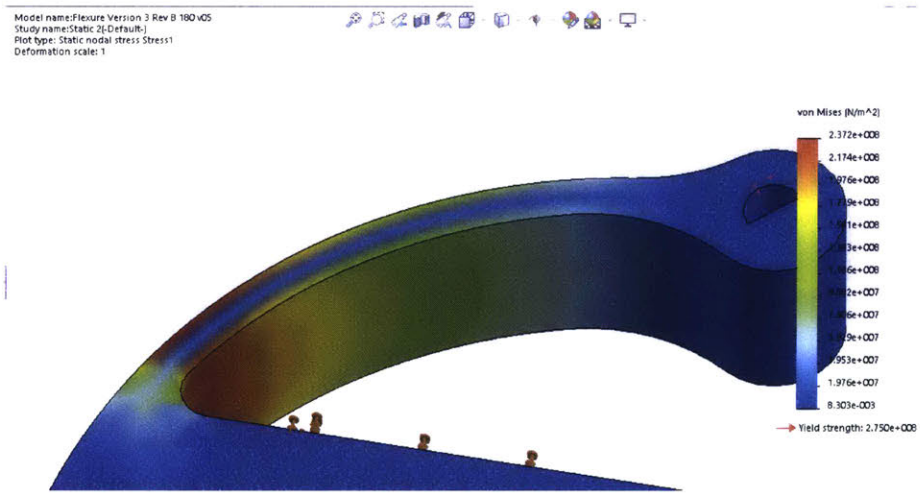

Figure 2-8: Optimal Solution Validation Finite Element Analysis - Von Mises Stress

2.6.3 Proof of Concept Prototype

Production of the curved beam proof of concept prototype was completed using dimensions that were convenient for production. Scaling of the components such that stock and fastening material procurement were simplified from a time and cost perspective was desired. Additionally, since this prototype's primary purpose was concept validation, the extent to which the modeling above could be used was maximized while taking manufacturing complexity into consideration. Stock material, ball bearing, dowel pins and shoulder bolts were all commercially procured. The curved beam element was cut from stock on a waterjet which enabled the production of the complex shape. Figure 2-9 provides a picture of the curved beam assembly used for this stage of the design validation.

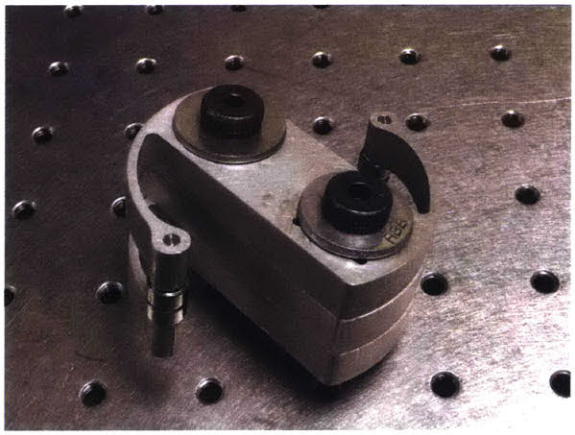

Figure 2-9: Proof of Concept Curved Beam Assembly

2.6.4 Test Based Validation

Following the verification of prototype fit-up, the final portion of concept validation was undertaken. This testing validation was a critical phase of the design effort, serving as the physical demonstration of concept feasibility. Test Based Validation was completed in a manner that minimized complexity of the setup and execution while still obtaining valuable insight and proof of concept.

Testing Set-Up

Since the production of a full prototype would be time intensive and higher in fidelity than required for the solution validation, a testing setup was required. This setup used a bench with 1/4-20 threaded holes on a 1 inch by 1 inch grid. For the purpose of the setup discussion, the load will be assumed as the fixed plate bolted to the bench using standoffs. Using the load plate, with indentations simulating the load cup, the curved beam prototype was placed in the system utilizing two balls to minimize friction with the table as shown in Figure 2-10.

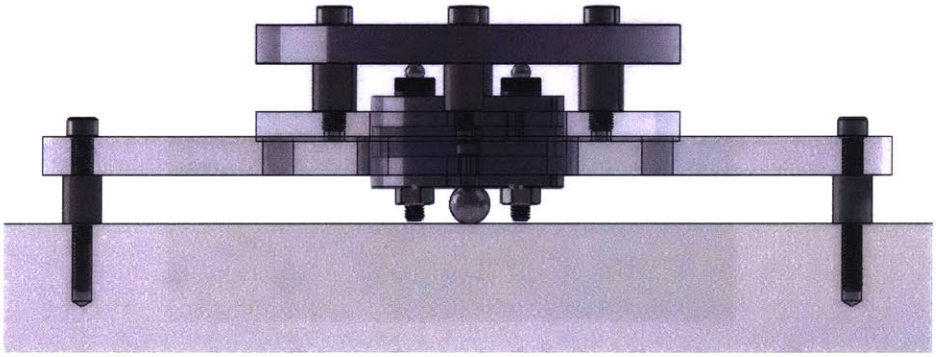

Figure 2-10: Validation Testing Setup - Frontal View

Another annular plate was cut to simulate the motor input. This plate was connected to an adapter plate using bolt, standoffs, and ball bearings to again provide separation and reduce friction. This setup allowed an input torque to be applied using a 10mm hex wrench. Another view of the testing setup is provided in Figure 2-11.

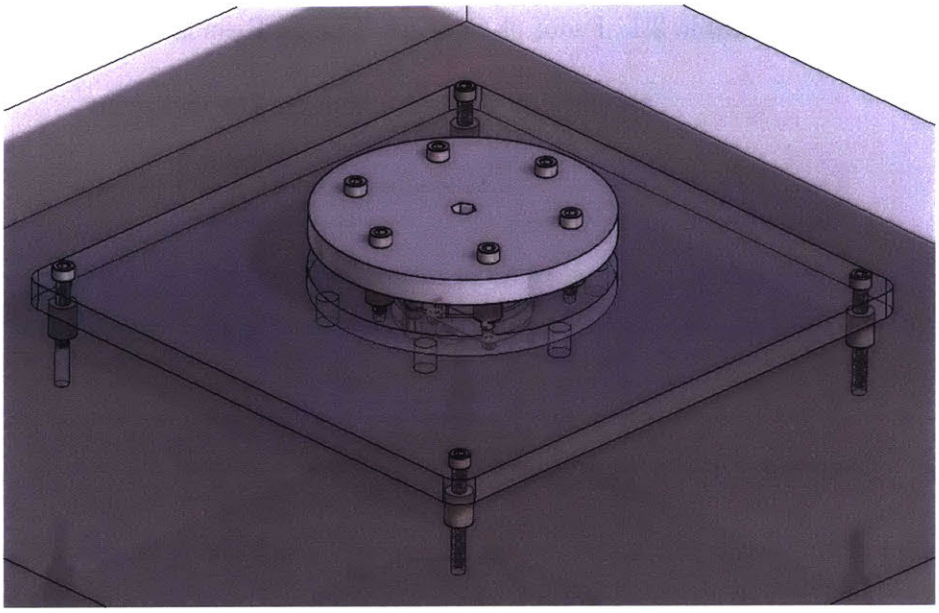

Figure 2-11: Validation Testing Setup - Modified Isometric View

The hex wrench was outfitted with a laser pointer such that, through the used of a cutting mat perpendicular and square to the test plate, angular displacement could be calculated. Despite the low sophistication of this method, it was adequate for the level of accuracy required, invoking a key tenant of deterministic design and design-build-test methodologies.

Test Expectations

The proof of concept prototype was not constructed in a manner to reflect the conditions experienced by the tilt drive section. As such, the torque at which the system would provide protection was not based on any specification, but was resultant from the dimensions of the curved beam and test plates. These calculations are presented in Appendix B.

Testing Results

The testing described above was executed twice and reasonable agreement was found between the calculations presented in Appendix B and the test results. The results are presented in Table 2.1.

Table 2.1: Proof of Concept Testing Results

	Breakaway Torque [in-lbf]	Angular Displacement [degrees]
Calculation	13.1	5.34
Test Run 1	16.5	5.49
Test Run 2	13.1	3.42

2.6.5 Testing Lessons Learned

The value of the design-build-test methodology was emphasized at this stage of the design. The value presented itself in the form of problems experienced during test execution. The validation tests conducted along with the problems formed a foundation upon which the rest of the design effort was built.

The first of these problems that was encountered became apparent through excessive angular deflection prior to the curved beam assembly disengagement. During the design of the testing setup, not all of the differences between the proof of concept prototype and the final component were anticipated. One of these is that the top test plate, or cup, was not supported radially as the shaft and cup combination would be in the final component. This lack of radial support resulted in radial displacement prior to a torque overload condition being achieved and resulted in excessive angular displacement. This was alleviated by using dowel pins between the test plate and curved beam assembly to provide a rudimentary level of radial support. The added friction of these dowel pins rolling on the inner circumference of the test plate was evaluated as insufficient to deem the test results invalid. This problem provided a lesson learned to the design process. Future design iterations would include radial support to prevent the angular displacement experienced during the first portion of validation testing.

The second lesson learned, which resulted in the limitation to the usefulness of the testing data, involved the method through which torque was measured. The torque wrench was a direct pawl clicker type wrench which does not provide a continuous

torque measurement, but only bends at the head when a specific torque is achieved. During the test, the measurement taken was the torque at which the curved beam assembly started to angularly displace or "breakaway". The second "laser pointed" measurement that allowed for the calculation of angular displacement was taken when the curved beam assembly released.

The lessons learned provided above helped to shape subsequent design efforts specifically, the planning for future testing plans. Despite the limitations to the testing resultant from the items cited above, the data was evaluated as adequate for the purpose of concept validation and progressing the design to the detailed engineering and design phase.

THIS PAGE INTENTIONALLY LEFT BLANK

Chapter 3

Detailed Engineering and Development

Following the decision to pursue the curved beam slip clutch as documented in Chapter 2, the design entered the phase of development that required an iterative approach. The goal of this design approach was to use the results of analysis to produce increasingly more detailed prototypes. Feedback from these prototypes and the associated test results allowed for the incorporation of an increasing level of detail into the design, either through the analytical or 3D model, or both. The prototypes will be used as a lens through which to view the evolution of the component. Most of the changes that were incorporated over the course of the design were cumulative. For this reason, the analytical and 3D models will be described in the following sections with only the changes specific to that iteration being described. Appendices C and D present the finalized models and serve as a cumulative product of the design iterations described below.

3.1 First Prototype Development

The evolutionary step from the Proof of Concept (POC) prototype to what will be deemed the "first prototype" was the most significant in scope and therefore requires the most explanation. The POC prototype served the purpose that it's name implies,

but was not viable for direct incorporation into the tilt drive for many reasons. The goal of the First Prototype was to address as many of these shortcomings as possible without investing an inordinate amount of time in it's development. It was understood that the form factor of the POC prototype was excessively large and that the next effort must decrease significantly in diameter. This became one of the primary focuses of the prototype.

3.1.1 Analytical Model Refinement

The analytical model used for the POC prototype as described in Section 2.6.1 formed the baseline for first prototype model. In order to serve as a reference for discussion later in this chapter, a comprehensive description of the entire model is presented in this section. As with all the analytical models in this chapter, the purpose of this model is to reflect the physical response of the curved beam in an effort to optimize its the design. The primary objective of the optimization effort is to minimize angular displacement prior to the clutch's disengagement at a specified torque threshold. The first step taken was the determination of the displacement of the ball bearing centerline axis due to loading in the vertical direction. This analysis employed energy methods to determine the deflection of the curved beam element, yielding values for vertical, horizontal and angular displacement. The equations presented below detail the contributions of each loading direction to these displacements. [10] The Area (A) and Moment of Inertia (I) terms, were varied over the length of the beam to account for curvature.

$$\delta_x = \frac{R}{EA}\left[F_x\left(\frac{2\phi+\sin 2\phi}{4}\right)-F_y\left(\frac{1-\cos^2\phi}{2}\right)\right]\Bigg|_{axial} - \frac{R}{GA}\left[F_x\left(\frac{2\phi-\sin 2\phi}{4}\right)-F_y\left(\frac{1-\cos^2\phi}{2}\right)\right]\Bigg|_{shear} -$$

$$\frac{1}{EI}\left[R^3F_x\left(\frac{6\phi-8\sin\phi-\sin 2\phi}{4}\right)-R^3F_y\left(\frac{1-2\cos\phi+\cos^2\theta}{2}\right)-M_oR^2(\phi-\sin\phi)\right]\Bigg|_{bending}$$

Figure 3-1: Curved Beam Deflection Equation - Horizontal Displacement

$$\delta_y = \frac{R}{EA}\left[-F_x\left(\frac{1-\cos^2\phi}{2}\right) - F_y\left(\frac{2\phi-\sin 2\phi}{4}\right)\right]\Bigg|_{axial} - \frac{R}{GA}\left[F_x\left(\frac{1-\cos^2\phi}{2}\right) - F_y\left(\frac{2\phi-\sin 2\phi}{4}\right)\right]\Bigg|_{shear} -$$

$$\frac{1}{EI}\left[R^3F_x\left(\frac{1-2\cos\phi-\cos^2\theta}{2}\right) - R^3F_y\left(\frac{2\phi-\sin 2\phi}{4}\right) - M_eR^2(1-\cos\phi)\right]\Bigg|_{bending}$$

Figure 3-2: Curved Beam Deflection Equation - Vertical Displacement

$$\theta = \frac{1}{EI}\left[R^2F_x(\phi-\sin\phi) - R^2F_y(1-\cos\phi) - M_eR\phi\right]\Bigg|_{bending}$$

Figure 3-3: Curved Beam Deflection Equation- Angular Displacement

Displacements were determined for a range of vertical loading conditions. A regression was then run on the vertical displacement versus the loading condition to determine the stiffness of the beam in the y-direction. Results of this regression are presented in Figure 3-4.

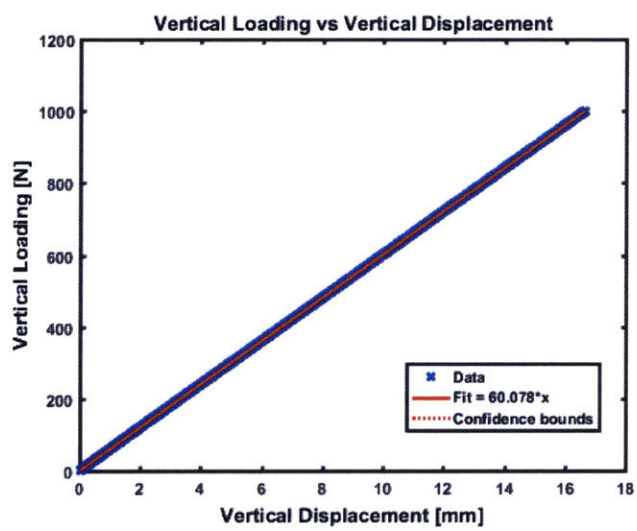

Figure 3-4: Vertical Displacement vs. Vertical Loading Regression Analysis

In order to address one of the limitations of the POC analytical model, an estimate of the ball and detent interface angle was made for the range of curved beam deflection. The goal was to perform this calculation for a range of initial interface angles such that an optimum could be selected. The initial interface angle is defined as that

angle at which the ball and detent make contact in the preloaded condition without a torque load being applied. This formulation of the interface angle as a function of beam deflection does not account for effect that the radius of the detent has upon the angle. This effect is addressed in Section

Once the vertical stiffness constant and the relationship between the interface angle and curved beam deflection were identified, the side force supported for a given preload force could be determined. This allowed for the calculation of the torque that could be supported for a range of initial interface angles, for a given curved beam preload condition. The results of these calculations, and the final output of this version of the analytical model, is provided in Figure 3-5 in graphical form.

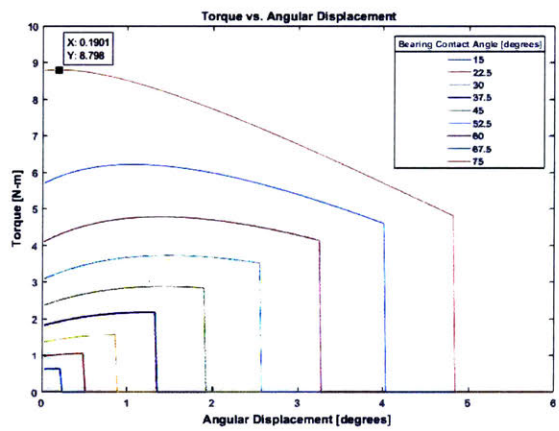

Figure 3-5: Torque vs. Angular Displacement as Determined by the First Prototype Analytical Model

Based on the results presented above, it was decided that an initial interface angle of 75 degrees would be incorporated into the design. This was because this angle resulted in a condition where a minimal angular displacement of 0.2 degrees was experienced prior to the release of the slip clutch. As with the analytical model presented in Section 2.4, there were acknowledged simplifications that yielded these excellent results. The intention at this stage was to produce a prototype from which to garner further insight into the design, rather than to develop a final and comprehensive product. The limitations of the model at this stage were:

- Interface Angle - The determination of the interface angle as a function of curved

beam deflection was solely based on the mechanics of the beam. The radius of the detent was not included as a variable in this determination.

- Stiffness Constant - The engagement force is a product of the displacement of the curved beam and the stiffness constant. There are both vertical and horizontal components of displacement, stiffness, and engagement force. For simplification, this stage of analysis only incorporated the vertical components.

- Hertzian Contact Stress - The cup detent and ball bearing experience line loading along their interface. Hertzian contact stress was not analyzed in relation to yield stress of the components.

3.1.2 CAD Model Refinement

Along with reducing the form factor of the proof of concept prototype, a main goal of this iteration was to "package" the curved beam assembly. This was done so that different constructions and arrangements for what would become the final product, could start to take shape. The initial concept for this packaging was done completed via the sketch presented in Figure 3-6 and then progressed to Solidworks.

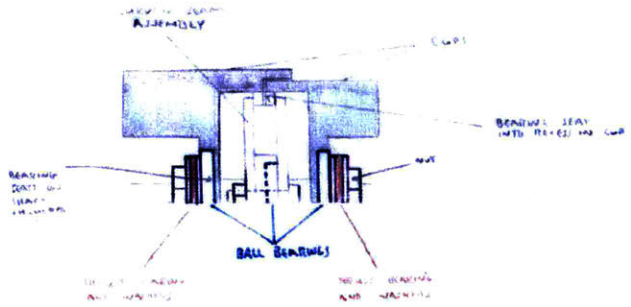

Figure 3-6: Sketch of First Prototype Initial Conceptualization

The main feature of the First Prototype was the arrangement of the major components. The design incorporated two opposing cups that interfaced such that the curved beam assembly fit between them and there was overlap between the cups. The two cups along and the curved beam assembly were located along a common shaft

with a series of ball and thrust bearings to maintain alignment and a small preload force, through the torquing of the nuts on either end. The purpose of the preload was to maintain the cups from separating during operation and to ensure the device was not reliant on the input and load shafts to maintain external preload. Also shown in Figure 3-7 are the shaft adapters at either end. The final connection between the slip clutch and the shafts was unknown at this point in the design, so an adapter that was flexible with respect to shaft configuration was desired, and what is presented below. The configuration shown accepts a D-profile shaft on both ends.

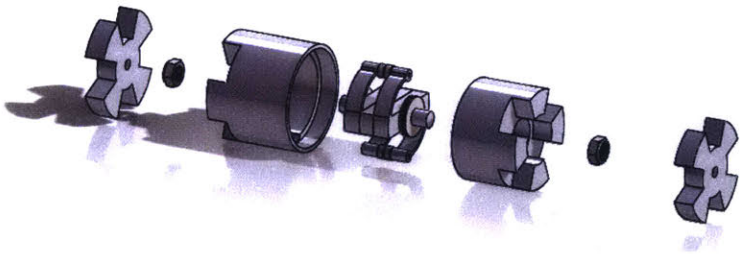

Figure 3-7: CAD model of First Prototype

3.1.3 Prototype Production

Since the purpose of this prototype was primarily to package the curved beam assembly, it was produced on the Stratasys uPrint SE Plus 3D printer available in the Precision Engineering Research Group (PERG) lab. Based on the size and concavity of the end cups, the decision was made to produce each of them in two pieces and then join them by glue following printing. Due to some preheating issues with the machine as well as tolerances that were too restrictive for the production method, the end cups could not overlap. This warping limited the usefulness of the printed prototype in accomplishing the main goal of the production, which was to verify fit-up. Pictures of the printed assembly are shown in Figure 3-8 detailing the distortion. Note the circumferential line, showing the interface of the two halves of the each end cup that were printed separately.

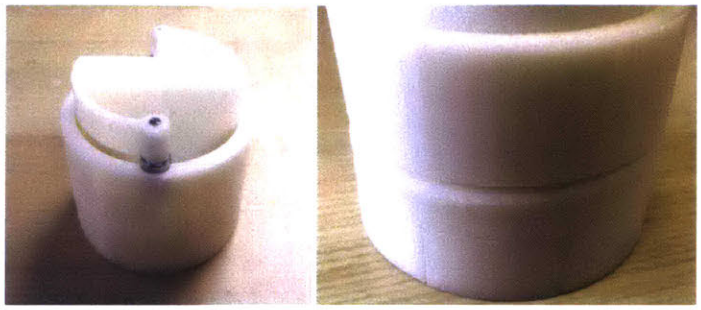

Figure 3-8: 3D Printed First Prototype - Partially Assembled

Despite the prototype failing in its main purpose, a great deal was learned through the process of building the component for the first time. The lessons learned were:

- Printer Capability - The end cups were printed in two halves because of a misjudgment of the 3D printer capability. The Stratasys uPrint SE Plus uses support material that allows the machine to print very complex shapes, and could have easily printed the end cups as single pieces. Additionally, the pre-heating issue that caused excessive warping of the end cups was a fault that, when cleared did not present itself again through the course this project.

- Tolerances - The tolerances used for this iteration, were in two cases, too tight for the level of prototype being produced. The holes for the dowel pins required that the pins be pressed into the curved beam assembly. Also, the gap between the end cups was not large enough to allow for them to overlap, in their normal means of interface.

3.2 Second Prototype Development

The first prototype offered several opportunities for improvement in the areas of the analytical and 3D models. Since it would carry through to both the models, a design decision with respect to the form factor was made. While the size of the first prototype was significantly reduced in comparison to that of the POC prototype, a further reduction was sought. The existing slip clutch for the tilt drive, the Zero-Max® Torque Tender Model TT2-C, was used for the basis of this change. This was

desirable, not only so that the prototype was more in line with commercially available slip clutches, but also because the 3D printing material and time resources would be reduced.

3.2.1 Analytical Model Refinement

As detailed previously the analytical model used through the development of the POC and first prototypes were limited in that many simplifications were used. The model was expanded in this iteration to address these limitations. The final analytical model presented in Appendix C was changed only slightly from the one used in this iteration. For this reason, the limitations present in the previous models will be addressed sequentially in the order they appear in the MATLAB script used. Along with the vertical, horizontal and angular displacements that were present for vertical loading conditions, this model also calculated the displacements for a range of horizontal loading conditions. This allowed for the calculation of stiffness constants in each direction for each loading direction. These calculations were completed using a regression analysis identical to that performed in 3.1.1. With these stiffness constants identified a calculation of the y-coordinate of the interface position could be identified and the incident angle calculated for the range of vertical displacement. With the incident angle calculated the side force and torque supported by the curved beam element could be determined. The angular displacement for the curved beam assembly was calculated using the x-coordinate of the interface position allowing for the plot of Torque versus Angular Displacement provided in 3-9. As noted, the torque following disengagement is modeled as zero, although some torque will be transmitted via friction on the surface of the ball bearing and end cup inner circumference.

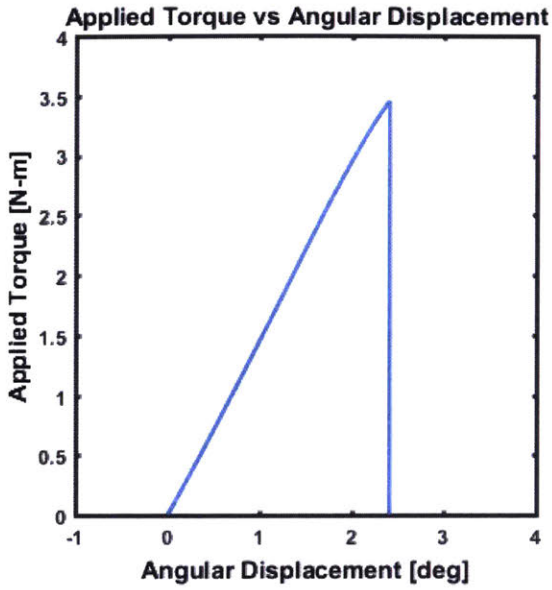

Figure 3-9: Second Prototype Analytical Model Output

3.2.2 3D Model Refinement

The major changes to the 3D model for the second prototype included a change to a smaller ball bearing to detent interface angle and the reduction in radial cross section. Both of these changes are shown most effectively in Figure 3-10

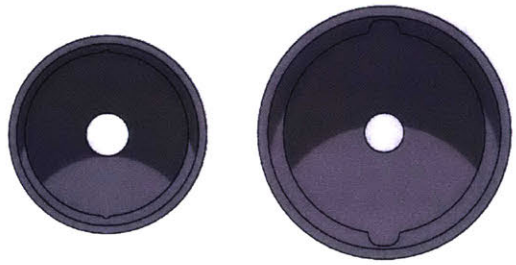

Figure 3-10: Left End Cup View of 1st (right) and 2nd (left) Prototypes

3.2.3 Prototype Production and Lessons Learned

The lessons learned from the production of the First Prototype with respect to 3D printer capability and tolerance were taken into account during this iteration. The end cups were printed as single pieces and were of excellent quality and mated to-

gether as expected in order to enclose the curved beam assembly. The major printed components of the Second Prototype are shown in Figure 3-11.

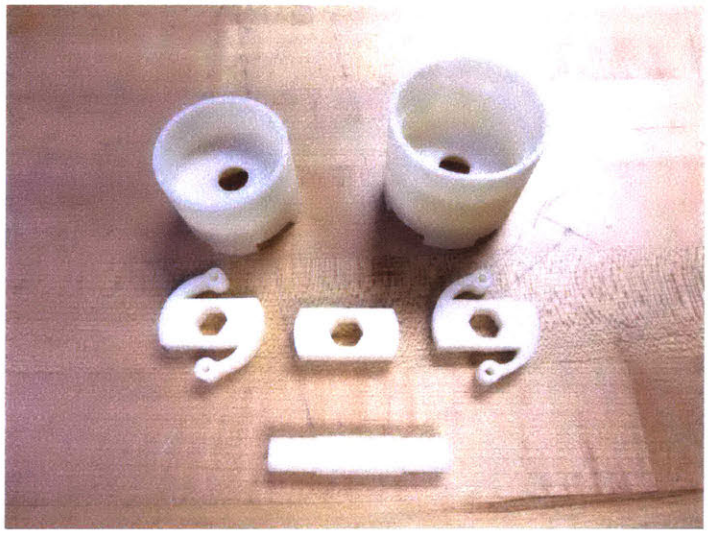

Figure 3-11: Second Prototype Major Components

Two lessons came out of the second prototype that were critical to the further development of the concept. Once the prototype was fully assembled, it became evident that it was not supporting torque as was expected. It was acknowledged that the torque supported by an ABS plastic printed part would not be the same as what would be supported by the analyzed material (Al 6061-T6), but the prototype was still deficient. It was recognized that the reason for the inability of the prototype to transmit torque was that one cup was interfacing the curved beam assembly prior to the other. This resulted in one cup carrying the majority of the preload, leaving the other without the ability to transmit the torque as expected. The second lesson that was taken from this prototype iteration was that the clutch assembly required radial support, as had been suggested by the POC prototype, during that component's testing. The resulting design changes to address these deficiencies were the incorporation of an angular contact bearing and two curved beam assemblies that could be preloaded separately. These design changes will be explained in further detail in the following section.

3.3 Third Prototype Development

The development of the third prototype required that several components be resized to accommodate the additional curved beam assembly and angular contact bearing. No changes were required to the analytical model and only minor changes were made to the 3D model.

3.3.1 Prototype Production and Lessons Learned

The goal of this iteration of prototype production was to ensure that the angular contact bearing could be accommodated along with the additional curved beam assembly. This was deemed of increasing importance because the next prototype produced was planned to be constructed of Aluminum vice printed from ABS plastic. The major components of this prototype are shown in Figure 3-12. Of note is the 1 millimeter spacer that was placed between the two curved beam assemblies to provide a standoff to allow for seperate preload. Also shown is a printed part that simulates the angular contact bearing in the lower right hand corner of the graphic.

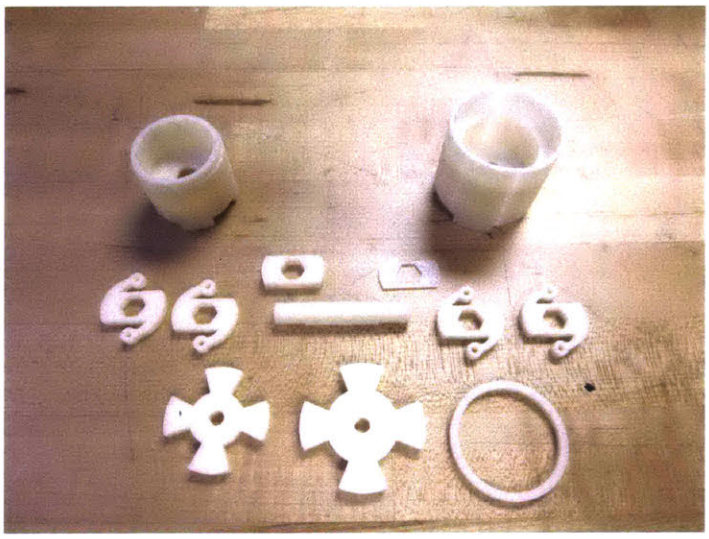

Figure 3-12: Third Prototype Major Components

One lesson learned arose out of this prototype that was again critical to the design evolution. It was recognized while assembling the component that the curved beam

assemblies could be preloaded in one cup, but preloading in the second cup presented difficulty. Without the ability to preload the second curved beam assembly, the slip clutch would not operate as intended. Required design changes to accommodate the ability to preload the component properly will be addressed in the following section.

3.4 Fourth Prototype Development

The goal of the fourth prototype was to progress the design to a point were the component could be produced in close to it's final form. In order to do this, there were design changes that required incorporation to support the preloading of both sides of the curved beam. A lead in feature was designed to provide a ramp which the ball bearing would be progressed through in order to become seated on the detent. A CAD rendering of this feature is provided in Figure 3-13 and shows the left end cup. The feature was included on both end cups to allow both sides to be properly assembled.

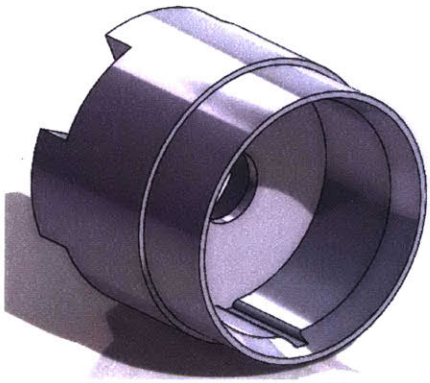

Figure 3-13: Right End Cup Lead In Feature

3.4.1 Prototype Production and Lessons Learned

The production of this prototype required a significant increase in time and financial resources to produce. All parts with were either procured commercially, or produced by the author. The majority of the processes used for this prototype are identical to those used for the High Fidelity Prototype and will be described in Chapter 4, and

not be covered here. The major lesson learned for this iteration was that the lead in feature was ineffective as accommodating the preload of the curved beam assemblies.

Figure 3-14: Right End Cup Lead In Feature - Damaged

Both of the end cups as well as the curved beam assemblies were damaged while trying to assemble the slip clutch. Figures 3-14 and 3-15 detail this damage.

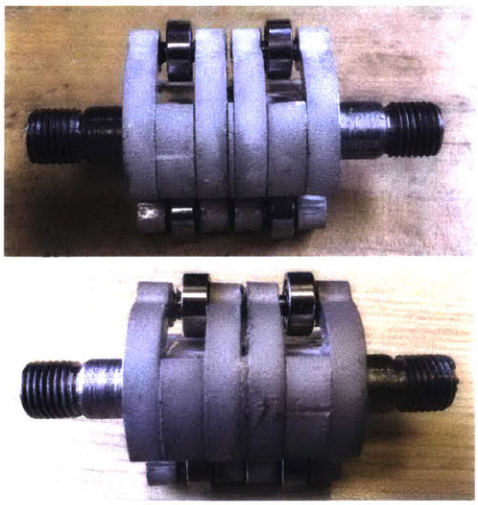

Figure 3-15: Original and Damaged Shaft Assemblies

3.5 Development of High Fidelity Prototype

The only changes to the prototype during this iteration was the redesign of the preload feature. As was seen in the fourth prototype, a lead in feature was ineffective and

resulted in damage that was costly from both and time and financial perspectives. It was decided that the simplest method of conducting this preload was to provide a slot in both end cups that allowed the curved beam assemblies to be inserted in the unloaded and rotated to a preload condition.

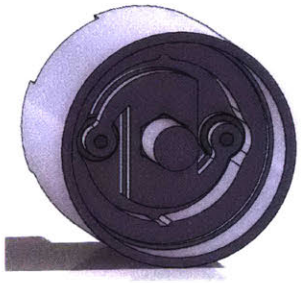

Figure 3-16: High Fidelity Prototype Preload Feature

A rendering from the 3D model reflecting this design feature is provided in Figure 3-16. Based on the High Fidelity Prototype (HFP) being the final prototype product of the present work, considerations for manufacturing and assembly are included in Chapter 4.

Chapter 4

Manufacturing and Testing

A primary goal throughout this design process was the realization of a slip clutch that could be produced without the use of extensive manufacturing resources. These considerations were taken into account as early as the concept selection phase where candidate solutions such as the spiral magnet slip clutch were abandoned, in part due to manufacturing complexity.

4.1 Manufacturing Processes

The manufacturing and final assembly of the curved beam slip clutch did not require extensive resources. The steps described below could be conducted in parallel, but will be described in the order that was followed during construction of the HFP. It is not expected that processes used for a production ready unit would differ significantly from those detailed below with the exception of scale.

4.1.1 Bearing Assembly Production

As reflected throughout the design effort, subcomponents to the slip clutch assembly were selected such that they could be easily procured commercially. This resulted in the selection of dowel pins and ball bearings that would form the bearing assembly. The bearing width was selected to maximize cup seating area and therefore reduce

Hertizian contact stress. The inner radius of the ball bearing dictated the dowel pin size. Dowel pin length was resultant from curved beam thickness and a required standoff. In order to produce a bearing assembly, the length of the dowel pin on either side of the ball bearing was calculated. A piece of aluminum was then counterbored to receive the ball bearing and drilled to a depth equal to the length of dowel pin calculated above. An arbor press was then used to produce the press fit between the dowel pin and the ball bearing. This allowed for the quick and repeatable production of the multiple bearing assemblies used in each prototype.

4.1.2 Curved Beam Assembly Production

The curved beam assembly required a modest amount of preparation in order to be ready for production. This preparation however, was independent of the amount of units produced. The primary tool used for the production of this component was the waterjet. Several waterjets were used throughout the prototype production effort, but it was found that the OMAX MicroMax, found in the MIT Hobby Shop produced the most high quality unit. In order to produce the g-code required for the waterjet to cut the part, two programs were used. The first, OMAX Layout, allowed for the import of a .dxf file, produced in Solidworks, and the definition of cutting path and quality. The critical dimensions of the curved beam that required attention during this phase were the hex shaft and dowel pin. For these dimensions, the highest cut quality of five was used. For all other cuts a quality of three, corresponding to general machining was used. Despite the use of the highest cut quality for the critical dimensions, it was necessary to account for the kerf of the cut which is associated with the waterjet nozzle performance. The kerf of the cut is defined using the offset function in the OMAX program and can be changed by the used. While the value of this setting is know in general, high tolerances required a more accurate determination of this value. This is done by performing and measuring test cuts and then adjusting the offset value to yield the desired dimension. This was done using the test plate shown in Figure 4-1

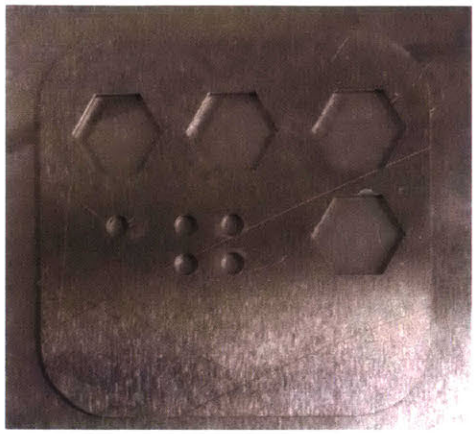

Figure 4-1: Test Plate For Establishment of Waterjet Offset

The file produced from OMAX Layout was then transferred to OMAX Make where material type and thickness was selected and the user sets the nozzle position to a the defined cut path start. After the nozzle height is set to zero such that an offset to the stock is maintained, the material is cut. A picture of the waterjet process being executed is provided in Figure 4-2.

Figure 4-2: Waterjetting of Curved Beam Elements

Another consideration regarding the waterjetting process was taken into account during the production of the curved beam element. As the cutting jet of water and grit traverses through the thickness of the stock, it is deflected, resulting in an angle across the thickness of the part produced. This angle is lower at higher cut qualities, but still present. Since the hex shaft and dowel pins were cut at the highest quality and would be potted with their respective components, they were not the sections of

the curved beam element that were of the most concern. The inner and outer radii of the curved beam itself were the areas where non-uniformity could yield the most effect on eventual performance with respect to that predicted. For this reason, the curved beam elements were cut in a manner that the cuts were reflected across a vertical axis. The resulting combination of these two elements produces a unit that is symmetric with respect to the bearing assemblies. A comparison between the asymmetry of the Fourth Prototype and the symmetry of the High Fidelity Prototype is provided in Figure 4-3.

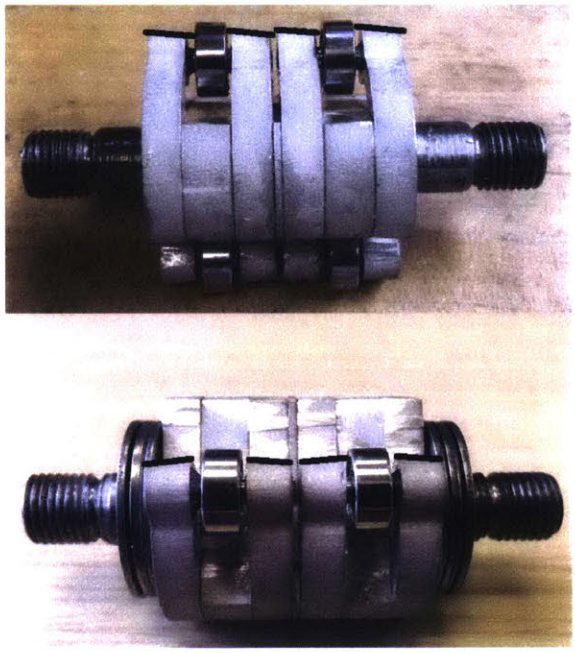

Figure 4-3: Curved Beam Assembly Symmetry Comparison 4th Prototype (Top) HFP (Bottom)

Along with the curved beam elements, the 1 millimeter and 6 millimeter spacers were cut on the waterject. The same .dxf file was used for their production, were the only difference was the changing of stock material on the cutting bed and the material thickness setting in OMAX Make. The tolerance on the hex shaft for the spacers was not as critical as those on the curved beam elements, because torque transmission is not required by these components. For this reason, the hex spaces were sized such that the shaft could pass through easily during the shaft potting process described in

Section 4.1.3.

After the curved beam elements and spacers were cut on the waterjet they were removed from the stock and the remainders of the tabs filed down to produce a smooth surface. This allowed for the potting of the bearing assemblies in the curved beam elements. The waterjet was used to produce sliding fits of these components, so a significant amount of potting material was not required. The process was started by placing potting material on the down pin end and placing this end in the curved beam element as shown in Figure 4-4. The 6 millimeter spacer was then placed on face of the first curved beam element and the second curved beam element placed on top while seating the exposed ends of the bearing assemblies. Following the curing of the potting material, the curved beam elements were ready to be combined with the shaft to produce the finalized shaft assembly.

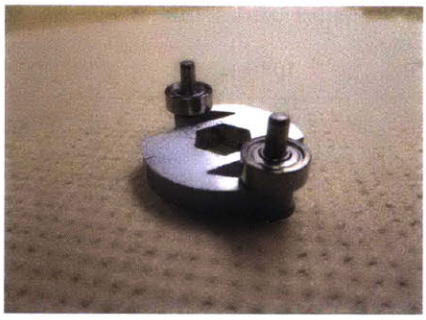

Figure 4-4: Dowel Pin Potting Into Curved Beam

4.1.3 Shaft Assembly Production

The shaft assembly is the combination of multiple commercially available and custom produced subcomponents. The shaft assembly is comprised of the 10 millimeter hex shaft, 4 needle thrust bearings, 2 self locking hex nuts, a one millimeter spacer, and two curved beam assemblies. The shaft was produced by cutting to approximate length a piece of hex stock. High tolerance hex shafting stock was not available in the size and length required, so basic hex stock was used. It is evaluated that the use of higher tolerance stock would not have realized performance benefits that could justify the added cost material cost. After the rough cut of the shaft was conducted,

it was faced and turned to length on the lathe. The hex shaft was then turned to produce seating surfaces for the thrust bearings and areas for external threading. A die was then used in the lathe tail stock to produce the threading to accept the self locking hex nuts, upon final assembly of the slip clutch unit. A picture of the hex shaft following production is provided in Figure 4-5

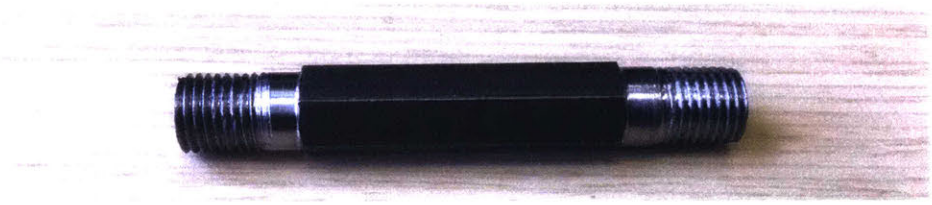

Figure 4-5: Fabricated Hex Shaft

Following production of the hex shaft, all shaft assembly subcomponents were ready for combination into a single unit. The first step in this was the potting of the curved beam assemblies and the 1 millimeter spacer onto the hex shaft. The potting material and then the small spacer and curved beam assemblies were fit over the shaft. The relative orientation of the curved beam assemblies was not of concern because they would self align with their respective cup ends. A earlier 3D printed prototype, along with sacrificial washers and nuts were used to provide clamping force during this process. Once the cure time of the potting material elapsed, the remaining components were fitted on the shaft producing the finalized hex shaft assembly as pictured in Figure 4-6.

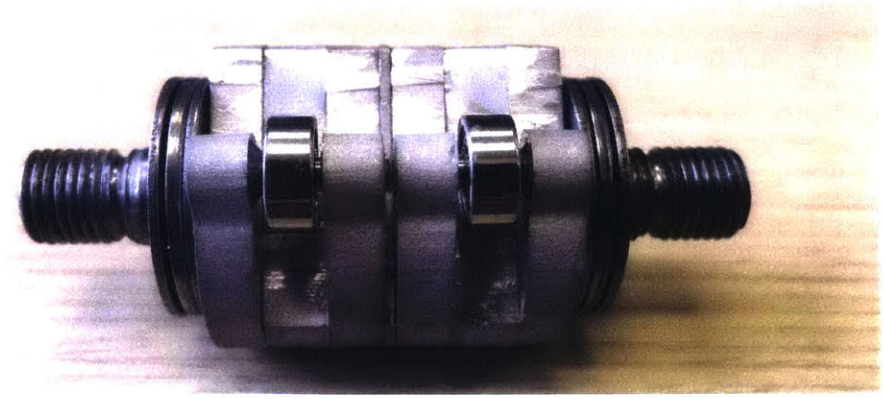

Figure 4-6: Fabricated Shaft Assembly

4.1.4 End Cup Production

There were several considerations taken into account with respect to the selection of the machining of the end cups. These considerations were primarily in the area of geometric features. The detents and to a lesser extent the preload features required a level of detail that would be difficult to obtain using a manual machining process. The shaft end of the cups that accommodated the shaft adapters also are fairly complex in shape. Taken together, if a manual machining process were used, the part could have to be turned down on the lathe and then machined on the mill. For these reasons, the complexity of the operations and tolerances involved supported the use of a CNC milling operation. The left and right end cups were produced in this fashion by an external entity. Figure 4-7 provides a picture of these completed cups. Some damage was incurred due to an error in the assembly process that was not a result of the design.

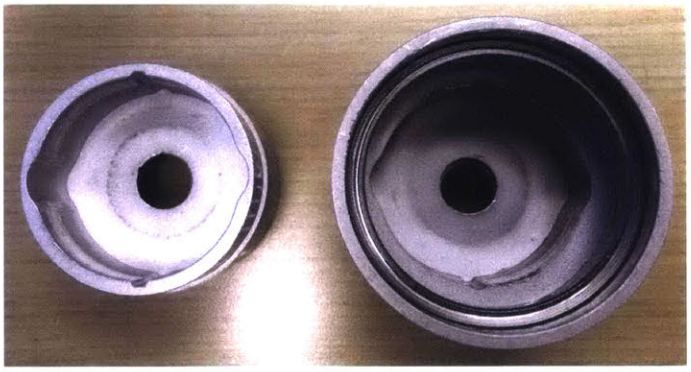

Figure 4-7: High Fidelity Prototype End Cups

4.1.5 Final Assembly

Following the completion of the sub assemblies described above, the final assembly of the high fidelity prototype couple be completed. The production of the shaft adapters were not discussed at length, but they were made to accommodate a 10mm hex shaft to allow for easy connection to the testing machine. The testing configuration of the slip clutch is shown in Figure 4-8. The end cups are shown with partial transpancy to display the location of the curved beam assemblies. Missing from the graphic are

lock nuts that fit on the threaded shaft and an angular contact bearing that produce axial force to keep the end cups together and maintain alignment of the curved beam assemblies.

Figure 4-8: High Fidelity Prototype Testing Configuration - Transparent View

4.2 Testing

Testing for the component was conducted on an Instron Model MT-10 at Wentworth Institute of Technology. The testing method used, held one cup in a fixed position and rotated the other cup at 0.5 degrees per second while taking torque measurements. Three runs of this testing method were performed with consistent results as displayed in Figure 4-9.

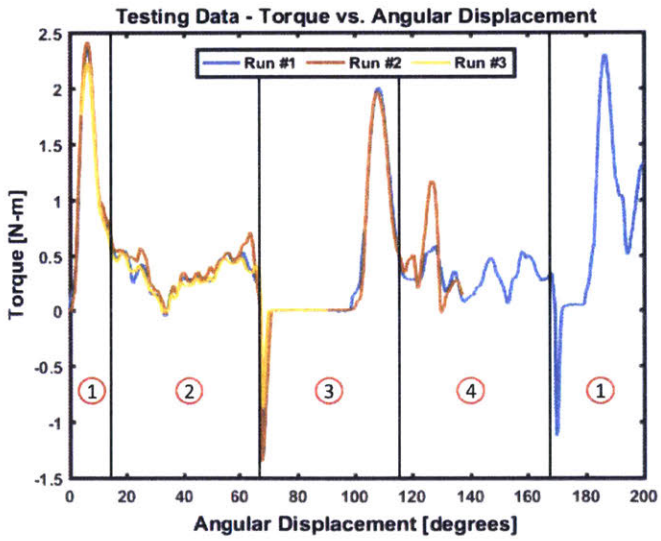

Figure 4-9: Testing Results With Regions Annotated

For the purpose of understanding these results, different regions of the testing

results are annotated with the position of the curved beam assembly with respect to the detent. Figure 4-10 provides a rendering of these positions and analysis is provided below. These positions are shown only for 0-180 degrees, but are identical for 180-360 degrees.

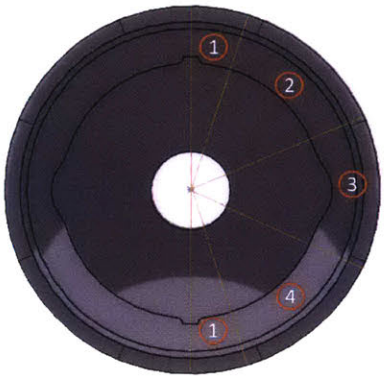

Figure 4-10: End Cup Torque Response Regions

- Region 1 (345-15) - This region covers the interaction of the ball bearing with the detent. At approximately 345 degrees the ball bearing seats into the detent and torque decreases sharply. At 0 degrees, the ball bearing begins to transmit torque and experience angular displacement until the detent is cleared at 015.

- Region 2 (15-65) - In this region the torque is not consistent, but is significantly lower than the maximum torque seen in Region 1. Inconsistencies in the inner radius of the cup resulted in the ball bearing transmitting more torque than would be expected. These inconsistencies are a result of excessive Hertzian contact stress, resulting in "ridges" which yielded the torque measurement oscillations.

- Region 3 (65-115) - This region spans the interaction of the ball bearing with the preload feature. At 65 degrees the ball bearing traverses down the slope of the feature resulting in a negative torque. On the upslope of the preload feature, at approximately 100 degrees, the torque increases until the ball bearing clears the feature at approximately 115.

- Region 4 (115-165) - In this region the ball bearing again is seated on the inner radius of the cup. The discussion presented for Region 2 applies to this case.

- Region 1 (165-195) -The device then repeats the process for another half revolution.

4.2.1 Comparison to Analytical Results

Figure 4-11 provides a comparison of the analytical model to the testing results. It was found that the maximum torque transmitted during testing was 2.4 N-m at an angular displacement of 6.3 degrees in comparison to 3.5 N-m at 4.8 degrees predicted by the model.

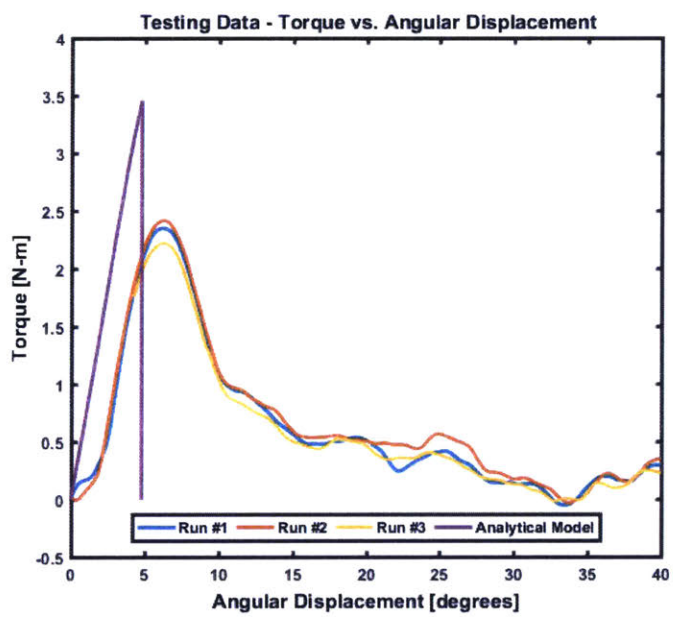

Figure 4-11: Testing vs. Analytical Model Results

It is hypothesized that this difference is a result of permanent deformation that was experienced by the curved beam elements. This condition was not discovered until after the testing was completed and the shaft assembly was removed from the end cups. Once this was done, it was found that the curved beam assembly that was used to disengage the clutch, was permanently deformed.

Figure 4-12: Deformation of High Fidelity Prototype Curved Beams

This deformation was apparent in comparison to the adjacent curved beam assembly. This condition also resulted in the inability to preload one side of the clutch. Figure 4-12 provides a picture of the deformed curved beam assembly and a 3D printed beam for comparison and visual proof of deformation.

In the condition as tested, the curved beam assembly is contained within the end cups and not visible for inspection. For this reason, the loading cycle that produced the deformation is not known absolutely. It is expected that that the deformation occurred while the component was being cycled by hand, prior to the use of the Instron testing machine. The permanent deformation that was experienced, resulted in the reduction in engagement for of the curved beam assembly, and a resultant torque capacity that was lower than expected.

4.3 Post Testing Design Iteration

The goal of this iteration was to address the shortcomings of the design, made apparent through testing, such that a prototype could be produced as a part of future work. The first of the shortcomings to be addressed was the amount of torque that was transmitted and its comparison to the tilt drive specifications. As documented previously, Aluminum Alloy 6061-T6 was used to produce the curved beam elements. Based on effect that the elastic modulus of steel has on the displacement equations presented in Section 3.1.1, a change of material for the curved beam assembly would allow for an increase in torque transmission. A change to the analytical model for AISI 4140H Steel and a reduction of initial interface angle to 16° produces a Torque

versus Angular Displacement curve that has a higher maximum torque value (8.5 N-m) but still has excessive angular displacement (4.2°). Although it is expected

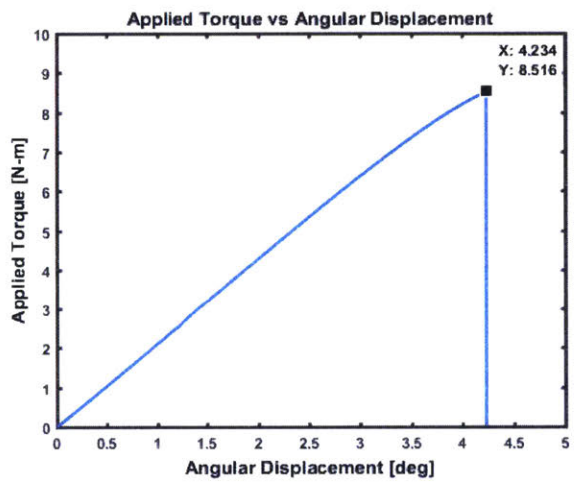

Figure 4-13: Torque vs. Angular Displacement for Steel Curved Beams with Interface Angle=16°

that the increased yield stress of steel would prevent the permanent deformation experienced by the HFP, the angular displacement is excessive and does not satisfy the functional requirement. This analysis along with the testing results, indicate that the curved beam arrangement is not adequate for the tilt drive application so Finite Element Analysis of the AISI 4140H curved beam was not conducted.

The second shortcoming of the HFP that was made apparent during the lead up to component testing was the inability to properly preload the device. The HFP only allowed for one cup to be properly preloaded because of the permanent deformation that occurred to one curved beam assembly and not the other. This inability to preload the component was compounded by the design of the end cup detents. The end cups were designed such that they were symmetric as displayed in Figure 4-14.

Figure 4-14: High Fidelity Prototype

While a symmetric detent should allow for the preloading of both sides of the slip clutch, it requires perfect alignment of the shaft assembly and identical preloading of the two curved beam assemblies. An asymmetric detent could be used to allow for some slight variation in the alignment and preload and enable the curved beam assemblies to seat on the detents of both end cups. While this would be a solution that would allow for the proper preloading of the component, the excessive angular displacement of this curved beam arrangement is limiting for the application.

The second and preferred method of overcoming the inability to preload both curved beam assemblies, is by shifting to an arch like curved beam configuration, conceptualized during the proof of concept phase and presented in Figure 4-15.

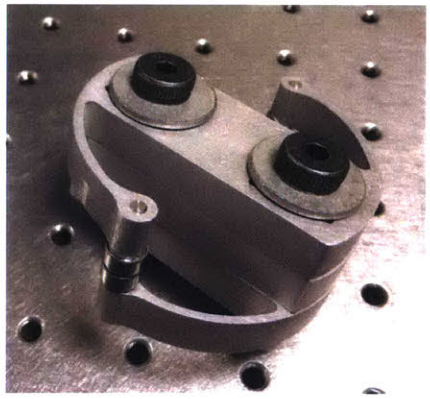

Figure 4-15: Post Testing Iteration Conceptual Configuration

This would allow for the elimination of the two end cup system because the arch

provides a bi-directional torque overload setpoint. One curved beam assembly could be used and have a direct coupling to the input shaft. This assembly would interface with a detent on the end cup coupled to the output shaft. The arch assembly would be provided with a housing such that it could be coupled to the shaft and so that proper component alignment could be maintained. An exploded isometric view of this arrangement is shown in Figure 4-16

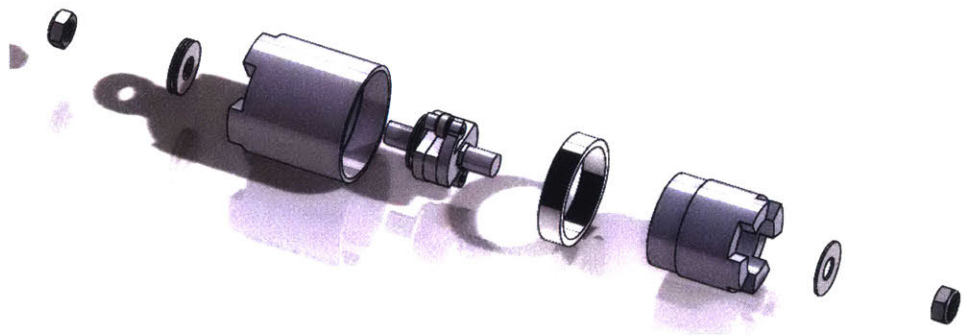

Figure 4-16: Post Testing Iteration Component Arrangement

This configuration operates on the same physical principles as the original curved beam arrangement, although the previously developed analytical model does not apply in its entirety. A static design study was conducted in Solidworks to conduct finite element analysis of the arch in order to assess the displacement and stress states in different loading conditions that the overload device would experience. Based on the deformation experienced by the original curved beam arrangement during the HFP testing, the first state analyzed was the beam arrangement following clutch disengagement. At this point in the devices rotation, the arch experiences the maximum displacement. This displacement is calculated using equation 4.1 dependent on the radii of the ball bearing (r_b) and detent (r_d), and the initial interface angle ($\alpha_{initial}$).

$$Displacement_{max} = (r_b + r_d) - (r_b + r_d) * \sin(90 - \alpha_{initial}) \tag{4.1}$$

A configuration with a ball bearing radius of 4mm, detent radius of 1mm and interface angle of 20 degrees yields a maximum displacement of 0.3mm in accordance with this equation. Static design studies were conducted for the arch configuration

for both 6061-T6 Aluminum and AISI 304 Steel, with the stress states presented in Figure

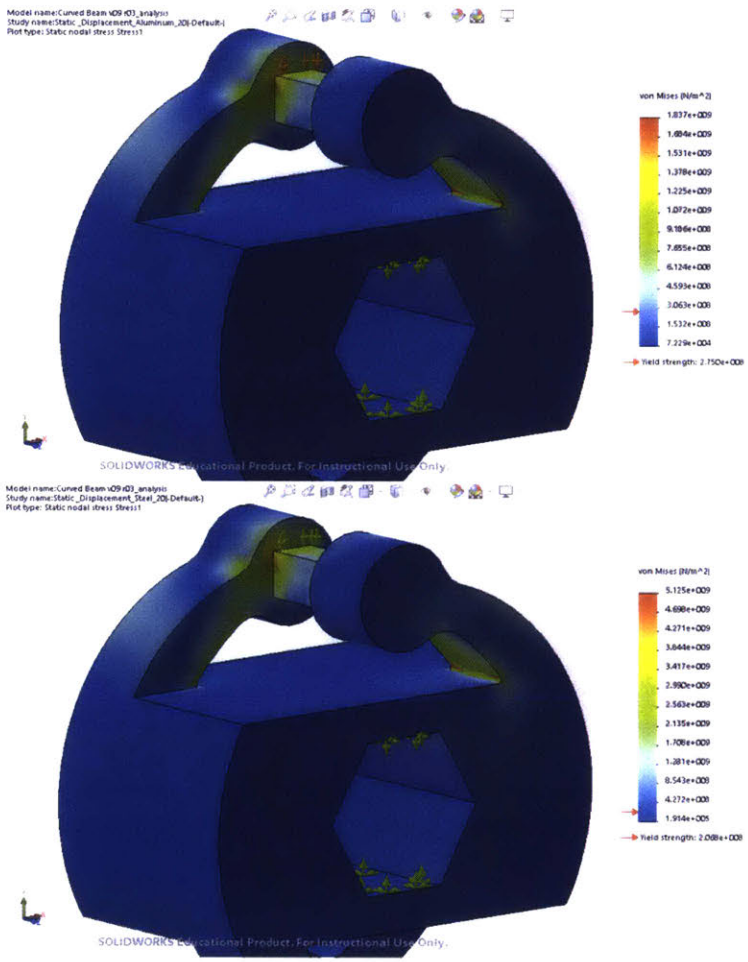

Figure 4-17: Arch Stress State for Aluminum (Top) and Steel (Bottom) Configurations

It is shown that, both the aluminum and steel variations of this configuration result in a stress state that exceeds the yield stress of the material for a displacement of 0.3mm. The maximum stress is found at the root of the curved beam that provides a fixed boundary condition and a stress concentration point. In order to avoid this limiting condition, a variation on the arch concept was explored to avoid the fixed boundary condition. In its simplest form, this evolution of the concept can be visualized as a pair of concentric rings with the inner having a protrusion seated on an outer ring detent, similar to that presented in Figure 4-18.

Figure 4-18: Rudimentary Presentation of Concentric Rings Concept

The inner ring would be connected to either the motor or load shafts through a dowel or shoulder bolt through a slot. This slot would allow for an increase in the "horizontal diameter" as the top and bottom of the component were compressed. This results in the ring being supported in what can be approximated as a rolling support.

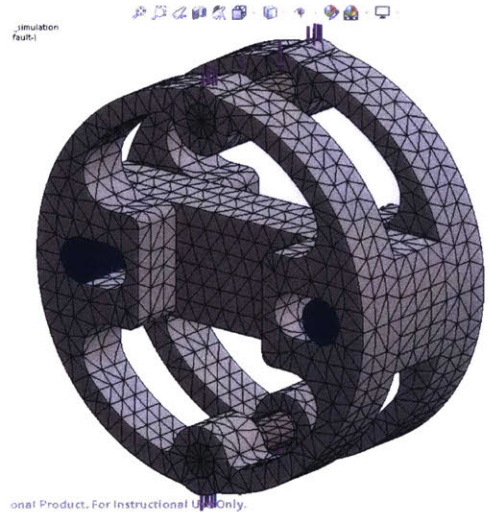

Figure 4-19: Rolling Support Approximated by Dowel Pin Location

Using equation 2.7 for a configuration that employs a ball bearing of 17.5mm outer diameter, a 1mm detent radius and an initial interface angle of 30 degrees yields a required preload force of 594 Newtons. This is a large engagement force that is driven by the low interface angle, but must be balanced with the static radial load of the ball bearing (C_0=756 Newtons). Lower interface angles require less displacement to clear the detent in an overload condition, but require a higher engagement force for a given torque. These factors have to be carefully optimized to prevent yielding the material or bearing damage. The stress state for both an aluminum and steel configuration is shown in Figure 4-20. It is seen that the highest stresses are at the root of the arch and the fillet closest to the dowel pin holes and are in excess of the yield stress. Despite this stress state, the revised arch configuration should be explored further to determine the optimal component geometry. It is expected that the optimal solution can be achieved without exceeding yield stress.

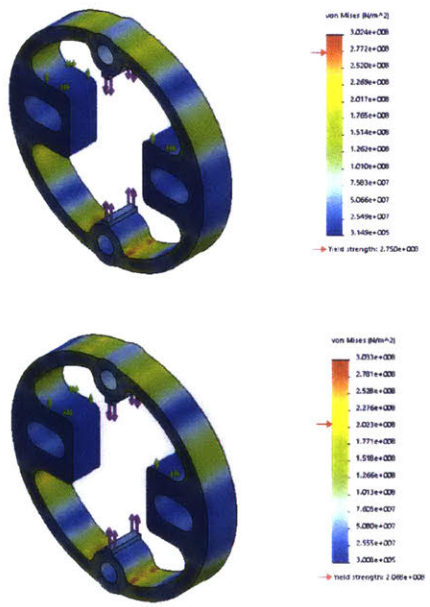

Figure 4-20: Revised Arch Stress State for Aluminum (Top) and Steel (Bottom) Configurations

A torque limiting clutch that used the revised arch configuration would take shape as presented in Figures 4-21 and 4-22. One shaft would be directly coupled to the arch assembly (green) through an interface piece (red). This interface piece would

accept shoulder bolts that would pass through the arch and spacer slots. Supported by the angular contact bearing (blue), the arch assembly would then transmit torque via the ball bearing to detent interface on the receiving cup (gray). The cup would be directly coupled and transmit torque to the receiving shaft.

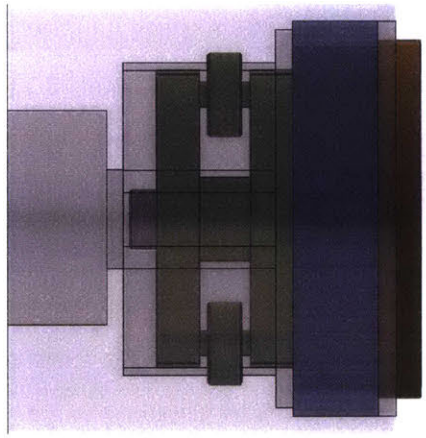

Figure 4-21: Revised Configuration of Arch Beam Torque Limiting Clutch - Side View

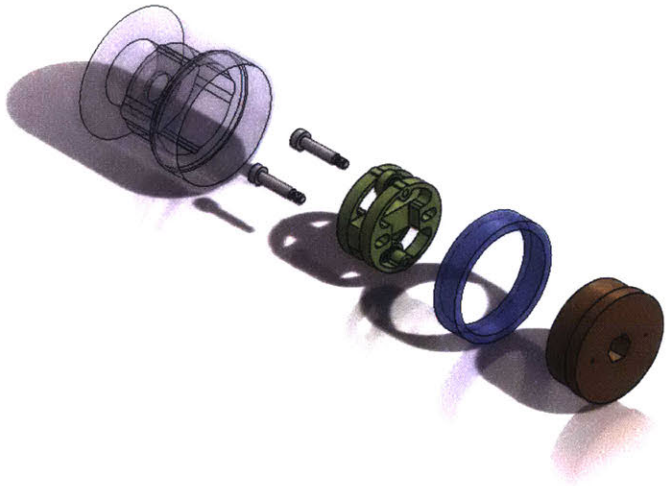

Figure 4-22: Revised Configuration of Arch Beam Torque Limiting Clutch - Exploded View

Chapter 5

Conclusion

Through the course of the design process documented in the preceding chapters, the development of the torque limiting clutch progressed significantly. The use of a curved beam as the actuating component of a torque overload device offers opportunity for systems with precise positioning requirements. Although the last prototyped iteration of the design produced results that did not meet the positioning requirements of the intended system, the curved beam based slip clutch concept is worthy of further investigation and development, specifically in the revised arch configuration. Development of the concept will be required to optimize system performance and analyze any system non-linearities. It is expected that such development would provide the a system that could be scaled and optimized for production.

5.1 Future Work

Based on the revised arch configuration being the next evolutionary step in the torque limiter development and as supported by preliminary results, it is the configuration that is recommended for further development to satisfy the functional requirements of the tilt drive. It is expected that detailed design analysis of the arch configuration would result in a component that would meet the required torque specification while minimizing position error.

Although the stresses presented in Section 4.3 are close to or in excess of the

yield stresses of the materials, the configuration is still a promising conceptual design solution. In order to assess the viability of this configuration the following areas require further analysis.

- Development of Analytical Model for the Revised Arch configuration to account for a 360 degree range of motion.
- Optimization of the driving variables (detent radius, roller bearing radius and curved beam dimensions) to balance the stress state in the arch and the displacement required to disengage the clutch.
- Detailed Prototype testing to confirm concept viability.

Appendix A

Candidate Solution Supporting Documentation

This appendix presents notebook pages that provide supporting documentation for the analysis of candidate solutions in the Strategy and Concept Development phase of the design. This documentation was used as a basis for establishing feasibility and dominance of those solutions that satisfied the functional requirements.

TITLE STRATEGY AND CONCEPT **PROJECT**

Continued from page 1-63

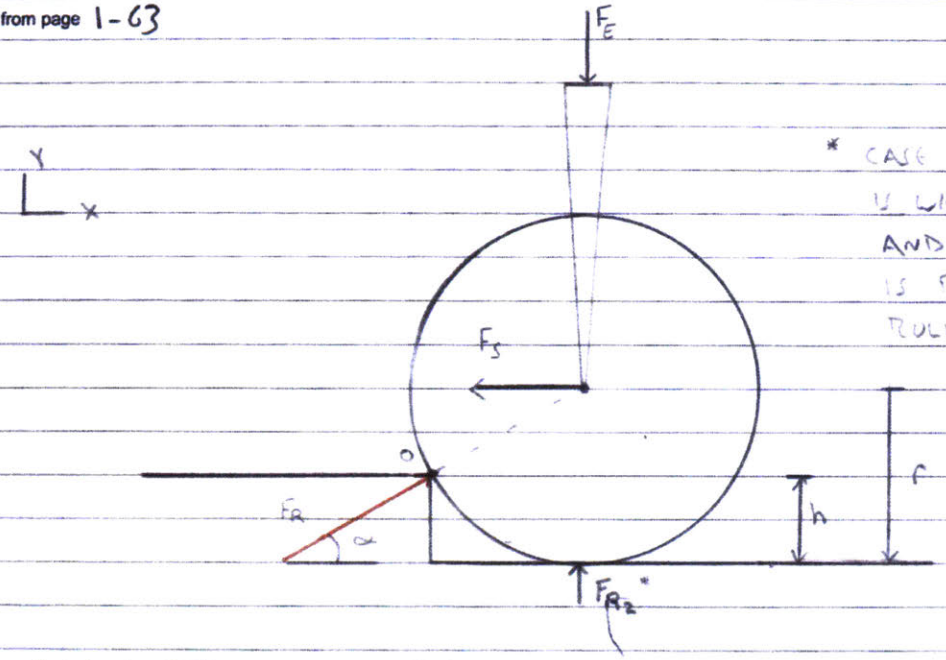

* CASE BEING DESCRIBED IS WHERE $F_{R_Y} = F_E$ AND $F_{R_Z} = 0$. THIS IS PRIOR TO THE ROLLER BEARING PASSING OVER THE STEP

ASSUMPTIONS : FLEXURE IS INFINITELY STIFF IN THE X-DIRECTION
FLEXURE HAS FINITE STIFFNESS IN THE Y-DIRECTION

KNOWNS : SIDE FORCE (F_S) FOR A GIVEN SLIP CLUTCH TORQUE CAPACITY AND LOCATION OF POINT O
HEIGHT OF STEP (h) AND ROLLER BEARING RADIUS (r)

UNKNOWNS : FORCE EXERTED BY FLEXURE IN THE Y-DIRECTION TO PREVENT MOVEMENT OF THE ROLLER BEARING (F_E)

$$\Sigma F_x = 0 = -F_S + F_{R_x} = -F_S + F_R \cos\alpha$$

$$F_R = \frac{F_S}{\cos\alpha}$$

$$\Sigma F_y = 0 = -F_E + F_{R_y} = -F_E + F_R \sin\alpha$$

$$F_E = \left(\frac{F_S}{\cos\alpha}\right)\sin\alpha = F_S \tan\alpha$$

$$F_E = F_S \tan\alpha \qquad (1)$$

Continued to page 1-65

SIGNATURE DATE 06OCT2016

DISCLOSED TO AND UNDERSTOOD BY DATE

TITLE STRATEGY AND CONCEPT PROJECT

Continued from page 1-64

α CAN BE DEFINED WITH RESPECT TO THE HEIGHT OF THE STEP (H) AND THE RADIUS OF THE ROLLER BEARING (R)

$$\alpha = \frac{h}{r}(90°)$$

SUBSTITUTING INTO EQUATION ①

$$F_E = F_S \tan\left[\frac{h}{r}(90°)\right] \quad ②$$

F_S CAN BE QUANTIFIED BY ASSUMING A DISTANCE OF POINT "O" FROM THE CLUTCH CENTERLINE (R) A DESIRED TORQUE CAPACITY (T_{CAP}) AND THE NUMBER OF ROLLER BEARING / FLEXURE "ARMS" (N)

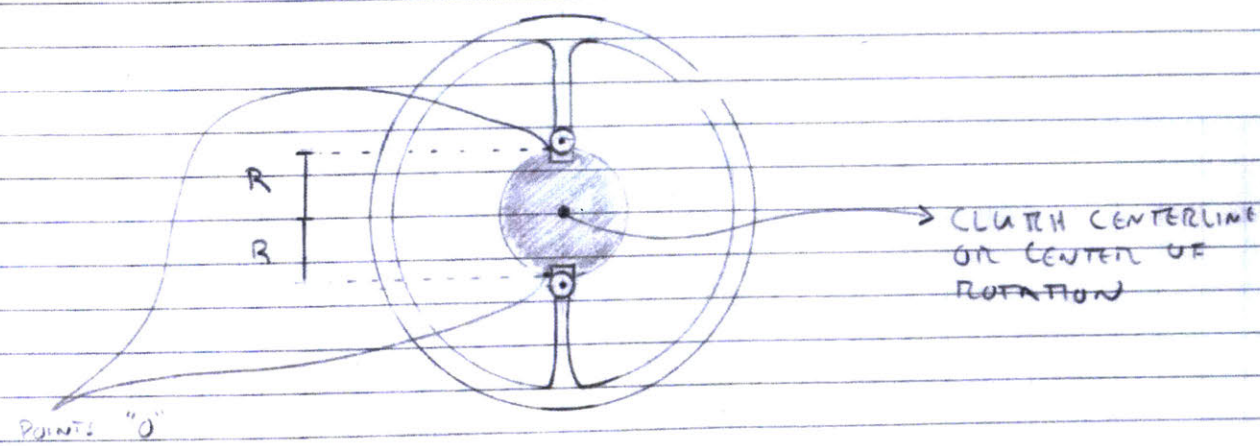

TORQUE CAPACITY $\equiv T_{CAP} = N \cdot F_S \cdot R$

$$F_S = \frac{T_{CAP}}{NR} \quad ③$$

Continued to page 1-66

SIGNATURE

DATE 06 OCT 2016

DISCLOSED TO AND UNDERSTOOD BY

DATE

PROPRIETARY INFORMATION

TITLE STRATEGY AND CONCEPT PROJECT

Continued from page 1-65

COMBINING EQUATIONS ② AND ③

$$F_E = \left(\frac{T_{CAP}}{NR}\right) \tan\left[\frac{h}{r}(90°)\right]$$

NOW, FOR A COUPLE OF ASSUMPTIONS TO CHECK FEASIBILITY

T_{CAP} = 85 in-lbs FOR TILT DRIVE

N = 3 BASED ON TUESDAY (10/4/16) MEETING AS MINIMUM NUMBER OF ROLLER BEARING/FLEXURE "ARMS" FOR STABILITY

R = 0.5 IN TO TRY TO MAINTAIN OVERALL CLUTCH DIAMETER < 2.5 IN

r = 0.138 IN THE SMALLEST DEEP GROOVE BALL BEARING I COULD FIND WAS TIMKEN 618/3 WITH AN OUTER DIAMETER OF 7mm = 0.276 IN

$\frac{h}{r}$ = 0.5 AS AN INITIAL ASSUMPTION FOR ITERATION

h = 0.069 IN

10 = RATIO OF FLEXURE SIZE TO TRAVEL OF ROLLER BEARINGS IN THE Y-DIRECTION

Continued to page 1-67

SIGNATURE DATE 06 OCT 2016

DISCLOSED TO AND UNDERSTOOD BY DATE

PROPRIETARY INFORMATION

TITLE STRATEGY AND CONCEPT PROJECT

Continued from page

SUBSTITUTING ASSUMPTIONS INTO EQUATION ④

$$F_E = \left(\frac{85\ in \cdot lb_f}{3 \cdot 0.5\ in}\right) \tan\left[0.5\,(90^\circ)\right]$$

$$F_E = 56.7\ lb_f$$

THIS SEEMS LIKE A REASONABLE VALUE TO ME WITH LIMITED KNOWLEDGE OF CIRCULAR FLEXURES.

NOW, LET'S CHECK SIZE

OVERALL CLUTCH DIAMETER (D_c)

$$D_c \approx 2 \cdot R + 2h \left(\frac{\text{FLEXURE SIZE}}{\text{VERTICAL DISPLACEMENT}}\right)$$

$$D_c \approx 2(0.5) + 2(0.069\ in)\ 10$$

$$D_c \approx 2.38\ in$$

THIS DIAMETER IS IN THE GENERAL RANGE BEING PURSUED (2.0 - 2.5 in)

Continued to page —

SIGNATURE

DATE 06 OCT 2016

DISCLOSED TO AND UNDERSTOOD BY

DATE

PROPRIETARY INFORMATION

TITLE STRATEGY AND CONCEPT **PROJECT** SPIRAL MAGNET SLIP CLUTCH

Continued from page 1-55

① MAGNETIC FORCE PROVIDED BY MAGNETS OF VARYING SIZES → COMMERCIALLY AVAILABLE

SAVED AS :

② THE SIZE OF MAGNET THAT CAN BE ACCOMODATED BY END AND CENTER PIECES OF A GIVEN DIAMETER

LENGTH :

PARAMETERS TO VARY: DIAMETER, OUTER DIAMETER STANDOFF, MAGNETIC FLUX STANDOFF, PITCH

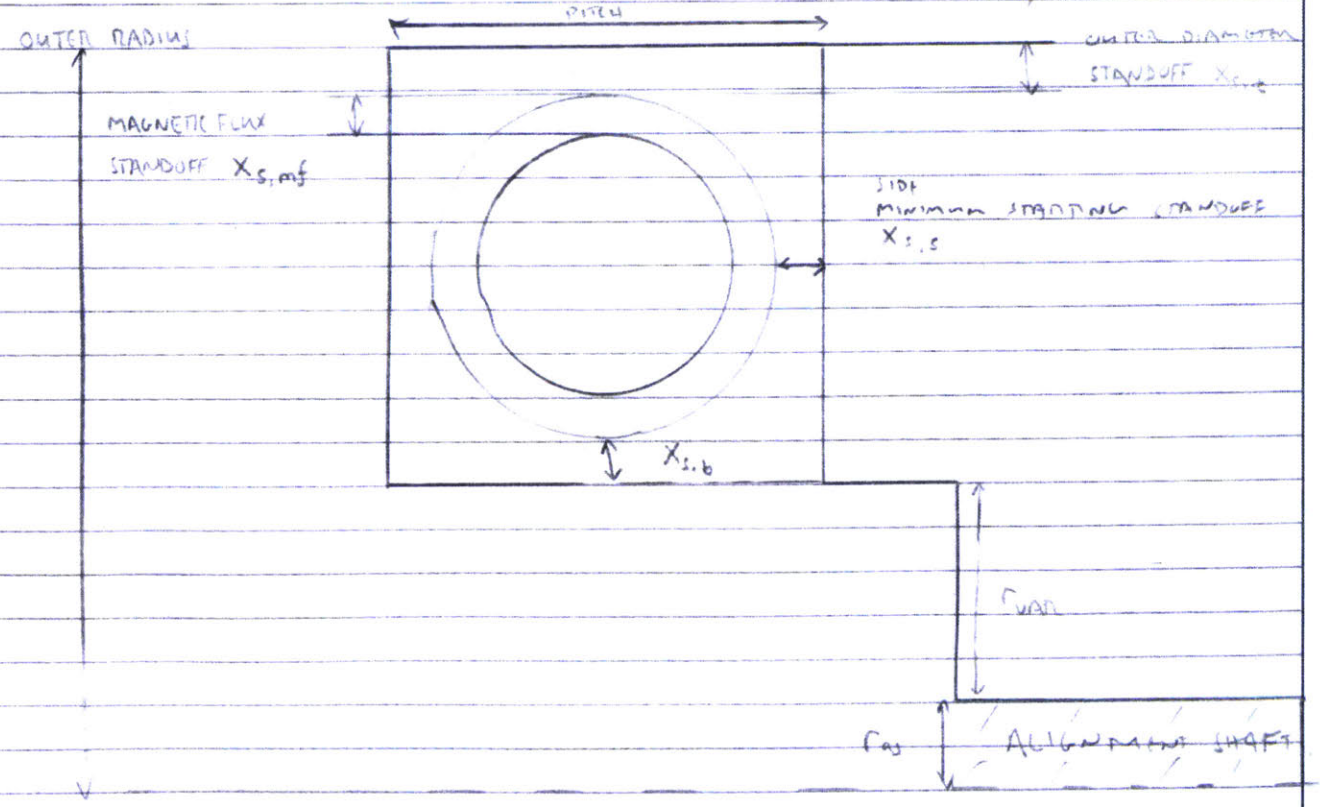

FRONT VIEW

Continued to page 1-57

SIGNATURE DATE 24 AUG 2016

DISCLOSED TO AND UNDERSTOOD BY DATE

TITLE STRATEGY AND CONCEPT **PROJECT** SPIRAL MAGNET SLIP CLUTCH

Continued from page 1-56

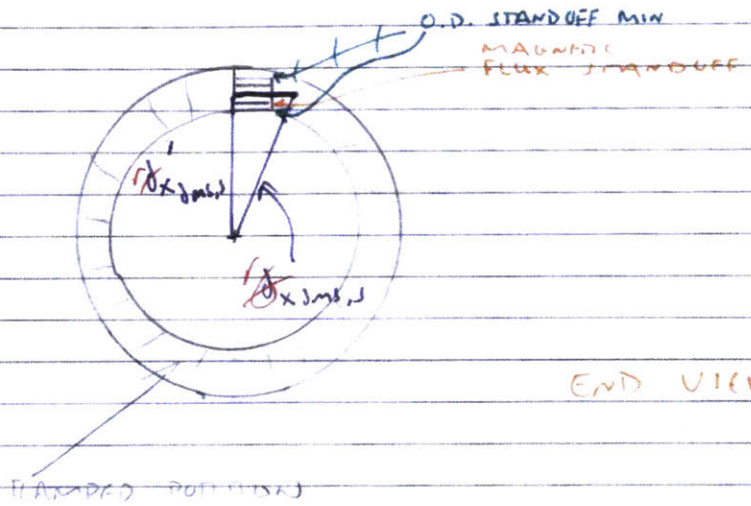

SIDE VIEW MINIMUM STANDOFF ($x_{dms,side}$) STARTING RADIUS ($r_{x_{dms,s}}$)

$$r'_{x_{dms,s}} = r_{as} + r_{AR} + x_{s,b} + x_{s,ms} + r_{MAG}$$

$$r_{x_{dms,s}} = \frac{l_{MAG}}{\sin\left(\tan^{-1}\left(\frac{l_{MAG}}{r'_{x_{dms,s}}}\right)\right)}$$

FRACTION OF REVOLUTION THE MAGNET OCCUPIES

$$f_{m,s} = \frac{\tan^{-1}\left(\frac{l_{MAG}}{r'_{x_{dms,s}}}\right)}{360}$$

FRACTION OF PITCH OVER MAGNET LENGTH

$$f_{p,s} = P \cdot f_{m,s}$$

Continued to page 1-58

SIGNATURE DATE 24 AUG 2016

DISCLOSED TO AND UNDERSTOOD BY DATE

PROPRIETARY INFORMATION

TITLE STRATEGY AND CONCEPT **PROJECT** SPIRAL MAGNET CONCEPT

Continued from page 1-57

$$X_{dms,side} = f_{p,s} + X_{min,s}$$

$X_{min,s}$ = DESIRED STANDOFF BETWEEN RECESS AND SPIRAL RAMP FALL.

TOP DIAMETER MINIMUM STANDOFF STANDING ($r_{dmt,top}$)

$$r_{dms,top,min} = r_{AS} + r_{VAR} + 2 \cdot r_{mag} + 2X_{mss}$$

INCLUDING ANGLE MAGNET OCCUPIES (α)

$$\alpha = \tan^{-1}\left(\frac{l_{mag}}{r_{dms,top,min}}\right)$$

RADIUS AT MINIMUM DIMENSION

$$r_{dms,top_{min}} = \frac{l_{mag}}{\sin\alpha}$$

$$r_{dms,top} = r_{dms,top_{min}} + X_{min,o}$$

$X_{min,o}$ = DESIRED STANDOFF BETWEEN RECESS AND OUTER DIAMETER OF CLUTCH BODY

③, ⑤ SKIP MAGNET RELOCATION FOR NOW

Continued to page 1-59

SIGNATURE DATE 24 AUG 2016

DISCLOSED TO AND UNDERSTOOD BY DATE

TITLE STRATEGY AND CONCEPT **PROJECT** SPIRAL MAGNET CONCEPT

Continued from page 1-58

④ TORQUE REQUIRED TO OVERCOME STATIC AND DYNAMIC FRICTION OF THE SPIRAL RAMP.

STATIC IS MORE IMPORTANT BECAUSE IT WILL BE ~~BIGGER~~ GREATER AND BECAUSE IT CONTRIBUTES TO THE SLIP CLUTCH TORQUE CAPACITY.

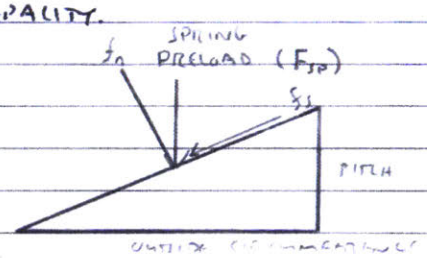

$$f_n = F_{SP} \cos\left(\tan^{-1}\left(\frac{\text{PITCH}}{\text{OUTSIDE CIRCUMFERENCE}}\right)\right)$$

FORCE OF STATIC FRICTION (f_s)

$$f_s = \mu_s f_n$$

BOTH OUTSIDE CIRCUMFERENCE AND SPRING PRELOAD ARE VARIABLE.

OUTSIDE CIRCUMFERENCE VARIES ALONG THE SPIRAL BASED ON MAGNET SIZE AND PITCH.

SPRING PRELOAD INCREASES IN THE OVERLOAD CONDITION AS THE LEFT AND RIGHT ENDS TRANSLATE AND THE ASSOCIATED PRELOAD / SPRING ARE COMPRESSED. ONLY STATIC CONDITION WILL BE ANALYZED INITIALLY SINCE $\mu_s > \mu_d$. SPRING SELECTION COULD BE EFFECTED BY THIS INTERACTION

Continued to page 1-60

SIGNATURE DATE 24 AUG 2016

DISCLOSED TO AND UNDERSTOOD BY DATE

PROPRIETARY INFORMATION

TITLE STRATEGY AND CONCEPT **PROJECT** SPIRAL MAGNET CONCEPT

Continued from page 1-59

RESULTANT f_s WILL ACT AT 2/3 THE DIFFERENCE BETWEEN THE INSIDE AND OUTSIDE RADIUS OF THE SPIRAL THEREFORE:

$$f_s = \mu_s F_{SP} \cos\left(\tan^{-1}\left(\frac{PITCH}{r_{eq}}\right)\right)$$

r_{eq} = SPIRAL INSIDE RADIUS + 2/3 ((SPIRAL INSIDE RADIUS + PITCH) − SPIRAL INSIDE RADIUS)

r_{eq} = SPIRAL INSIDE RADIUS + 2/3 PITCH = $r_{as} + r_{VAR}$ + 2/3 PITCH

$$f_s = \mu_0 F_{SP} \cos\left(\tan^{-1}\left(\frac{PITCH}{r_{as} + r_{VAR} + \frac{2}{3} PITCH}\right)\right)$$

ASSUMING $P = 20\,mm$

$r_{IN} = r_{as} + r_{VAR} = 6.5\,mm$

$FSP = 100$ lbs

$r_{IN} = r_{as} + r_{VAR}$ =

FSP = 100 lbs

=> 14 in-lbs

THE CONTRIBUTION OF STATIC FRICTION TO THE TORQUE CAPACITY IS ~14 in-lbs

Continued to page 1-61

SIGNATURE DATE 24AUG2016

DISCLOSED TO AND UNDERSTOOD BY DATE

TITLE STRATEGY AND CONCEPT **PROJECT** TRI-SOCKET BALL CONCEPT

Continued from page 1-60

FIRST ORDER ANALYSIS OF TRI-SOCKET CONCEPT

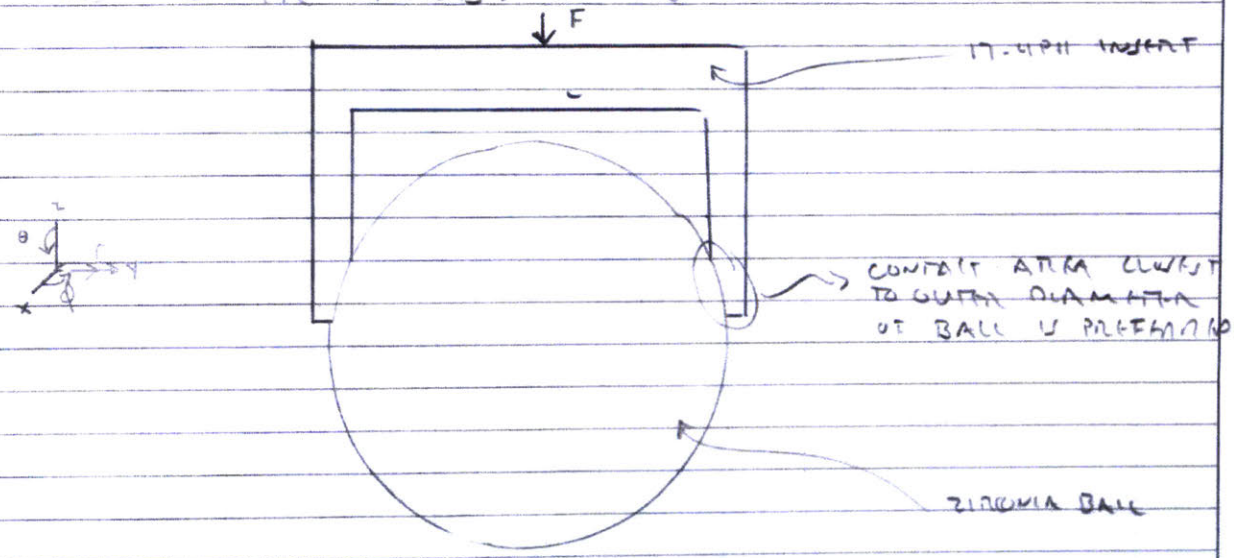

GOAL: TO MOVE THE CONTACT AREA OF THE INSERT AS FAR AS POSSIBLE TOWARDS THE OUTER RADIUS. THIS WILL ALLOW FOR THE GREATEST TORQUE TRANSMISSION.

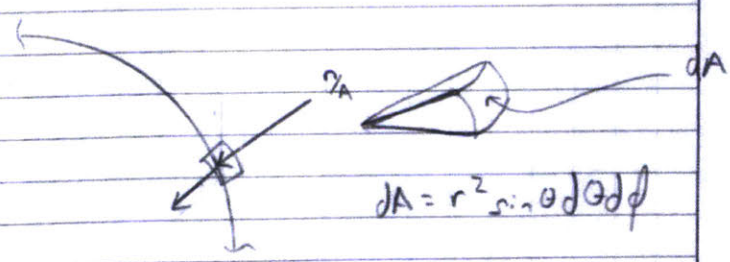

$$dA = r^2 \sin\theta \, d\theta \, d\phi$$

$$f_{friction} = \mu n$$

$$dT = \int_{\theta=\theta_i}^{\theta=\theta_f} f_{friction} \cdot r \, d\theta = \int_{\theta=\theta_i}^{\theta=\theta_f} f_{friction} \, r_{sphere} \cos\theta \, d\theta$$

Continued to page 1-62

SIGNATURE

DATE 03 OCT 2016

DISCLOSED TO AND UNDERSTOOD BY

DATE

PROPRIETARY INFORMATION

TITLE STRATEGY AND CONCEPT **PROJECT** TRI-SOCKET BALL CONCEPT

Continued from page 1-61

$$T = \mu n r_{SPHERE} \sin\theta \Big|_{\theta=\theta_i}^{\theta=\theta_f}$$

$$T = \mu n r_{SPHERE} (\sin\theta_f - \sin\theta_i)$$

EFFECTIVE RADIUS

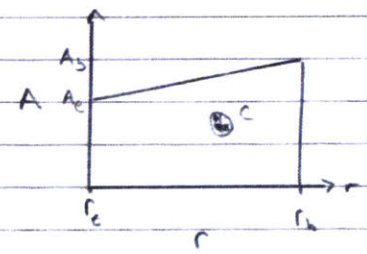

A = CIRCUMFERENCE FOR A GIVEN RADIUS

$$C_x = \frac{A_t(r_b - r_t)\cdot\left(\frac{r_b - r_t}{2}\right) + \left(\frac{r_b - r_t}{2}\right)(A_b - A_t)\left(\frac{r_b - r_t}{3}\right)}{A_t(r_b - r_t) + (A_b - A_t)\left(\frac{r_b - r_t}{2}\right)}$$

$$C_x = \frac{(r_b - r_t)^2}{(r_b - r_t)} \frac{\frac{A_t}{3} + \frac{A_b}{6}}{\left(\frac{A_b + A_t}{2}\right)}$$

$$C_x = (r_b - r_t)\frac{\left(\frac{2A_t + A_b}{3}\right)}{A_t + A_b}$$

$$C_x = (r_b - r_t)\frac{2A_t + A_b}{3(A_t + A_b)}$$

SUBSTITUTE $A = C = 2\pi r$

$$C_x = (r_b - r_t)\frac{4\pi r_t + 2\pi r_b}{6\pi(r_t + r_b)}$$

$$C_x = \left(\frac{r_b - r_t}{r_t + r_b}\right)(2r_t + r_b)$$

Continued to page 1-63

SIGNATURE

DATE 03 OCT 2016

DISCLOSED TO AND UNDERSTOOD BY

DATE

PROPRIETARY INFORMATION

TITLE STRATEGY AND CONCEPT **PROJECT** TRI-SOCKET BALL CONCEPT

Continued from page 1-62

TORQUE

$$T = f_{friction} r_{eff} = \mu n \frac{(r_b - r_t)}{(r_t + r_b)} \frac{(2r_t + r_b)}{3}$$

Continued to page 1-64

SIGNATURE		DATE 03 OCT 2016
DISCLOSED TO AND UNDERSTOOD BY	DATE	PROPRIETARY INFORMATION

THIS PAGE INTENTIONALLY LEFT BLANK

Appendix B

Proof of Concept Testing Calculations

This appendix presents design notebook pages which provide supporting documentation for the analysis conducted in support of Proof of Concept Prototype validation testing. This documentation was used as a basis for establishing feasibility of this concept.

TITLE PROTOTYPE DEFLECTION **PROJECT** CURVED BEAM CONCEPT

Continued from page NA

PROBLEM STATEMENT: DETERMINE THE EXPECTED TORQUE CAPACITY OF THE CURVED BEAM SLIP CLUTCH PROTOTYPE FOR COMPARISON WITH TEST DATA

METHOD*:

1. USE FEA TO DETERMINE STIFFNESS IN THE VERTICAL PLANE. THIS PLANE CORRESPONDS TO THE DEFLECTION THAT ENABLES THE CLUTCH TO RELEASE ON OVERLOAD

2. USE GIVEN GEOMETRY TO DETERMINE THE SYSTEM PRELOAD

3. USE PRELOAD TO DETERMINE TORQUE CAPACITY.

* THIS METHOD IS REQUIRED IN ORDER TO ADDRESS TO A MACHINE EXAMPLE DESIGN WHICH A SPECIFIC TORQUE CAPACITY REQUIREMENT IS MADE. THE METHOD WILL NOT BE USED FOR A PROTOTYPE PROOF OF CONCEPT

Continued to page 1-93

SIGNATURE DATE 30 OCT 2015

DISCLOSED TO AND UNDERSTOOD BY DATE

TITLE [illegible] DEFLECTION **PROJECT** CUTOUT BEAM CONCEPT

Continued from page 1-97

STEP 1 : STIFFNESS DETERMINATION

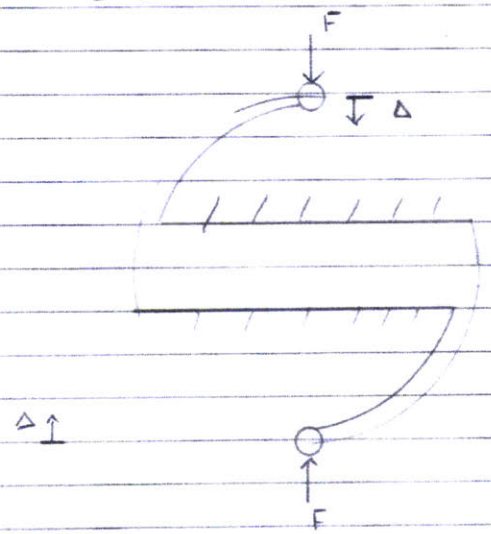

FEA WAS PERFORMED IN SOLIDWORKS WITH LOADS AND BOUNDARY CONDITIONS GENERALIZED ABOVE. ANALYSIS YIELDED THE FOLLOWING DATA.

LOAD	DISPLACEMENT (Δ) [mm]	$K = \frac{LOAD}{\Delta}$ [N/mm]
1 N	0.0247	40.5
10 N	0.2469	40.5

Continued to page 1-94

SIGNATURE DATE 04 DEC 2016

DISCLOSED TO AND UNDERSTOOD BY DATE

TITLE PROTOTYPE DEFLECTION **PROJECT** CURVED BEAM COUPLING

Continued from page 1-93

2. PRELOAD DETERMINATION

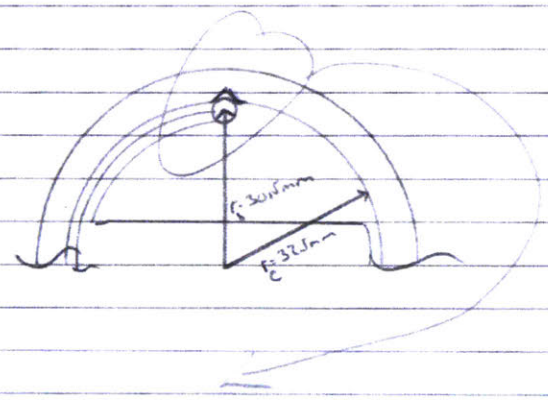

FROM CAD
THIS POINT OF
THE "CUP" IS
AT $r = 32.690mm$

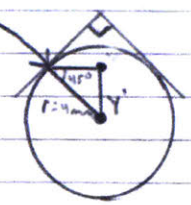

DEFLECTION OF THE CURVED BEAM IN THE STATIC CONDITION (Δy_{static}) IS THE DIFFERENCE IN THE Y POSITION OF THE POINT WHERE THE CURVED BEAM MEETS THE CUP AND THE POSITION OF THAT POINT IF THE CURVED BEAM WERE NOT PRELOADED.

$$\Delta y_{static} = Y_s - (r_b + y') = 32.7\ mm - (30.5mm + \sin 45(4mm))$$

$$\Delta y_{static} = 0.6mm$$

Continued to page 1-95

SIGNATURE DATE 04 DEC 2015

DISCLOSED TO AND UNDERSTOOD BY DATE

TITLE PROTOTYPE DEFLECTION **PROJECT** CURVED BEAM CONCEPT

Continued from page

$F_{PRELOAD} = \Delta y_{STATIC} \, k = 0.6\,mm \, (40\,N/mm)$

$F_{PRELOAD} = 24.3\,N$

GIVEN CALCULATION ON PAGE 1-65 AND 1-66

$F_{PRELOAD} = \frac{T_{CAPACITY}}{N \cdot r_c}$

$T_{CAPACITY} = F_{PRELOAD} \cdot N \cdot r_c$

$N = 2$ BASED ON TWO CURVED BEAMS

$T_{CAPACITY} = (24.3\,N)(2)(0.0305\,m)$

$$\boxed{T_{CAPACITY} = 1.48\,N \cdot m = 13.1\,in\text{-}lb}$$

DURING TESTING PROTOTYPE RELEASED AT ~16 IN-lbs. THIS IS CONSIDERED REASONABLE AGREEMENT OF INITIAL CALCULATION AND TEST DATA.

Continued to page

SIGNATURE DATE

DISCLOSED TO AND UNDERSTOOD BY DATE

TITLE PROJECT

Continued from page

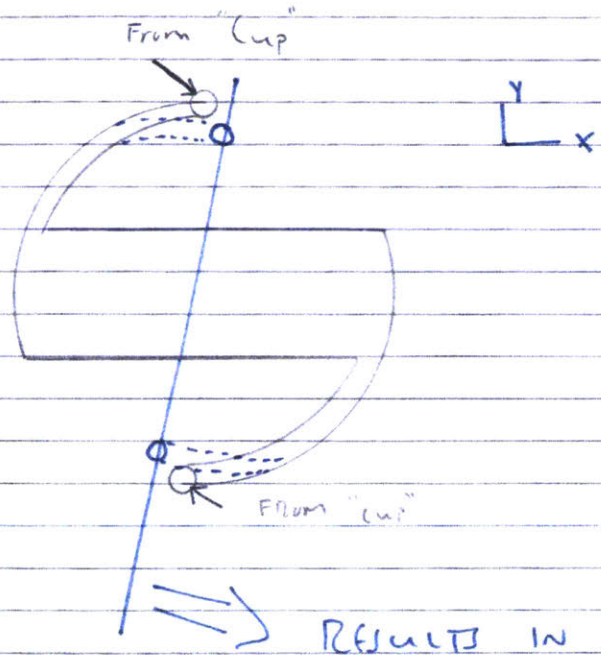

RESULTS IN LOW TORSIONAL STIFFNESS

Continued to page

SIGNATURE DATE

DISCLOSED TO AND UNDERSTOOD BY DATE

PROPRIETARY INFORMATION

TITLE PRELIMINARY DEFLECTION **PROJECT** CURVED BEAM

Continued from page

PRELIMINARY DEFLECTION AND STRESS ANALYSIS IN ACCORDANCE WITH Beam_curved.xls

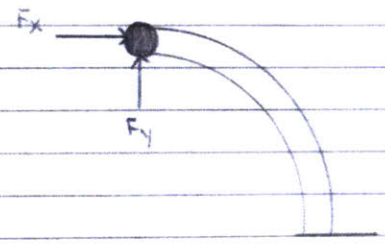

$F_y = F_{PRELOAD} - F_{INSTALL} = 243N - 243N = 0$

$F_x = F_\perp = F_{PRELOAD}$ (SINCE $\alpha = 45°$)

$F_x = 243N$

INPUT INTO Beam_curved.xls

$\delta_{x\,TOTAL} = 1.420$ mm

$\delta_{y\,TOTAL} = 1.988$ mm ⇒ THIS MAKES SENSE FOR SLIP CLUTCH DISENGAGEMENT SINCE BALL DRAWING RADIUS = 4mm

Continued to page

SIGNATURE DATE

DISCLOSED TO AND UNDERSTOOD BY DATE

PROPRIETARY INFORMATION

TITLE PROTOTYPE DEFLECTION **PROJECT** CURVED BEAM CONCEPT

Continued from page 1-97

GIVEN $F_x = 24.3\,N$ AND $F_y = 0$ ON DRIVING CUP

$$\delta_x = 1.420\,mm$$
$$\delta_y = 1.988\,mm$$

AND $F_x = -24.3\,N$ AND $F_y = 0$ ON DRIVEN CUP

$$\delta_x = -1.420\,mm$$
$$\delta_y = -1.988\,mm$$

EACH "SIDE" IS RESPONSIBLE FOR

$$\alpha = 2\sin^{-1}\left(\frac{C}{2R}\right) = 2\sin^{-1}\left(\frac{1.420\,mm}{2 \cdot 30.5\,mm}\right)$$

$$\alpha = 2.67^\circ$$

$\Rightarrow$ TOTAL ANGULAR TRANSMISSION ERROR (θ)

$$\theta = 2(2.67^\circ)$$

$$\theta = 5.34^\circ$$

Continued to page

SIGNATURE DATE

DISCLOSED TO AND UNDERSTOOD BY DATE

PROPRIETARY INFORMATION

TITLE PROTOTYPE TESTING **PROJECT**

Continued from page 1.99

1ST TEST

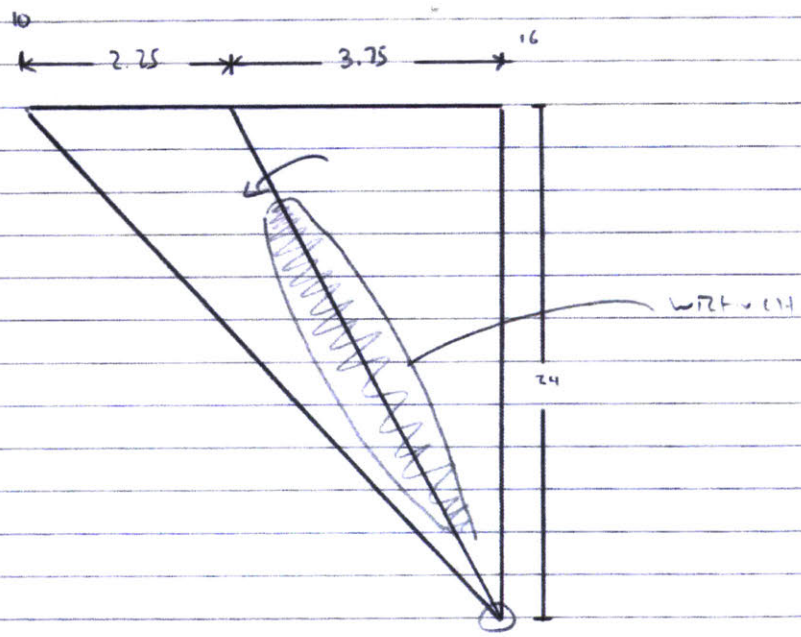

ERROR (ϕ) = $\sin^{-1}\left(\frac{6}{24}\right) - \sin^{-1}\left(\frac{3.75}{24}\right)$

ϕ = 3.488 @ 16.5 in·lbs = 1.86 N·m

Continued to page

SIGNATURE DATE

DISCLOSED TO AND UNDERSTOOD BY DATE

TITLE PROTOTYPE TUNING **PROJECT**

Continued from page 100

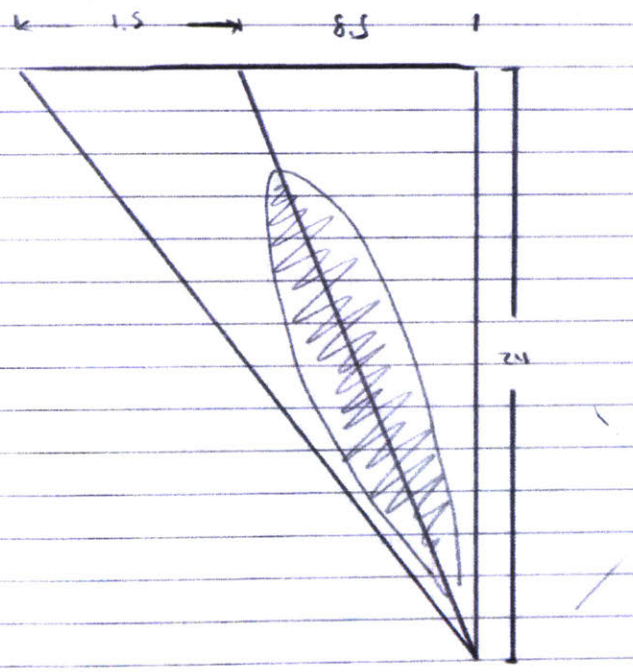

ENGAGEMENT FORCE DETERMINATION, 14

@ 45° $F_{PRELOAD}$ = 24.3N ϕ = 3.416

@ 1.484 N·m

AGREEMENT IN MODEL AND TEST DATA

Continued to page

SIGNATURE DATE

DISCLOSED TO AND UNDERSTOOD BY DATE

PROPRIETARY INFORMATION

Appendix C

Finalized Analytical Model

This appendix presents that finalized version of the analytical model. This model was generated using MATLAB and the script along with selected graphed output is provided.

Curved Beam Analytical Model

```
The purpose of this script is to optimize the design of the curved
beam based slip clutch.  The primary objective of this optimization is
to minimize angular displacment following the threshold torque (torque
capacity) being met.  This optimization will be completed in several
steps, which form the basis for the sections of this script as listed
below;
```

(1) Required Preload/Engagement Force Determination For a given torque capacity (T_capacity) and initial ball bearing to detent incident angle (gamma_initial), determine the engagement or preload force (F_engagement)required for the curved beam element.

(2) Vertical, Horizontal and Angular Displacment Due to Vertical Loading This section uses energy methods to calculate the displacement of the ball bearing centerline axis due to loading in the vertical direction.

(3) Horizontal, Vertical and Angular Stiffness Calculation The displacements calculated in step (2) are used to determine their respective directional stiffness (k_xy, k_yy and k_phi_y) based on vertical loading.

(4) Vertical, Horizontal and Angular Displacment Due to Horiz. Loading This section uses energy methods to calculated the displacement of the ball bearing centerline axis due to loading in the horizontal direction.

(5) Horizontal, Vertical and Angular Stiffness Calculation The displacements calculated in step (4) are used to determine their respective directional stiffness (k_xx, k_yx and k_phi_x) based on horizontal loading.

(6) Determination of Y Coordinate of Ball Bearing to Detent Interface The y coordinate of the ball bearing to detent interface is set to zero for the vertical loading conditions presented in Step (2) that are less than the calculated preload force. This reflects that the curved beam element will not displace until the preload force is overcome. The y coordinate for the vertical loading conditions that are larger than the preload force are set to equal the difference in the position of the interface from the preloaded condition.

(7) Ball Bearing and Detent Incident Angle vs. Y Coordinate The vertical displacement calculated in step (2) along with the geometry of the ball bearing and detent are used to derive the incident angle as a function of vertical displacement.

(8) Torque Determination For the range of vertical loading conditions determined in Step (2), those that are less than the preload force are set to zero. Those that are greater are set equal to the engagement force plus the stiffness constant multiplied by the vertical displacement. This quantity is then divided by the cosine of gamma to yield the side force that can be supported. The torque associated to this side force is then calculated.

(9) The Horizontal Location of the Interface Position of the Ball The horizontal location of the interface position will be calculated to support determination of angular displacement. This location is determined using the interface incident angle which is calculated in Step (6) as a function of vertical displacement.

(10) Angular Displacement Determination The angular displacment of the curved beam element is determined based on the horizontal displacement calculated in step (2) and the horizontal location of the inteface position calculated in step (9). (11) Testing Results and Comparison This portion of the code, loads and displays the testing data and plots on the same axes as the analytical model. This allows for comparison between test results and the output of the script above.

```
close all
clear all
clc
```

```
A=ones(9,1001);
num_rows=size(A,1);
num_cols=size(A,2);
B=ones(1,1001);

% (1) Required Preload/Engagement Force Determination
%     For a given torque capacity (T_capacity) and initial ball bearing
%     to detent incident angle (gamma_initial), determine the engagement
%     or preload force (F_engagement)required for the curved beam element.

T_capacity=0;                 %Torque Capacity                        [N-m]
gamma_initial=20;                %Initial Ball Bearing/Detent Incident Angle
                                 %                                 [degrees]
N=2;                             %Number of Ball Bearing Elements
R=14;                            %Radius to Ball Bearing Centerline     [mm]
R=R/1000;                        %Radius to Ball Bearing Centerline      [m]

Fs_capacity=(T_capacity/(N*R)).*B;
                                 %Side Force for given Torque Capacity   [N]

% (2) Vertical, Horizontal and Angular Displacment Due to Vertical Loading
%     This section uses energy methods to calculate the displacement of
%     the ball bearing centerline axis due to loading in the vertical
%     direction.

Fy=linspace(0,1000,1001);        %Vertical Loading                       [N]
Fx=0;                            %Horizontal Loading                     [N]
Mo=0;                            %Moment Loading                         [N]
R_curvature=14;                  %Radius of Curvature of Curved Beam    [mm]
E=69800;                         %Modulus of Elasticity (Al 6061-T6)[N/mm^2]
nu=0.29;                         %Poisson's Ratio       (Al 6061-T6)
G=E/(2*(1+nu));                  %Shear Modulus         (Al 6061-T6)[N/mm^2]
b=10;                            %Curved Beam Thickness                 [mm]
h_i=4;                           %Curved Beam Initial Height            [mm]
h_f=2;                           %Curved Beam Final Height              [mm]
w_i=8;                           %Half Width of Curved Beam Element     [mm]
theta_i=asin(w_i/R_curvature);   %Initial Angle of Beam            [radians]
theta_f=pi()/2;                  %Final Angle of Beam              [radians]
y_f=0;                           %Assumes final cross section is on the
                                 %Neutral Axis

% Horizontal Displacement (delta_xy)

for i=1:num_cols
        fun_delta_x_axial=@(theta) (R_curvature./(E*(b*(((h_f-h_i)/...
                                   (theta_f-theta_i))*theta+h_i)))).*....
                                   (Fx.*(cos(theta).^2)-...
                                   Fy(i).*sin(theta).*cos(theta));
        delta_x_axial(i)=integral(fun_delta_x_axial,theta_i,theta_f);

        fun_delta_x_shear=@(theta) (R_curvature./(G*(b*(((h_f-h_i)/...
                                   (theta_f-theta_i))*theta+h_i)))).*...
                                   (Fx.*(sin(theta)).^2-...
                                    Fy(i).*cos(theta).*sin(theta));
        delta_x_shear(i)=integral(fun_delta_x_shear,theta_i,theta_f);

        fun_delta_x_bending= @(theta) (R_curvature./(E*((b*(((h_f-h_i)/...
```

```
                                (theta_f-theta_i))*theta+h_i).^3)/12+b*...
                                (((h_f-h_i)/(theta_f-theta_i)).*theta+h_i).*...
                                ((((y_f-((h_i-h_f)/2))/(theta_f-theta_i))*...
                                theta+((h_i-h_f)/2))).^2))).*...
                                (Fx.*R_curvature^2*(1-cos(theta)).^2+...
                                Fy(i).*R_curvature^2.*sin(theta).*...
                                (1-cos(theta))+Mo*R_curvature.*(1-cos(theta)));
        delta_x_bending(i)=integral(fun_delta_x_bending,theta_i,theta_f);

        delta_xy_total(i)=(delta_x_axial(i)+delta_x_shear(i)+....
                           delta_x_bending(i));
end

%Vertical Displacement (delta_yy)

for i=1:num_cols
        fun_delta_y_axial=@(theta) (R_curvature./(E*(b*(((h_f-h_i)/...
                                   (theta_f-theta_i))*theta+h_i)))).*....
                                  ((-Fx.*cos(theta).*sin(theta))+...
                                     Fy(i).*(sin(theta)).^2);
        delta_y_axial(i)=integral(fun_delta_y_axial,theta_i,theta_f);

        fun_delta_y_shear=@(theta) (R_curvature./(G*(b*(((h_f-h_i)/...
                                   (theta_f-theta_i))*theta+h_i)))).*...
                                   (Fx.*cos(theta).*sin(theta)+...
                                   (Fy(i).*(cos(theta)).^2));
        delta_y_shear(i)=integral(fun_delta_y_shear,theta_i,theta_f);

        fun_delta_y_bending= @(theta) (R_curvature./(E*((b*(((h_f-h_i)/...
                             (theta_f-theta_i))*theta+h_i).^3)/12+b*...
                             (((h_f-h_i)/(theta_f-theta_i)).*theta+h_i).*...
                             ((((y_f-((h_i-h_f)/2))/(theta_f-theta_i))*...
                             theta+((h_i-h_f)/2))).^2))).*...
                             (Fx.*R_curvature^2*sin(theta).*(1-cos(theta))+...
                              Fy(i).*R_curvature^2.*(sin(theta)).^2+...
                              Mo*R_curvature.*sin(theta));
        delta_y_bending(i)=integral(fun_delta_y_bending,theta_i,theta_f);
end

        delta_yy_total=(delta_y_axial+delta_y_shear+delta_y_bending);

%Angular Displacment(phi_y)

for i=1:num_cols

        fun_phi=@(theta) (R_curvature./(E*((b*(((h_f-h_i)/...
                             (theta_f-theta_i))*theta+h_i).^3)/12+b*...
                             (((h_f-h_i)/(theta_f-theta_i)).*theta+h_i).*...
                             ((((y_f-((h_i-h_f)/2))/(theta_f-theta_i))*...
                             theta+((h_i-h_f)/2))).^2))).*...
                             (Fx.*R_curvature*(1-cos(theta))+...
                              Fy(i).*R_curvature*sin(theta)+Mo);

        phi(i)=integral(fun_phi,theta_i,theta_f);
end

% (3) Horizontal, Vertical and Angular Stiffness Calculation
```

```
%     The displacements calculated in step (2) are used to determine their
%     respective directional stiffness (k_xy, k_yy and k_phi_y) based on
%     vertical loading.

% Horizontal Stiffness (k_xy)

[reg_x,k_xy,b_x]=regression(delta_xy_total(1,:),Fy(1,:));
k_xy=k_xy.*B;

% figure
% plot(delta_xy_total(1,:),Fy(1,:));
% xlabel('Displacement in X Direction [mm]','FontSize',12,...
%     'FontWeight','bold','Color','k');
% ylabel('Resultant Y Force [N]','FontSize',12,...
%     'FontWeight','bold','Color','k');
% title('Resultant Y Force vs Displacement in X direction','FontSize',12,...
%     'FontWeight','bold','Color','k');

% Vertical Stiffness (k_yy)

[reg_y,k_yy,b_y]=regression(delta_yy_total(1,:),Fy(1,:));
k_yy=k_yy.*B;

% figure
% plot(delta_yy_total(1,:),Fy(1,:));
% xlabel('Displacement in Y Direction [mm]','FontSize',12,...
%     'FontWeight','bold','Color','k');
% ylabel('Resultant Y Force [N]','FontSize',12,...
%     'FontWeight','bold','Color','k');
% title('Resultant Y Force vs Displacement in Y direction','FontSize',12,...
%     'FontWeight','bold','Color','k');

% Angular Stiffness (k_phi_y)

[reg_phi,k_phi_y,b_phi]=regression(phi(1,:),Fy(1,:));

% figure
% plot(phi(1,:),Fy(1,:));
% xlabel('Displacement in Phi Direction [rad]','FontSize',12,...
%     'FontWeight','bold','Color','k');
% ylabel('Resultant Y Force [N]','FontSize',12,...
%     'FontWeight','bold','Color','k');
% title('Resultant Y Force vs Displacement in Phi direction','FontSize',12,...
%     'FontWeight','bold','Color','k');

%(4) Vertical, Horizontal and Angular Displacment Due to Horizontal Loading
%    This section uses energy methods to calculated the displacement of
%    the ball bearing centerline axis due to loading in the horizontal
%    direction.

Fy=0;                           %Vertical Loading                    [N]
Fx=linspace(0,1000,1001);       %Horizontal Loading                  [N]

% Horizontal Displacement (delta_xx)

for i=1:num_cols
        fun_delta_xx_axial=@(theta) (R_curvature./(E*(b*(((h_f-h_i)/...
```

```
                                (theta_f-theta_i))*theta+h_i)))).*....
                                (Fx(i).*(cos(theta).^2)-...
                                Fy.*sin(theta).*cos(theta));
        delta_xx_axial(i)=integral(fun_delta_xx_axial,theta_i,theta_f);

        fun_delta_xx_shear=@(theta) (R_curvature./(G*(b*(((h_f-h_i)/...
                                (theta_f-theta_i))*theta+h_i)))).*...
                                (Fx(i).*(sin(theta)).^2-...
                                 Fy.*cos(theta).*sin(theta));
        delta_xx_shear(i)=integral(fun_delta_xx_shear,theta_i,theta_f);

        fun_delta_xx_bending= @(theta) (R_curvature./(E*((b*(((h_f-h_i)/...
                            (theta_f-theta_i))*theta+h_i).^3)/12+b*...
                            (((h_f-h_i)/(theta_f-theta_i)).*theta+h_i).*...
                            ((((y_f-((h_i-h_f)/2))/(theta_f-theta_i))*...
                            theta+((h_i-h_f)/2))).^2))).*...
                            (Fx(i).*R_curvature^2*(1-cos(theta)).^2+...
                             Fy.*R_curvature^2.*sin(theta).*(1-cos(theta))+...
                             Mo*R_curvature.*(1-cos(theta)));
        delta_xx_bending(i)=integral(fun_delta_xx_bending,theta_i,theta_f);
end

delta_xx_total=(delta_xx_axial+delta_xx_shear+delta_xx_bending);

%Vertical Displacement (delta_yx)

for i=1:num_cols
        fun_delta_yx_axial=@(theta) (R_curvature./(E*(b*(((h_f-h_i)/...
                                (theta_f-theta_i))*theta+h_i)))).*....
                               ((-Fx(i).*cos(theta).*sin(theta))+...
                                 Fy.*(sin(theta)).^2);
        delta_yx_axial(i)=integral(fun_delta_yx_axial,theta_i,theta_f);

        fun_delta_yx_shear=@(theta) (R_curvature./(G*(b*(((h_f-h_i)/...
                                (theta_f-theta_i))*theta+h_i)))).*...
                                (Fx(i).*cos(theta).*sin(theta)+...
                                (Fy.*(cos(theta)).^2));
        delta_yx_shear(i)=integral(fun_delta_yx_shear,theta_i,theta_f);

        fun_delta_yx_bending= @(theta) (R_curvature./(E*((b*(((h_f-h_i)/...
                            (theta_f-theta_i))*theta+h_i).^3)/12+b*...
                            (((h_f-h_i)/(theta_f-theta_i)).*theta+h_i).*...
                            ((((y_f-((h_i-h_f)/2))/(theta_f-theta_i))*...
                            theta+((h_i-h_f)/2))).^2))).*...
                            (Fx(i).*R_curvature^2*sin(theta).*(1-cos(theta))+...
                             Fy.*R_curvature^2.*(sin(theta)).^2+...
                             Mo*R_curvature.*sin(theta));
        delta_yx_bending(i)=integral(fun_delta_yx_bending,theta_i,theta_f);
end

delta_yx_total=(delta_yx_axial+delta_yx_shear+delta_yx_bending);

%Angular Displacment(phi_x)

for i=1:num_cols

        fun_phi_x=@(theta) (R_curvature./(E*((b*(((h_f-h_i)/...
```

```
                                (theta_f-theta_i))*theta+h_i).^3)/12+b*...
                                (((h_f-h_i)/(theta_f-theta_i)).*theta+h_i).*...
                                ((((y_f-((h_i-h_f)/2))/(theta_f-theta_i))*...
                                theta+((h_i-h_f)/2))).^2))).*...
                                (Fx(i).*R_curvature*(1-cos(theta))+...
                                 Fy*R_curvature*sin(theta)+Mo);

        phi_x(i)=integral(fun_phi_x,theta_i,theta_f);
end

% (5) Horizontal, Vertical and Angular Stiffness Calculation
%     The displacements calculated in step (4) are used to determine their
%     respective directional stiffness (k_xx, k_yx and k_phi_x) based on
%     horizontal loading.

% Horizontal Stiffness (k_xx)

[reg_xx,k_xx,b_xx]=regression(delta_xx_total(1,:),Fx(1,:));
k_xx=k_xx.*B;

% figure
% plot(delta_xx_total(1,:),Fx(1,:));
% xlabel('Displacement in X Direction [mm]','FontSize',12,...
%     'FontWeight','bold','Color','k');
% ylabel('Resultant X Force [N]','FontSize',12,...
%     'FontWeight','bold','Color','k');
% title('Resultant X Force vs Displacement in X direction','FontSize',12,...
%     'FontWeight','bold','Color','k');

% Vertical Stiffness (k_yx)

[reg_yx,k_yx,b_yx]=regression(delta_yx_total(1,:),Fx(1,:));
k_yx=k_yx.*B;

% figure
% plot(delta_yx_total(1,:),Fy(1,:));
% xlabel('Displacement in Y Direction [mm]','FontSize',12,...
%     'FontWeight','bold','Color','k');
% ylabel('Resultant X Force [N]','FontSize',12,...
%     'FontWeight','bold','Color','k');
% title('Resultant X Force vs Displacement in Y direction','FontSize',12,...
%     'FontWeight','bold','Color','k');

% Angular Stiffness (k_phi)

[reg_phi_x,k_phi_x,b_phi_x]=regression(phi_x(1,:),Fx(1,:));

% figure
% plot(phi_x(1,:),Fx(1,:));
% xlabel('Displacement in Phi Direction [rad]','FontSize',12,...
%     'FontWeight','bold','Color','k');
% ylabel('Resultant X Force [N]','FontSize',12,...
%     'FontWeight','bold','Color','k');
% title('Resultant X Force vs Displacement in Phi direction','FontSize',12,...
%     'FontWeight','bold','Color','k');

% (6) Determination of Y Coordinate of Ball Bearing to Detent Interface
```

```
Fs=-(k_yy.*delta_yy_total+k_yx.*delta_xy_total).*tand(gamma_initial)+...
    (k_xx.*delta_xy_total+k_xy.*delta_xy_total);

[min_difference,a]=...          %Determines at which index
    min(abs(Fs-Fs_capacity));   %in the Fy matrix, the Fy is
                                %greater than F_engagement.
y_coordinate=B;

for i=1:num_cols
    if Fs(i)<Fs_capacity(i)
        y_coordinate(i)=0;
    else
        y_coordinate(i)=delta_yy_total(i)-delta_yy_total(a);
    end
end

% (7) Ball Bearing and Detent Incident Angle vs. Y Coordinate
%      The vertical displacement calculated in step (2) along with the
%      geometry of the ball bearing and detent are used to derive the
%      incident angle as a function of vertical displacement.

r_1=1;                  %Radius of Detent Fillet                        [mm]
r_2=5;                  %Radius of Roller Bearing                       [mm]

for i=1:num_cols
    if y_coordinate(i)>(r_2+r_1)*(1-cosd(gamma_initial))
    y_coordinate(i)=(r_2+r_1)*(1-cosd(gamma_initial));
    delta_xy_total(i)=0;
    end
end

gamma=acosd(((r_2+r_1)*cosd(gamma_initial)+y_coordinate)/(r_2+r_1));
%plot(gamma,y_coordinate);

% (8) Torque Determination
%      For the range of vertical and horizontal displacements calculated in
%      Step (2), the side force that can be supported by the curved beam is
%      calculated.  For vertical displacement that exceed the sum of the
%      ball bearing and detent radii, indicating slip clutch disengagement,
%      the side force is set to zero. This is a simplification as there is
%      friction and torque resultant at the ball bearing and inner end cup
%      radius.

for i=1:num_cols
    if y_coordinate(i)<(r_2+r_1)*(1-cosd(gamma_initial))
     Fs(i)=((-(k_yy(i).*delta_yy_total(i)+k_yx(i).*delta_xy_total(i)).*...
         tand(gamma(i)))+(k_xx(i).*delta_xy_total(i)+...
         k_xy(i).*delta_xy_total(i)));
    else Fs(i)=0;
    end
end

T_applied=B;                            %                               [N-m]
for i=1:num_cols
            T_applied(i)=Fs(i)*N*R;
end
```

```
% (9) The Horizontal Location of the Interface Position of the Ball
%      The horizontal location of the interface position will be calculated
%      to support determination of angular displacement.  This location is
%      determined using the interface incident angle which is calculated in
%      Step (6) as a function of vertical displacement.

x_coordinate=round(r_1*sind(gamma_initial)-r_1*sind(gamma),10);
                         %Rounded to the 10th Decimal place so that results
                         %to large negative powers of 10 are approximated as
                         %zero.

% figure
% plot(x_coordinate(1,:),y_coordinate(1,:));
% %axis([0,10, 0,50])
% xlabel('Horizontal Position of Ball/Detent Interface [mm]','FontSize',12,...
%     'FontWeight','bold','Color','k');
% ylabel('Vertical Position of Ball/Detent Interface','FontSize',12,...
%     'FontWeight','bold','Color','k');

% (10) Angular Displacement Determination
%       The angular displacment of the curved beam element is determined
%       based on the horizontal displacement calculated in step (2) and
%       the horizontal location of the inteface position calculated in
%       step (9).

x_disp=x_coordinate+delta_xy_total;

alpha=B;

 for i=a
    alpha(i)=0;
 end
d=a+1;

[max_difference,b]=...                  %Determines at which index in the
    max(abs(x_coordinate-...            %x_disp matrix corresponds to
    delta_xy_total));                   %slip clutch release
c=b-1;

for i=d:num_cols
    if T_applied(i)>0
        alpha(i)=(atand((2.*x_disp(i))/(R_curvature-y_coordinate(i))));
    else
        alpha(i)=alpha(c);
    end
end

alpha(1001)=alpha(1000);

figure
plot(alpha,T_applied);
%axis([-1,6, 0,4])
xlabel('Angular Displacement [deg]','FontSize',12,...
    'FontWeight','bold','Color','k');
ylabel('Applied Torque [N-m]','FontSize',12,...
    'FontWeight','bold','Color','k');
```

```
title('Applied Torque vs Angular Displacement','FontSize',...
    12,'FontWeight','bold','Color','k');

% (11) Testing Results and Comparison
%   This portion of the code, loads and displays the testing data and plots
%   on the same axes as the analytical model.  This allows for comparison
%   between test results and the output of the script above.
load('testing_data_run_1')

avg_torque_zero_run_1=mean(Torque_run_1(5330:5429));
Torque_run_1=Torque_run_1-avg_torque_zero_run_1;
Torque_run_1=Torque_run_1*0.112984829333;
Rotation_run_1=Rotation_run_1-8.527;

% figure
% plot(Rotation_run_1,Torque_run_1)
% axis([0,190, -3,3])

load('testing_data_run_2')

avg_torque_zero_run_2=mean(Torque_run_2(5320:5425));
Torque_run_2=Torque_run_2-avg_torque_zero_run_2;
Torque_run_2=Torque_run_2*0.112984829333;
Rotation_run_2=Rotation_run_2-5.2;

% figure
% plot(Rotation_run_2,Torque_run_2)
% axis([0,190, -3,3])

load('testing_data_run_5')
avg_torque_zero_run_5=mean(Torque_run_5(5280:5349));

Torque_run_5=Torque_run_5-avg_torque_zero_run_5;
Torque_run_5=Torque_run_5*0.112984829333;
Rotation_run_5=Rotation_run_5+4.2;

% figure
% plot(Rotation_run_5,Torque_run_5)

figure
plot(Rotation_run_1,Torque_run_1,Rotation_run_2,Torque_run_2,...
    Rotation_run_5,Torque_run_5)
hold on
plot(alpha,T_applied);
axis([0,40, -1,4])
lgd = legend('Run #1','Run #2','Run #3','Analytical Model','Location',...
    'south','Orientation','horizontal');
%title(lgd,'Bearing Contact Angle [degrees]')
xlabel('Angular Displacement [degrees]','FontSize',12,...
    'FontWeight','bold','Color','k');
ylabel('Torque [N-m]','FontSize',12,...
    'FontWeight','bold','Color','k');
title('Testing Data - Torque vs. Angular Displacement',...
    'FontSize',12,'FontWeight','bold','Color','k');
```

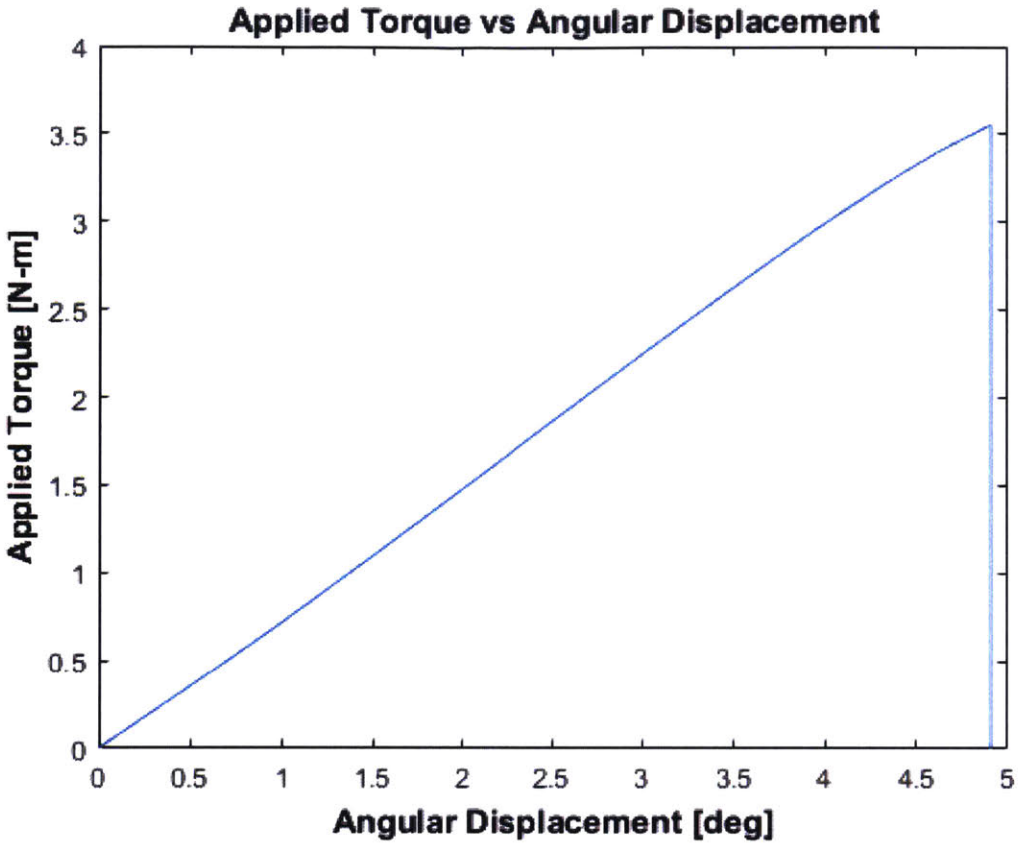
Applied Torque vs Angular Displacement
Applied Torque [N-m]
Angular Displacement [deg]
0
0.5
1
1.5
2
2.5
3
3.5
4
4.5
5

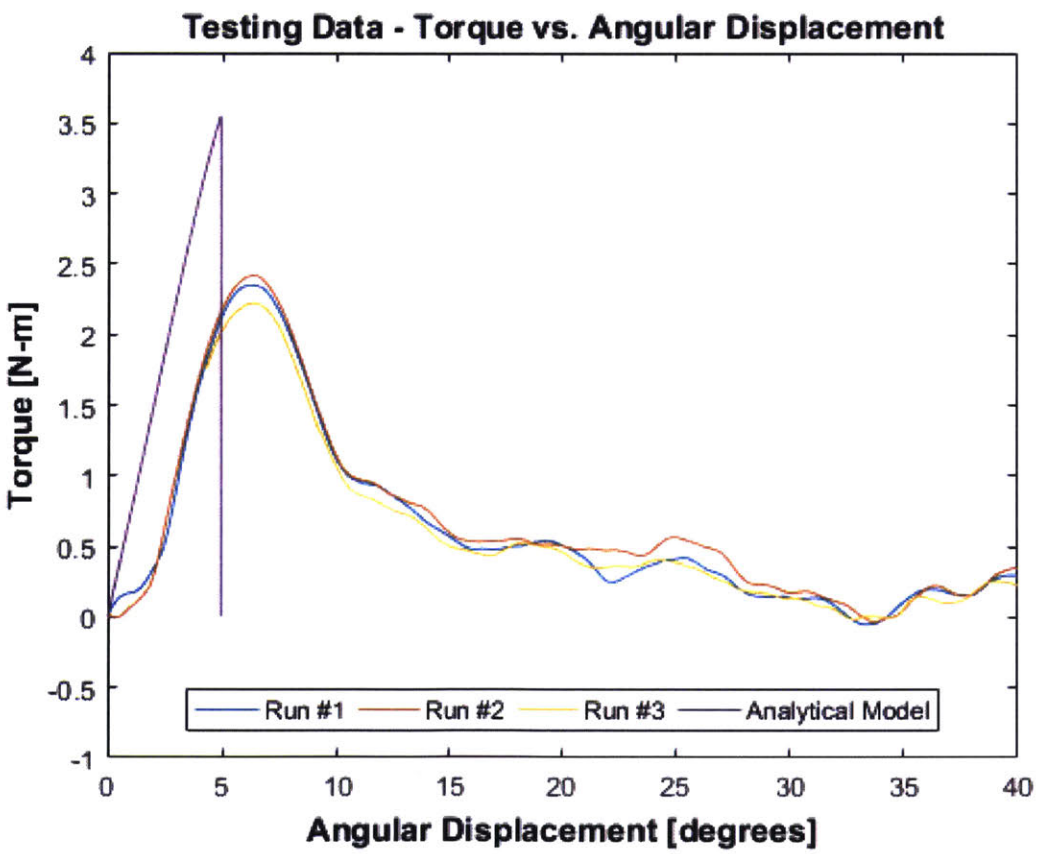
Testing Data - Torque vs. Angular Displacement
Torque [N-m]
Angular Displacement [degrees]
Run #1
Run #2
Run #3
Analytical Model
-1
-0.5
0
0.5
1
1.5
2
2.5
3
3.5
4
0
5
10
15
20
25
30
35
40

THIS PAGE INTENTIONALLY LEFT BLANK

Appendix D

High Fidelity Prototype CAD Model

The drawings presented in this Appendix provided details on the geometry of the High Fidelity Prototype.

ITEM NO.	PART NUMBER	DESCRIPTION	QTY.
1	Shaft	10mm Hex Shaft with 3/8-24 threading	1
2	Curved Beam		4
3	Dowel Pin	3mm Diameter 16mm Long	4
4	Roller Bearing	10mm Outer Radius, 3mm Inner Radius	4
5	6mm Spacer		2
6	1mm Spacer		1
7	Thrust Bearing	24mm Outer Diameter 10mm Inner Diameter	4
8	Thrust Bearing Washer	24mm Outer Diameter 10mm Inner Diameter	8
9	Left Cup		1
10	Right Cup		1
11	Hex Nut	3/8-24 Stainless Steel with Nylon Insert	2

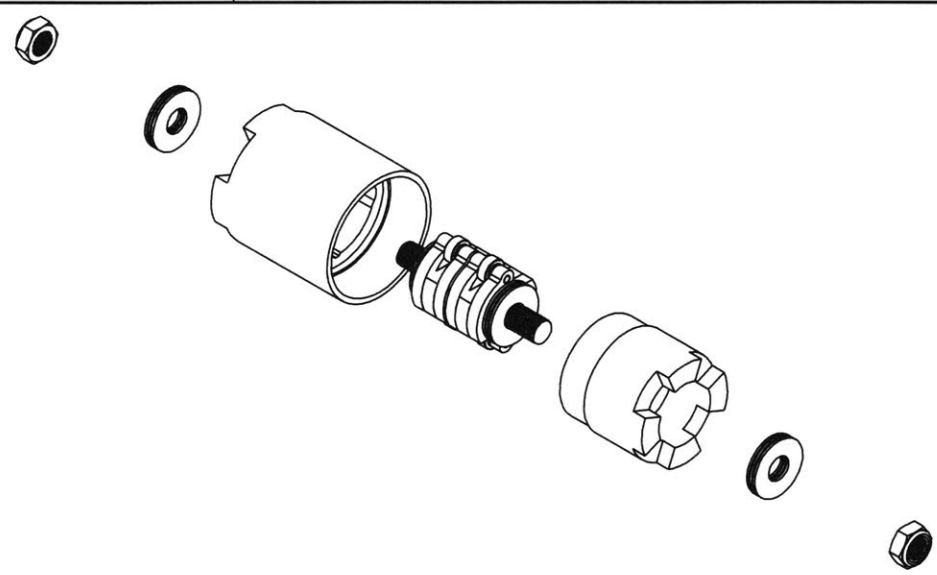

PROPRIETARY AND CONFIDENTIAL

THE INFORMATION CONTAINED IN THIS DRAWING IS THE SOLE PROPERTY OF <INSERT COMPANY NAME HERE>. ANY REPRODUCTION IN PART OR AS A WHOLE WITHOUT THE WRITTEN PERMISSION OF <INSERT COMPANY NAME HERE> IS PROHIBITED.

NEXT ASSY | USED ON

APPLICATION

UNLESS OTHERWISE SPECIFIED:

DIMENSIONS ARE IN MILLIMETERS
TOLERANCES:
FRACTIONAL ±
ANGULAR: MACH ± BEND ±
TWO PLACE DECIMAL ±
THREE PLACE DECIMAL ±

INTERPRET GEOMETRIC TOLERANCING PER:

MATERIAL

FINISH

DO NOT SCALE DRAWING

	NAME	DATE
DRAWN		
CHECKED		
ENG APPR.		
MFG APPR.		
Q.A.		

COMMENTS:

TITLE:

Slip Clutch Assembly

SIZE **A** | DWG. NO. Assembly | REV

SCALE: 1:5 | WEIGHT: | SHEET 1 OF 1

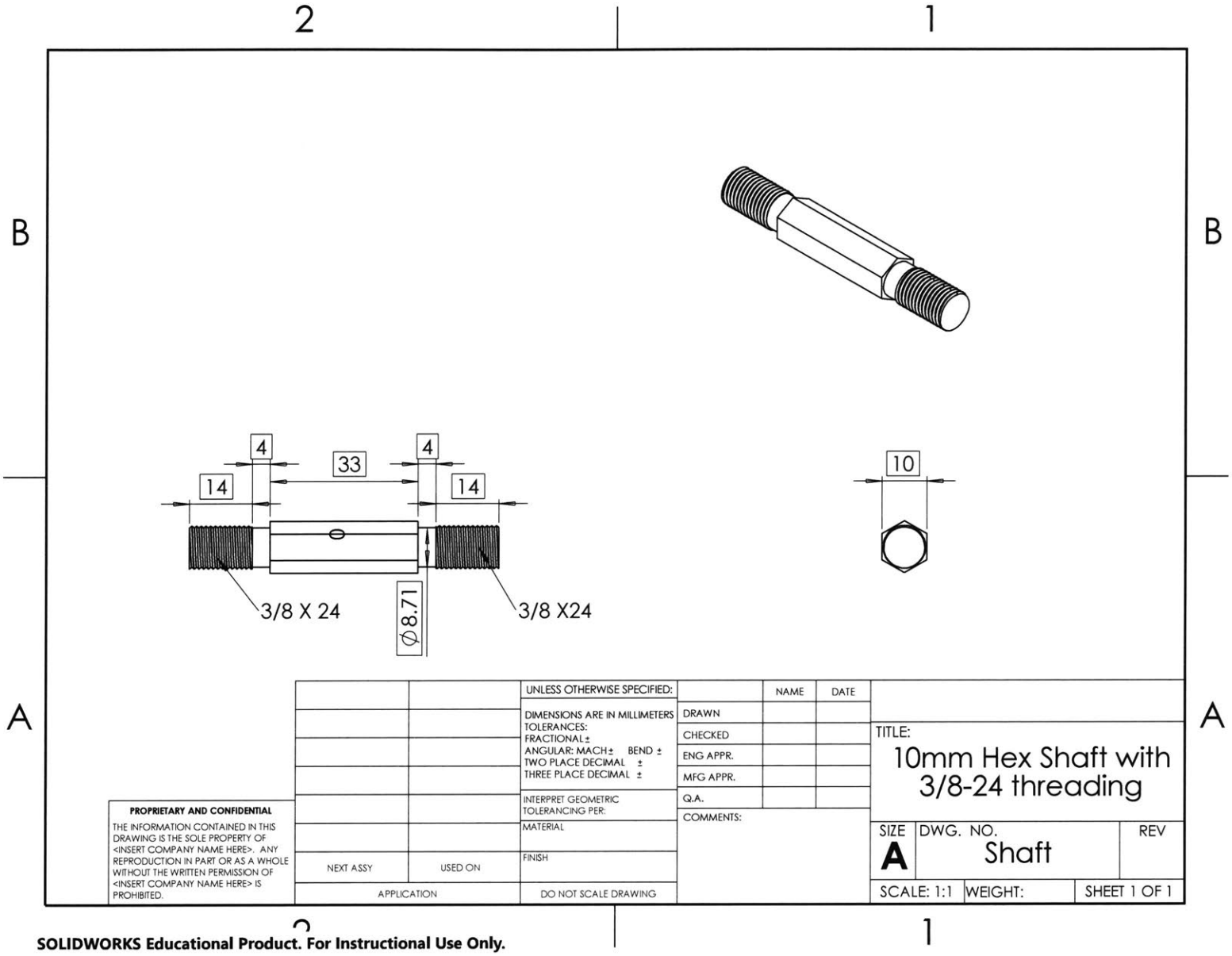
2
1
B
A
4
33
4
14
14
3/8 X 24
Ø8.71
3/8 X24
10
UNLESS OTHERWISE SPECIFIED:
DIMENSIONS ARE IN MILLIMETERS
TOLERANCES:
FRACTIONAL ±
ANGULAR: MACH ± BEND ±
TWO PLACE DECIMAL ±
THREE PLACE DECIMAL ±
INTERPRET GEOMETRIC TOLERANCING PER:
MATERIAL
FINISH
DO NOT SCALE DRAWING
NEXT ASSY
USED ON
APPLICATION
NAME
DATE
DRAWN
CHECKED
ENG APPR.
MFG APPR.
Q.A.
COMMENTS:
TITLE:
10mm Hex Shaft with 3/8-24 threading
SIZE
A
DWG. NO.
Shaft
REV
SCALE: 1:1
WEIGHT:
SHEET 1 OF 1
PROPRIETARY AND CONFIDENTIAL
THE INFORMATION CONTAINED IN THIS DRAWING IS THE SOLE PROPERTY OF <INSERT COMPANY NAME HERE>. ANY REPRODUCTION IN PART OR AS A WHOLE WITHOUT THE WRITTEN PERMISSION OF <INSERT COMPANY NAME HERE> IS PROHIBITED.
SOLIDWORKS Educational Product. For Instructional Use Only.

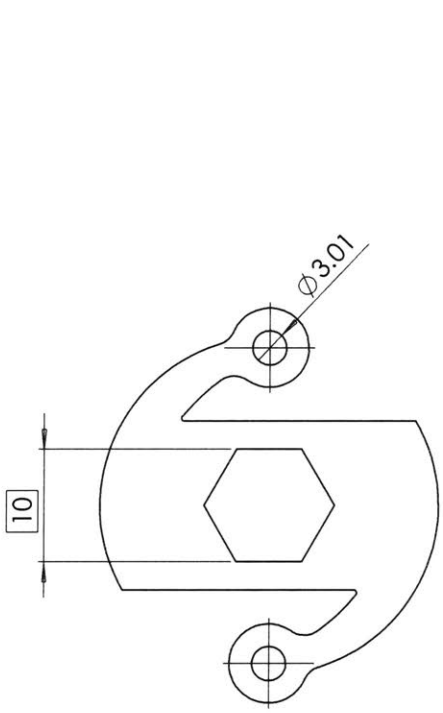

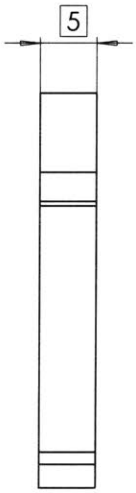

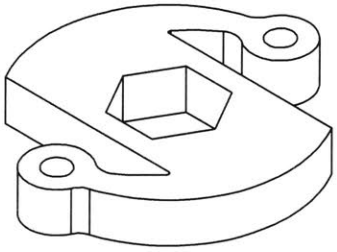

All dimensions are not shown based on complex geometry fabricated on waterjet. Refer to Curved Beam.sldprt for fabrication.

				NAME	DATE
		UNLESS OTHERWISE SPECIFIED:			
		DIMENSIONS ARE IN MILLIMETERS TOLERANCES: FRACTIONAL ± ANGULAR: MACH ± BEND ± TWO PLACE DECIMAL ± THREE PLACE DECIMAL ±	DRAWN		
			CHECKED		
			ENG APPR.		
			MFG APPR.		
		INTERPRET GEOMETRIC TOLERANCING PER:	Q.A.		
		MATERIAL	COMMENTS:		
NEXT ASSY	USED ON	FINISH			
APPLICATION		DO NOT SCALE DRAWING			

TITLE:
Slip Clutch: Curved Beam

SIZE	DWG. NO.	REV
A	Curved Beam	
SCALE: 2:1	WEIGHT:	SHEET 1 OF 1

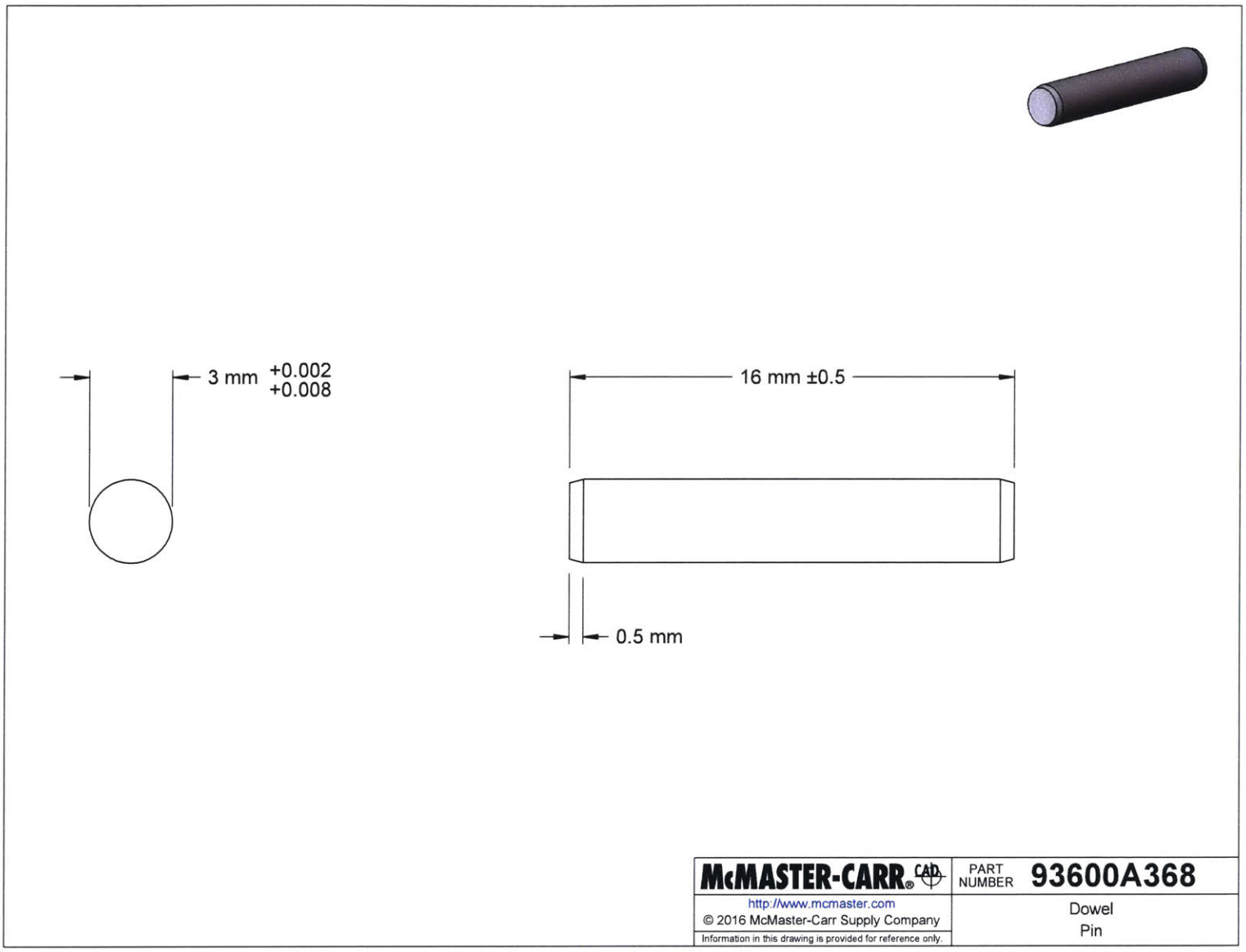
3 mm +0.002 +0.008
16 mm ±0.5
0.5 mm
McMASTER-CARR® CAD
PART NUMBER 93600A368
http://www.mcmaster.com
© 2016 McMaster-Carr Supply Company
Information in this drawing is provided for reference only.
Dowel Pin

Trade Number: 623-2Z

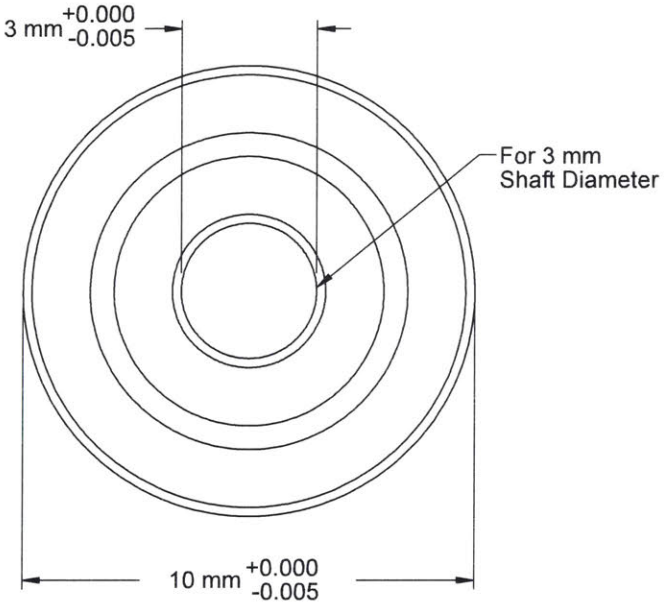

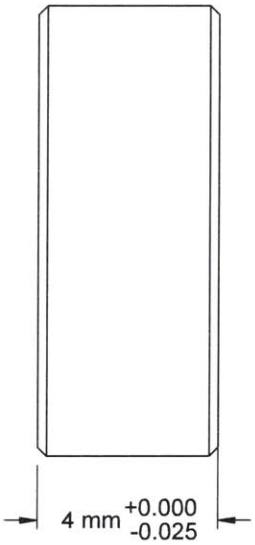

McMASTER-CARR® CAD	PART NUMBER	7804K128
http://www.mcmaster.com © 2015 McMaster-Carr Supply Company Information in this drawing is provided for reference only.	Premium Stainless Steel Ball Bearing	

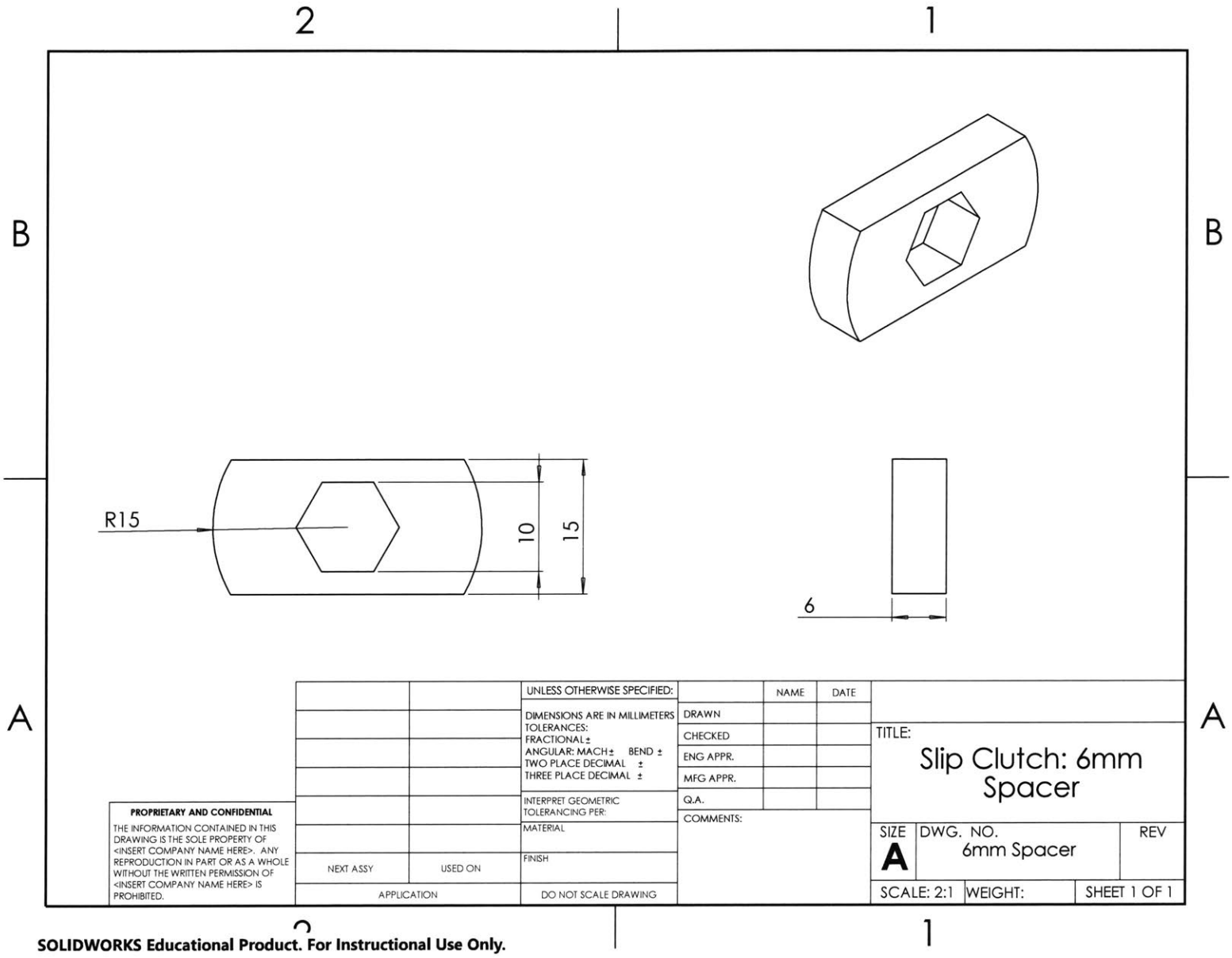

SOLIDWORKS Educational Product. For Instructional Use Only.

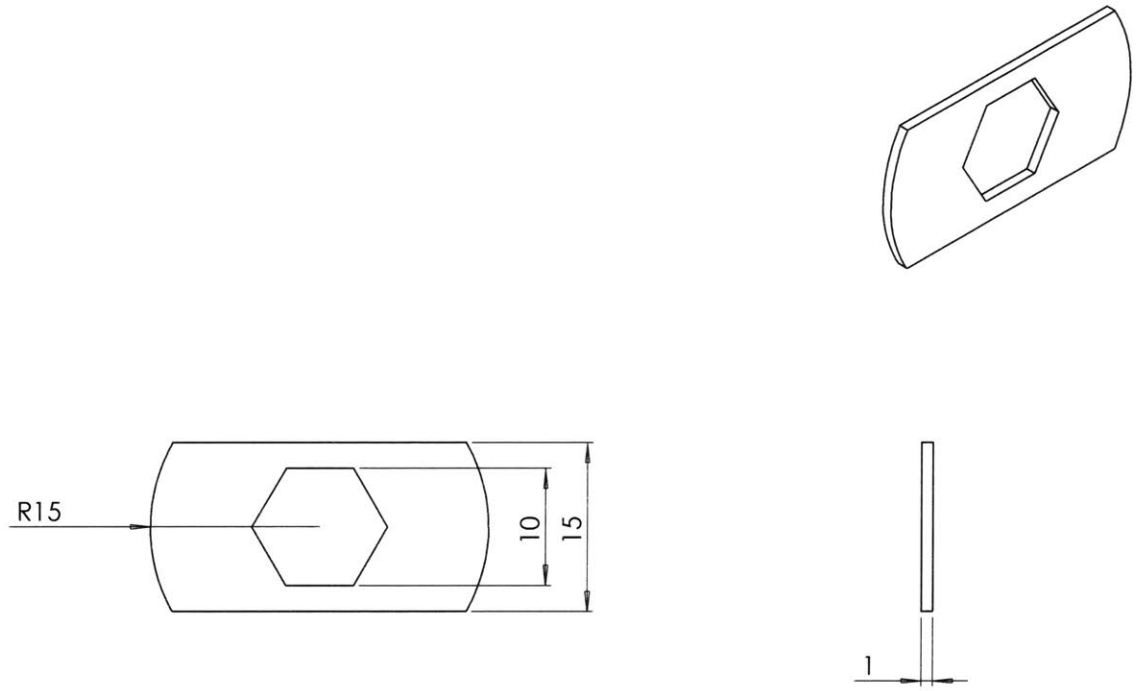

		UNLESS OTHERWISE SPECIFIED:		NAME	DATE
		DIMENSIONS ARE IN MILLIMETERS TOLERANCES: FRACTIONAL ± ANGULAR: MACH ± BEND ± TWO PLACE DECIMAL ± THREE PLACE DECIMAL ±	DRAWN		
			CHECKED		
			ENG APPR.		
			MFG APPR.		
		INTERPRET GEOMETRIC TOLERANCING PER:	Q.A.		
		MATERIAL	COMMENTS:		
NEXT ASSY	USED ON	FINISH			
APPLICATION		DO NOT SCALE DRAWING			

TITLE:

Slip Clutch: 1mm Spacer

SIZE	DWG. NO.	REV
A	1mm Spacer	
SCALE: 2:1	WEIGHT:	SHEET 1 OF 1

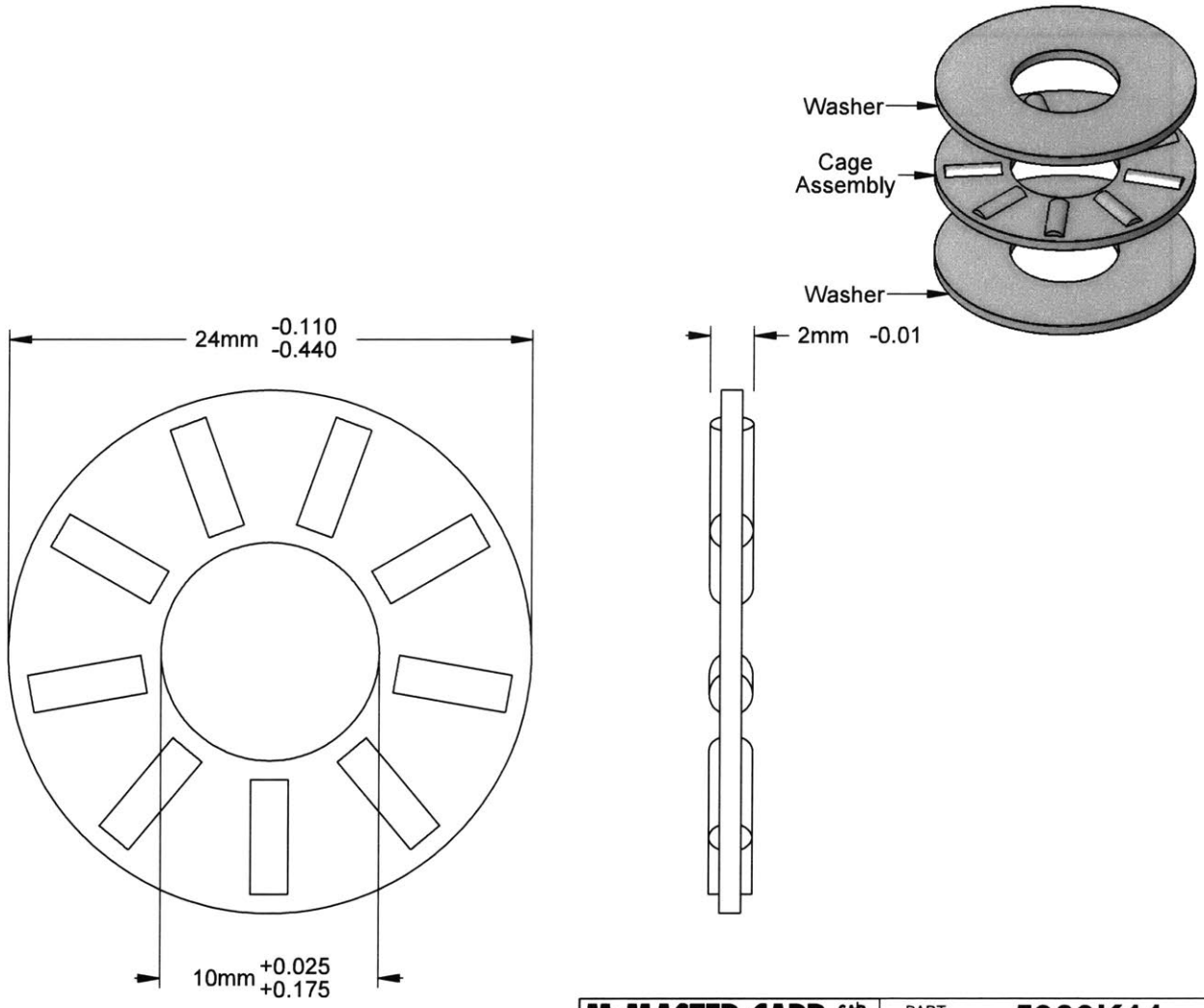

McMASTER-CARR® CAD

http://www.mcmaster.com

PART NUMBER **5909K11**

Steel Cage Assembly for Thrust Needle-Roller Bearing

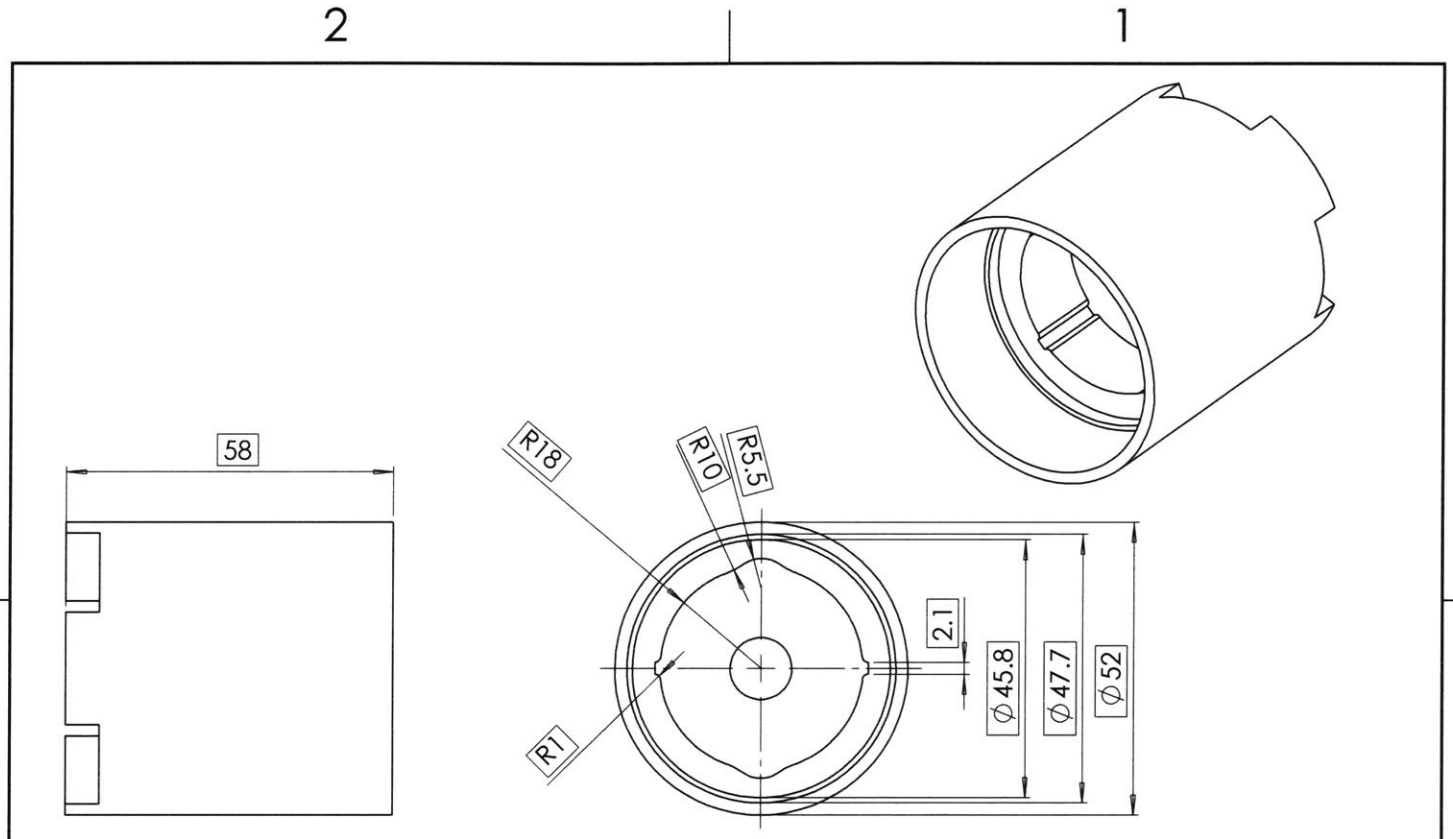

		UNLESS OTHERWISE SPECIFIED:		NAME	DATE
		DIMENSIONS ARE IN MILLIMETERS TOLERANCES: FRACTIONAL ± ANGULAR: MACH ± BEND ± TWO PLACE DECIMAL ± THREE PLACE DECIMAL ±	DRAWN		
			CHECKED		
			ENG APPR.		
			MFG APPR.		
		INTERPRET GEOMETRIC TOLERANCING PER:	Q.A.		
		MATERIAL	COMMENTS:		
NEXT ASSY	USED ON	FINISH			
APPLICATION		DO NOT SCALE DRAWING			

TITLE:

Slip Clutch: Left End Cup

SIZE	DWG. NO.	REV
A	Left End Cup	
SCALE: 1:1	WEIGHT:	SHEET 1 OF 2

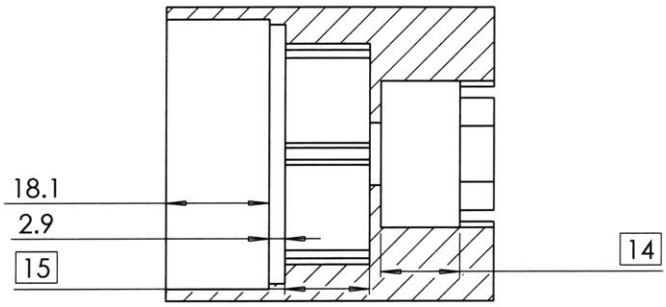

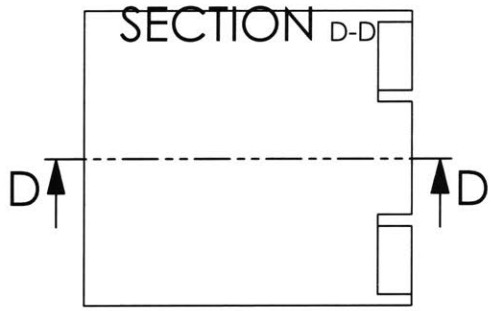

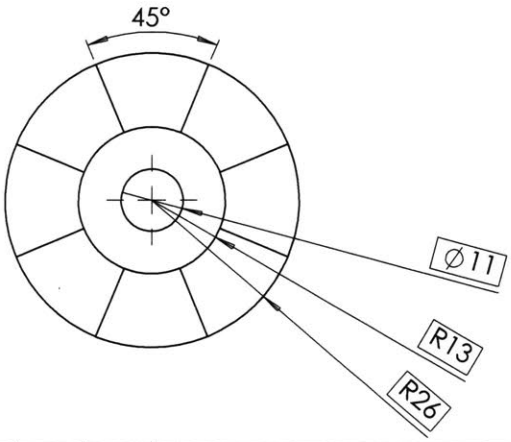

		UNLESS OTHERWISE SPECIFIED:		NAME	DATE
		DIMENSIONS ARE IN MILLIMETERS TOLERANCES: FRACTIONAL ± ANGULAR: MACH ± BEND ± TWO PLACE DECIMAL ± THREE PLACE DECIMAL ±	DRAWN		
			CHECKED		
			ENG APPR.		
			MFG APPR.		
		INTERPRET GEOMETRIC TOLERANCING PER:	Q.A.		
		MATERIAL	COMMENTS:		
NEXT ASSY	USED ON	FINISH			
APPLICATION		DO NOT SCALE DRAWING			

TITLE:

Slip Clutch: Left End Cup

SIZE	DWG. NO.	REV
A	Left End Cup	
SCALE: 1:1	WEIGHT:	SHEET 2 OF 2

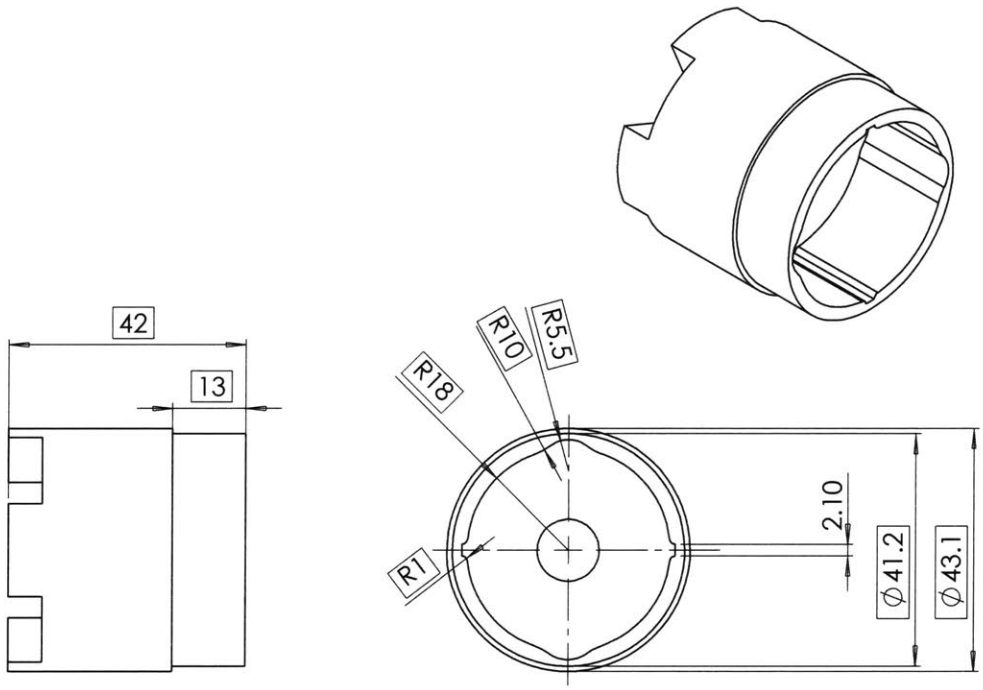

		UNLESS OTHERWISE SPECIFIED:		NAME	DATE
		DIMENSIONS ARE IN MILLIMETERS TOLERANCES: FRACTIONAL ± ANGULAR: MACH ± BEND ± TWO PLACE DECIMAL ± THREE PLACE DECIMAL ±	DRAWN		
			CHECKED		
			ENG APPR.		
			MFG APPR.		
		INTERPRET GEOMETRIC TOLERANCING PER:	Q.A.		
		MATERIAL	COMMENTS:		
NEXT ASSY	USED ON	FINISH			
APPLICATION		DO NOT SCALE DRAWING			

TITLE:
Slip Clutch: Right End Cup

SIZE	DWG. NO.	REV
A	Right End Cup	
SCALE: 1:1	WEIGHT:	SHEET 1 OF 2

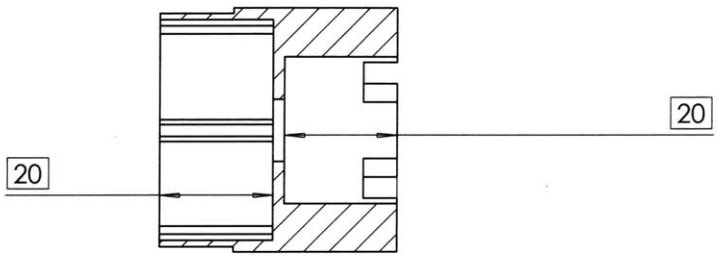

SECTION A-A

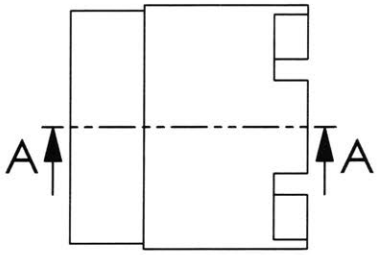

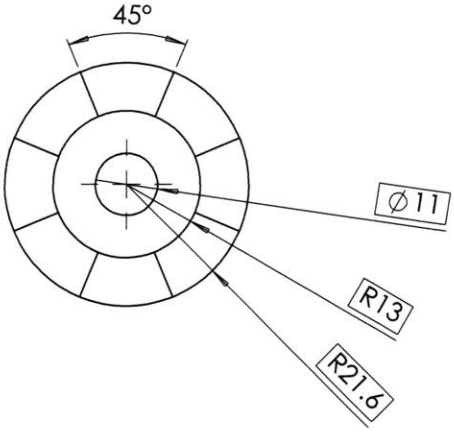

		UNLESS OTHERWISE SPECIFIED:		NAME	DATE
		DIMENSIONS ARE IN MILLIMETERS TOLERANCES: FRACTIONAL ± ANGULAR: MACH ± BEND ± TWO PLACE DECIMAL ± THREE PLACE DECIMAL ±	DRAWN		
			CHECKED		
			ENG APPR.		
			MFG APPR.		
		INTERPRET GEOMETRIC TOLERANCING PER:	Q.A.		
		MATERIAL	COMMENTS:		
NEXT ASSY	USED ON	FINISH			
APPLICATION		DO NOT SCALE DRAWING			

TITLE:
Slip Clutch: Right End Cup

SIZE	DWG. NO.	REV
A	Right End Cup	
SCALE: 1:1	WEIGHT:	SHEET 2 OF 2

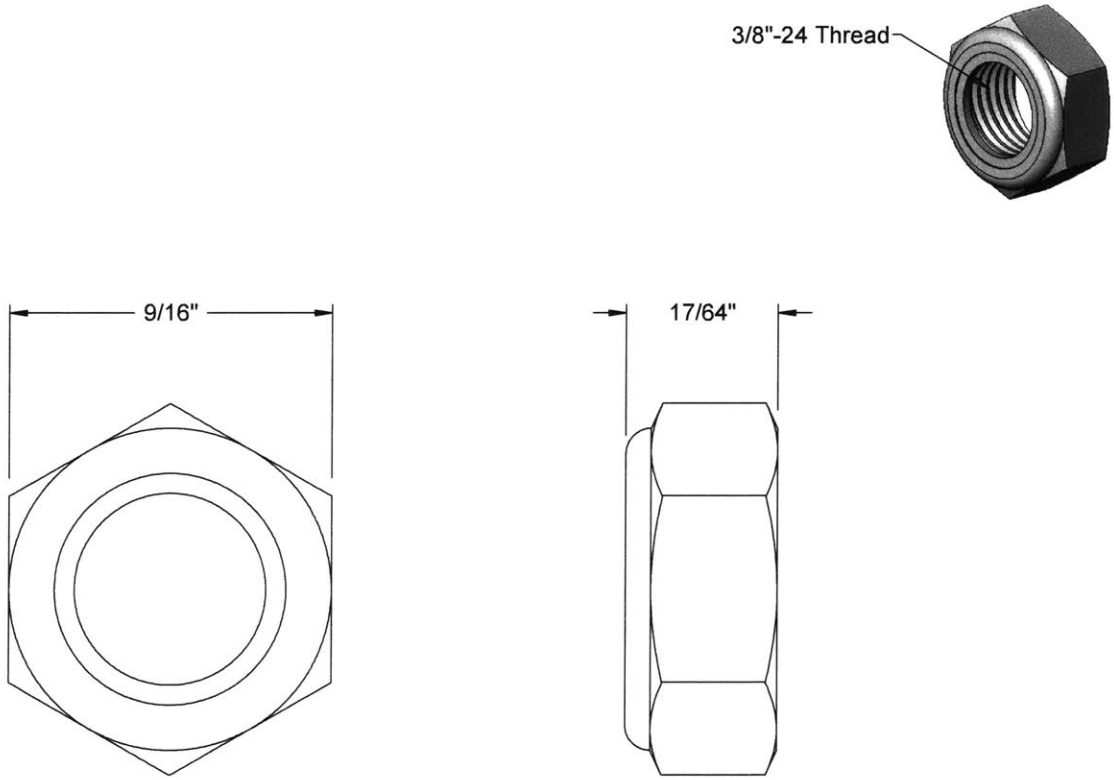

McMASTER-CARR® CAD

http://www.mcmaster.com

PART NUMBER **94945A218**

Thin Nylon-Insert Locknut

Bibliography

[1] R. G. Budynas, J. K. Nisbett, and J. E. Shigley. *Shigley's mechanical engineering design.* Mcgraw-Hill series in mechanical engineering. New York, NY : McGraw-Hill Education, [2015], 2015.

[2] Dynatect. Torque Limiter Technical Information. http://www.dynatect. Accessed: 2016-08-12.

[3] M. Graham, A. Slocum, and R. Sanehez. Teaching high school students and college freshmen product development by deterministic design with prep. *JOURNAL OF MECHANICAL DESIGN*, 129(7):677 – 681, n.d.

[4] S. Kalpakjian and S. R. Schmid. *Manufacturing engineering and technology.* Upper Saddle River, NJ : Pearson, [2014], 2014.

[5] L. S. Marks. *Marks' standard handbook for mechanical engineers.* New York : McGraw-Hill, [c1978-, 1978.

[6] Mayr. EAS Compact Torque Limiting Device Technical Information. http://www.mayr.com/en/products/torque-limiters/eas-compact-r-ra. Accessed: 2016-08-12.

[7] N. Mills. Design and Testing of a Pan-tilt Mechanism for Severe Environments. Master's thesis, Massachusetts Institute of Technology, Mechanical Engineering Department, May 2016.

[8] MITiCampus. PREP-Deterministic Design. http://icampus.mit.edu/projects/prep-peer-review-evaluation-process/prep-deterministic-design. Accessed: 2017-02-15.

[9] E. Oberg, F. D. Jones, H. L. Horton, and H. H. Ryffel. *Machinery's handbook.* South Norwalk : Industrial Press, Incorporated, 2016., 2016.

[10] A. H. Slocum. Course 2.75-Curved Beam Design Spreadsheet. http://web.mit.edu/2.75/fundamentals/FUNdaMENTALSspreadsheets.html. Accessed: 2016-10-25.

[11] A. H. Slocum. Course 2.75-FUNdaMENTALS of Design. http://web.mit.edu/2.75/fundamentals/FUNdaMENTALS.html. Accessed: 2016-09-20.

[12] A. H. Slocum. Course 2.75-FUNdaMENTALS of Design Chapter 3. http://web.mit.edu/2.75/fundamentals/FUNdaMENTALs Accessed: 2016-09-20.

[13] A. H. Slocum. Proposal for A Low-Torque Pan Tilt System for Directional Scanning in a Marine Environment. Unpublished Work, 2014.

[14] A. C. Ugural and S. K. Fenster. *Advanced strength and applied elasticity.* Upper Saddle River, N.J. : Prentice Hall PTR, c2003., 2003.

[15] ZeroMax. H-TLC Torque Tender Technical Information. http://www.zeromax.com/documents/H-TLC20catalog20pages.pdf. Accessed: 2017-02-17.